Abstract

This report deals with the thermal-hydraulic analysis of the helium-cooled pebble bed (HCPB) test blanket module (TBM) to be tested in the International Thermonuclear Experimental Reactor (ITER). It represents a poloidal section of the corresponding European blanket concept being developed at FZK in collaboration with other European research organizations for a DEMO reactor. This concept employs alternating layers of ceramic breeder material and beryllium as multiplier, which are separated by radial-toroidal cooling plates.

The analysis is performed with the computer code RELAP/MOD3.1 which is one-dimensional in terms of the fluid dynamics but permits heat transfer across flow channel walls. Thus, modeling of the complex cooling flow pattern present in the TBM, in combination with the time-dependent volumetric heat as well as surface heat flux applied to the first wall, is described in detail. The model includes also the complete cooling circuit with circulator, heat exchanger, pressure and temperature control provisions, and the coupling to the secondary cooling system.

The performance of the TBM and cooling circuit during normal operation (i.e., steady state and pulsed operation) and accidents was investigated. Four accident families were analysed with a variety of input parameters: (1) loss of flow accidents, (2) loss of coolant accidents, (3) leak inside test module accidents, and (4) loss of heat sink accidents. Typical transients for pressure, temperature, velocity, and mass flow rate at various locations in the TBM and in the circuit are presented and discussed in terms of safety aspects. Overall, no critical safety issues were identified.

Thermohydraulische Analysen des ITER-Testmoduls für das heliumgekühlte Feststoffblanket unter normalen Betriebsbedingungen und bei Störfällen

Zusammenfassung

Gegenstand dieses Berichtes sind thermo-hydraulische Analysen des sogenannten Test-Blanket-Moduls (TBM) für das heliumgekühlte Feststoffblanket (engl.: helium-cooled pebble bed, HCPB), das in dem "International Thermonuclear Experimental Reactor" (ITER) erprobt werden soll. Es stellt einen Ausschnitt des entsprechenden europäischen Blanketkonzeptes dar, welches im FZK in Zusammenarbeit mit anderen europäischen Forschungseinrichtungen für den Einsatz in einen Demonstrationsreaktor (DEMO) entwikkelt wird. Dieses Blanket ist aus abwechselnden Schichten aus keramischen Brutstoff- und Berylliumkugeln aufgebaut, die ihrerseits durch radial-toroidal angeordnete Kühlplatten voneinander getrennt sind.

Die Analysen wurden mit dem Rechenprogramm RELAP5/MOD3.1 durchgeführt. RELAP ist in Bezug auf die Fluiddynamik eindimensional, erlaubt aber die Berücksichtigung von Wärmetransport durch die Wandstrukturen der Kühlkanäle. Die Modellierung der sehr komplexen Strömungsführung im TBM in Verbindung mit der zeitabhängigen Wärmeerzeugung im Innern des TBM und an der "Ersten Wand" ist daher im einzelnen dargelegt. Das Modell enthält zudem den kompletten Kühlkreislauf mit Gebläse, Wärmetauscher, Vorkehrungen für Druck- und Temperaturregelung sowie die Ankopplung an das sekundäre Kühlsystem.

Es wurde das Verhalten des TBM mit Kühlkreislauf während des normalen Betriebes (d. h. bei stationärer und gepulster Betriebsweise) sowie bei Störfällen untersucht. Für letztere wurden vier Gruppen von Ereignissen unter Variation mehrerer Parameter betrachtet, nämlich (1) Durchflußstörungen, (2) Kühlmittelverluststörfälle, (3) Lecks innerhalb des Testmoduls und (4) Verlust der Wärmesenke. Typische Zeitverläufe für Druck, Temperatur, Geschwindigkeit und Massenstrom an verschiedenen Stellen im TBM und im Kreislauf werden dargestellt und bezüglich der Sicherheit diskutiert. Insgesamt ergeben sich daraus keine Bedenken zur Sicherheit des Gesamtsystems.

Contents

1 Introduction **1**

2 HCPB Test Blanket Module **3**
2.1 Design . . . 3
2.2 Power Generation . . . 4
2.2.1 Nominal Power . . . 4
2.2.2 Decay Heat Power . . . 7

3 RELAP5/MOD3.1 Cooling System Model **15**
3.1 Primary Side Piping . . . 16
3.2 Test Module . . . 20
3.2.1 Flow Channels . . . 20
3.2.2 Structure . . . 24
3.2.3 Power Generation . . . 30
3.3 Circulator . . . 32
3.4 Heat Exchanger . . . 34
3.5 Pressure Control System . . . 35
3.6 Temperature Control System . . . 36
3.7 Secondary Side Piping . . . 37

4 Normal Operation Analyses **47**
4.1 Steady State Analysis . . . 47
4.2 Pulsed Operation Analysis . . . 50

5 Accident Analyses **57**
5.1 Loss of Flow Accidents . . . 57
5.1.1 Loss of Electrical Power of Circulators (LOFA2) . . . 57
5.1.2 Inadvertent valve closure (LOFA2A) . . . 70
5.2 Loss of Coolant Accidents . . . 73
5.2.1 Ex-vessel Loss of Coolant (LOCA2EX) . . . 73
5.2.2 In-vessel Loss of Coolant (LOCA2IN) . . . 78
5.3 Leak Inside Test Module Accidents (LEAK2TM) . . . 84
5.4 Loss of Heat Sink Accidents . . . 93
5.4.1 Total Loss of Heat Sink (LOHS2HX) . . . 93
5.4.2 Loss of Secondary Side Flow (LOSF2HX) . . . 94

6 Summary and Conclusions **101**

List of Figures

2.1 Isometric view of a poloidal portion of the HCPB DEMO blanket 4
2.2 Radial-poloidal cut through TBM (status of 7/96) 5
2.3 Radial-toroidal cut through TBM (status of 7/96) 6
2.4 Detail of first wall and cooling plates 9
2.5 Decay heat power vs. time in HCPB TBM 13

3.1 Location of the HCPB TBM in ITER and pipe routing (status of 7/96) . . 17
3.2 RELAP5/MOD3.1 nodalization of one cooling loop of the HCPB TBM . . 18
3.3 Detailed RELAP5/MOD3.1 nodalization of the HCPB TBM 19
3.4 Location of orifices in TBM model 23
3.5 Sharp-edge orifice 23
3.6 Modelling of first wall with RELAP5 heat structures 25
3.7 Modelling of breeding zone with RELAP5 heat structures 27
3.8 Characteristic curves of the helium circulator 33
3.9 Mixing of bypass and HX flow 37

4.1 ITER pulsed operation: Structural temperature vs. time in toroidal midplane 52
4.2 ITER pulsed operation: Temperatures and mass flow rates vs. time 53
4.3 ITER pulsed operation: Helium temperature vs. time 54
4.4 ITER pulsed operation: Structural temperatures vs. time 55

5.1 LOFA2: circulator coast-down behaviour 59
5.2 LOFA2 case I: maximum structural temperatures vs. time 60
5.3 LOFA2 cases II to VII: maximum FW MANET temperature vs. time . . . 61
5.4 LOFA2 case II: maximum structural temperature vs. time 62
5.5 LOFA2 case III: maximum structural temperature vs. time 63
5.6 LOFA2 case IV: maximum structural temperature vs. time 63
5.7 LOFA2 case V: maximum structural temperature vs. time 64
5.8 LOFA2 case VI: maximum structural temperature vs. time 64
5.9 LOFA2: maximum FW MANET temperature vs. time for first hour 65
5.10 LOFA2: maximum FW MANET temperature vs. time for first day 66
5.11 LOFA2: controlled mass flow rates vs. time 66
5.12 LOFA2: corrected heat transfer coefficients vs. time 67
5.13 LOFA2: main loop flow rates vs. time 67
5.14 LOFA2: maximum FW beryllium temperature during the first hour 68
5.15 LOFA2: maximum FW beryllium temperature during the first day 69
5.16 LOFA2: cold leg wall temperature vs. time 69
5.17 LOFA2A case I: maximum structural temperatures during the first hour . . 71
5.18 LOFA2A case I: maximum structural temperatures during the first day . . 72
5.19 LOFA2A cases I-III: maximum FW MANET temperature vs. time 72

5.20 RELAP5/MOD3.1 nodalization for ex-vessel LOCA analyses 74
5.21 LOCA2EX: pressure, helium velocity and mass flow rate vs. time 76
5.22 LOCA2EX: heat transfer coefficients, temperatures and mass flow rates . . 77
5.23 RELAP5/MOD3.1 nodalization for in-vessel LOCA analysis 79
5.24 LOCA2IN case I: loop pressure, VV pressure and VV helium temperature . 81
5.25 LOCA2IN case I: mass flow rates, circulator head, and helium temperatures 82
5.26 LOCA2IN case II: maximum structural temperatures vs. time 83
5.27 RELAP5/MOD3.1 nodalization for leak inside test module analysis 85
5.28 LEAK2TM case I: pressure histories, circulator head, and leak mass flow rate 88
5.29 LEAK2TM case I: controlled mass flow rates vs. time 89
5.30 LEAK2TM case I: maximum structural temperatures vs. time 89
5.31 LEAK2TM case II: maximum structural temperatures vs. time 90
5.32 LEAK2TM case III: maximim structural temperature vs. time 90
5.33 LEAK2TM case IV: pressure, circulator head and mass flow rate 91
5.34 LEAK2TM case IV: maximum structural temperatures vs. time 92
5.35 LOHS2HX case I: maximum structural temperatures vs. time 94
5.36 LOHS2HX case II: maximum structural temperatures vs. time 95
5.37 LOSF2HX: maximum structural temperature vs. time 96
5.38 LOSF2HX: mass flow rates vs. time 97
5.39 LOSF2HX: HX secondary temperature vs. time 98
5.40 LOSF2HX: HX secondary void fractions vs. time 99

List of Tables

2.1 Power densities inside the HCPB TBM (status of 7/96) 7
2.2 Power production inside the HCPB TBM 8
2.3 Ratio of decay heat/nominal power density for DEMO MANET 10
2.4 Ratio of decay heat/nominal power density for DEMO beryllium 11
2.5 Ratio of decay heat/nominal power density for DEMO breeder 12
2.6 Decay heat power inside the HCPB TBM 13

3.1 Design parameters for different pipe components 16
3.2 Division of cooling plates in six cooling zones 21
3.3 Main parameters of TBM model hydrodynamic components 38
3.4 Energy loss coefficients and geometry of actual orifices 39
3.5 Heat transfer areas of breeding zone heat structures 39
3.6 Heat transfer equivalent diameters of breeding zone heat structures 40
3.7 Decay heat power generation in blanket box MANET 40
3.8 Decay heat power generation in blanket box beryllium coating 41
3.9 Nominal power densities in the six cooling zones 41
3.10 Nominal power generation in breeding zone structures 42
3.11 Decay heat power vs. time in breeding zone heat structure 1 43
3.12 Decay heat power vs. time in breeding zone heat structure 2 44
3.13 Homologous parameters of helium circulator 45

4.1 Steady state structural temperatures 48
4.2 Steady state heat transfer coefficients 49

5.1 Investigated LOFAs - loss of electrical power 58
5.2 Investigated leak inside test module accidents 86
5.3 Overview of the main temperature results obtained for the cases investigated 100

Chapter 1

Introduction

The European Helium-Cooled Pebble Bed (HCPB) DEMO blanket concept is one of the blanket concepts selected for further development within the EU fusion programme [1]. A representative test module of the HCPB blanket will be tested in the International Thermonuclear Experimental Reactor (ITER), scheduled for test begin around the year 2010. The purpose of the tests is to demonstrate tritium breeding and recovery as well as extraction of high grade heat suitable for generation of electricity.

For integration in ITER the Test Blanket Module (TBM) has to assure a number of features. These are to provide adequate shielding, accommodate surface and nuclear heating, handle static and dynamic loads, support vacuum requirements, conform to safety criteria, have minimal impact on operational availability, and to conform to remote handling criteria. In terms of safety, the operation of the TBM should have as low as possible impact on the safe operation of ITER during postulated accidents [2]. The present work is a first scoping study to identify key parameters in the thermo-dynamic behaviour of the TBM subsystem in the ITER environment.

The HCPB TBM represents a poloidal section of the corresponding DEMO blanket segment. It employs alternating layers of ceramic breeder material (the current reference material being Li_4SiO_4) and beryllium, both in form of small pebbles. The material layers of 1.1 cm and 4.5 cm thickness, respectively, are separated by cooling plates with integral cooling channels. The stack of layers and plates is encapsulated in a strong and actively cooled structure, the fabrication techniques of which are being developed in parallel [3]. Many of the geometric parameters adopted here are still subject of optimization. The configuration analyzed in this report corresponds to the status as of July 1996 and is termed in [1] as BTM-I. Please note that meanwhile the terminology has changed from Blanket Test Module, BTM, to Test Blanket Module, TBM. Hence, BTM-I will henceforth be denoted simply as TBM.

The second element in the study is the helium cooling system pertaining to the TBM. It consists of two separate primary heat removal loops which, for sake of simplicity, have been lumped to a single loop in the analysis. The loop architecture also corresponds to the status as of 1996 as outlined in [1], when the system was supposed to be accommodated in the tritium building of ITER rather distant from the TBM proper. This has changed in the meantime, entailing much shorter and smaller pipe dimensions [4]. Therefore, many of the results reported will change quantitatively, however the principal trends and conclusions are expected to be maintained when the analysis will be revised on the grounds of this work. The analysis was carried out with the thermal-hydraulic computer code RELAP5/MOD3.1 [5].

The TBM design and the power generation are described in the following chapter. After

a brief characterization of the RELAP code and a detailed description of the geometrical and thermo-dynamic system model in chapter 3, the report deals essentially with the analysis of the dynamics of the TBM, including its cooling system. The behaviour during normal operation, both in the steady state and in the pulsed power mode, is described in chapter 4. The main part, chapter 5, is then devoted to different types of accidents. These are: (1) loss of flow accidents (LOFAs), (2) loss of coolant accidents (LOCAs), (3) leak inside test module accidents (LEAK), and (4) loss of heat sink accidents (LOHS). Summary and conclusions are drawn in chapter 6.

Chapter 2

HCPB Test Blanket Module

2.1 Design

The HCPB TBM represents a poloidal section of a HCPB DEMO blanket segment. An isometric view of a poloidal portion of the HCPB DEMO outboard blanket segment is shown in Fig. 2.1 [6]. The overall dimensions of the TBM are determined by the constraints of the ITER horizontal port which is supposed to accommodate both the HCPB TBM and a similar test module developed by the Japanese group. A maximum size of 2.56 m high by 1.56 m wide is available for the two modules installed [1].

The present calculations are based on the design status of the TBM of July 1996. Radial-poloidal and radial-toroidal cuts of the TBM at this design state are shown in Figures 2.2 and 2.3. The current reference design of the TBM differs slightly from that shown in the figures and, additionally, the reference material has changed from MANET to EUROFER. However, these modifications do not influence the relevance of the present analyses. Details of the current reference design can be found in [4].

The test module consists of a rigid box with 8 mm thick radial-toroidally arranged cooling plates in the interior. The plasma facing part of the blanket box constitutes the first wall (FW) of the TBM. Both blanket box and cooling plates are made of the martensitic steel MANET. On the plasma side the FW is coated with a 5 mm beryllium layer which serves as a protection against the plasma interaction. Between the cooling plates, alternating pebble beds of the breeder material Li_4SiO_4 (11 mm bed thickness) and of the neutron multiplier beryllium (45 mm bed thickness) are located. The back of the blanket box is formed by a massive MANET block housing the main coolant feed lines and exhaust lines. A detail of the first wall with adjacent cooling plates and integrated cooling channels is shown in Fig. 2.4 on page 9.

Blanket box and structure are cooled in series by helium at 8 MPa. The helium flow path is as follows: First the helium is distributed from the main coolant feed lines to the blanket box (FW) cooling channels, then streams through the blanket box, is afterwards collected in poloidal headers and redistributed to the cooling plates, flows through the cooling plates, and is finally collected in the main coolant exhaust lines.

For safety reasons the helium cooling system is divided into two independent cooling loops with equal capacity. The arrangement of the two loops is such that adjacent blanket box cooling channels and adjacent cooling plates belong to different cooling loops. The flow directions in the two sets of channels pertaining to each loop are opposite to equalise the toroidal temperature profile in the TBM. The nominal inlet and outlet temperatures of the helium gas are 250 °C and 350 °C, respectively, at a total mass flow rate of 3.7 kg/s for both cooling loops.

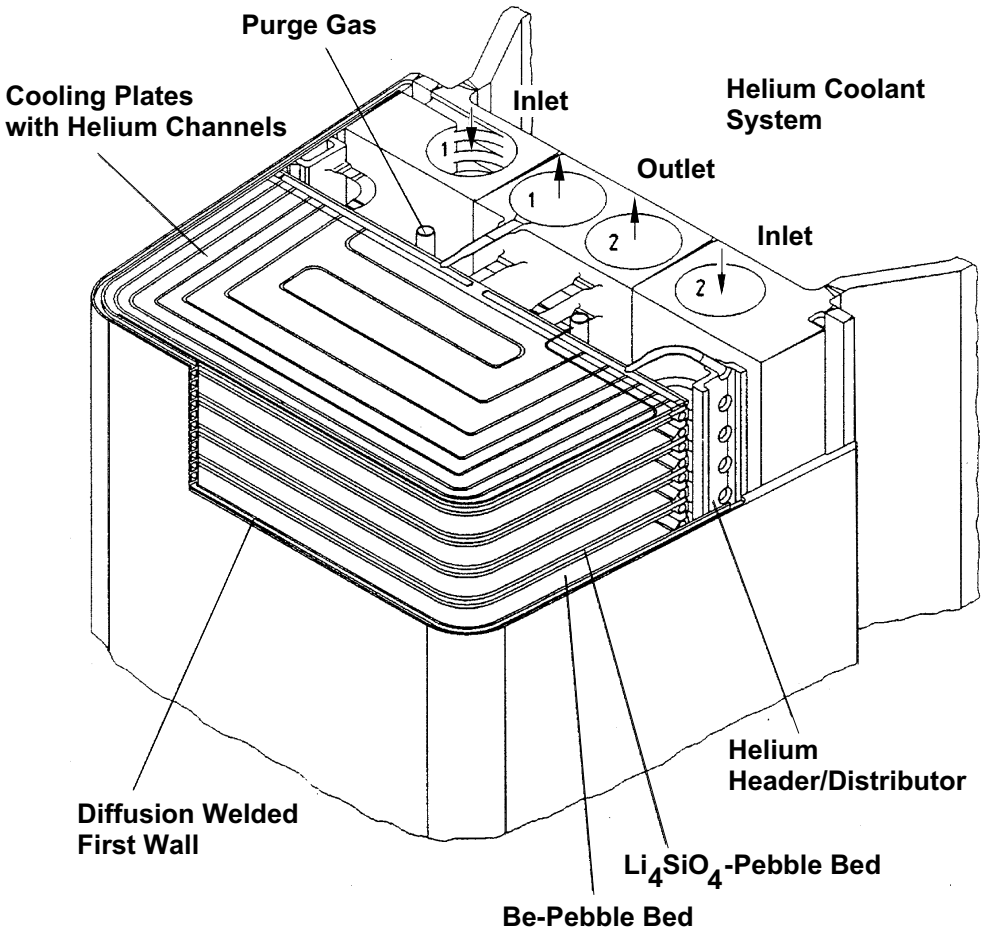

Figure 2.1: Isometric view of a poloidal portion of a HCPB DEMO outboard blanket segment at the torus equatorial plane.

Top and bottom of the TBM are closed by cover plates (caps) made of MANET. Like the FW the cover plates are protected by a 5 mm thick beryllium coating on the plasma facing edge. The cooling manner of the cover plates, i.e. number and shape of cooling channels, has not yet been elaborated.

To facilitate handling procedures the TBM will be attached to a water-cooled support frame which is part of the ITER design. This support frame constitutes an additional heat sink in the case that all active cooling inside the TBM is lost. However, no credit has been given to this effect in the present analysis.

2.2 Power Generation

2.2.1 Nominal Power

The power load on the TBM during the ITER burn cycles consists of surface heating and volumetric heating.

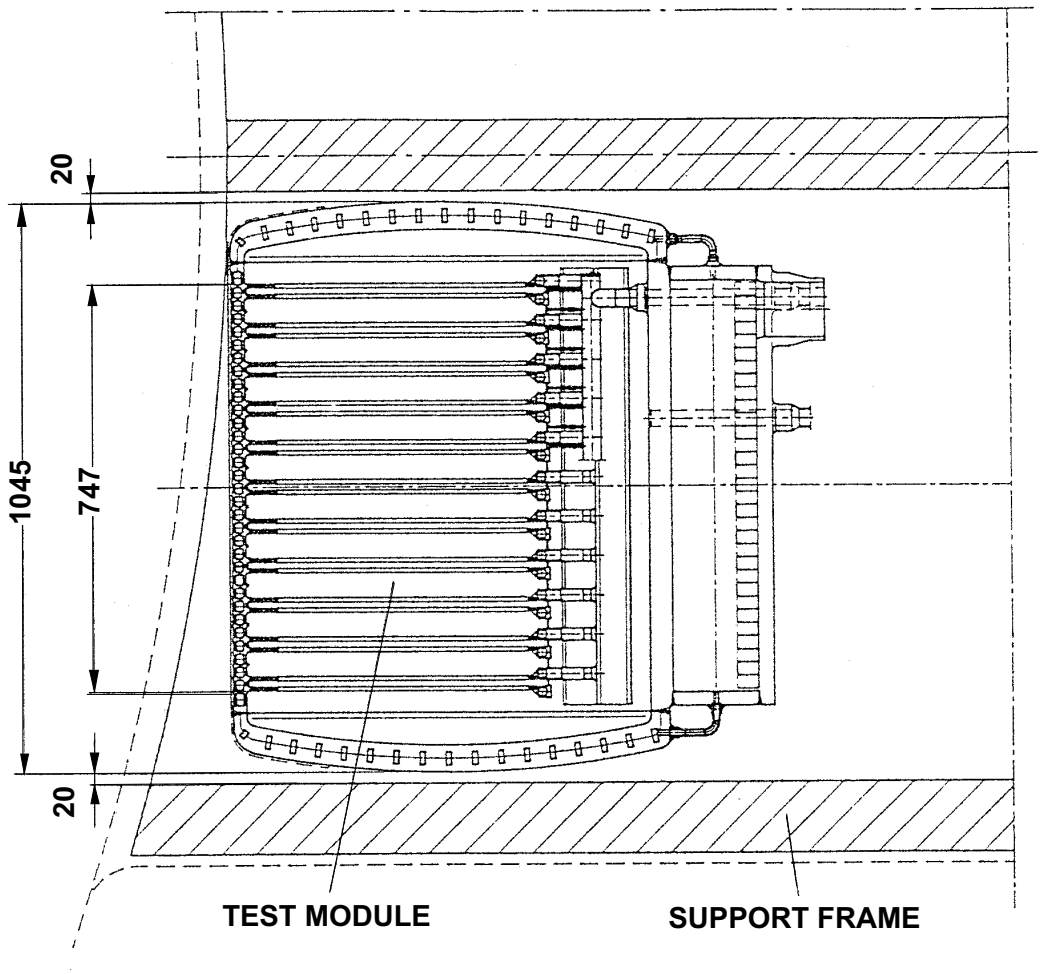

Figure 2.2: Radial-poloidal cut through TBM (status of 7/96)

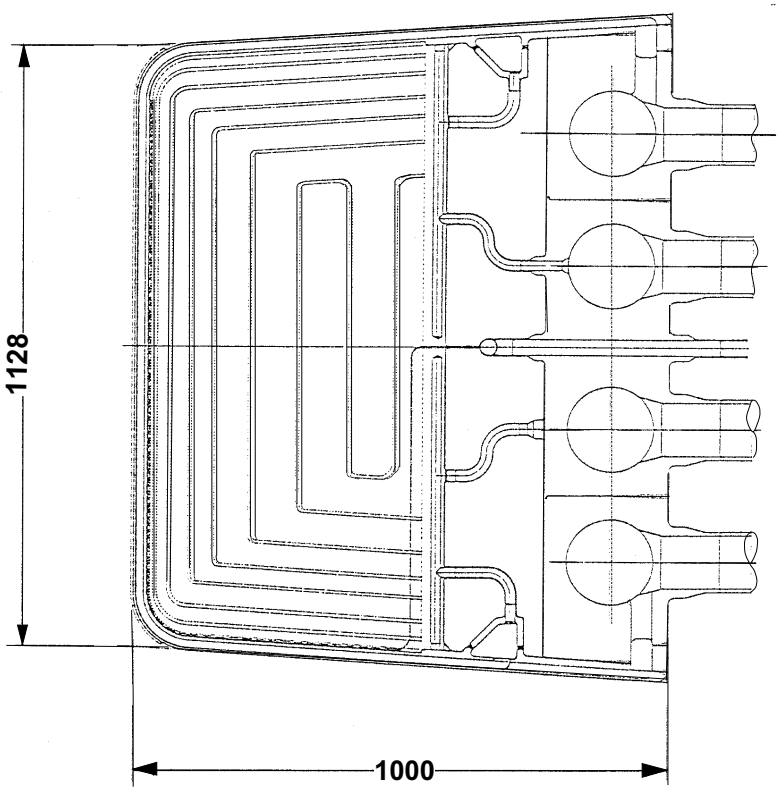

Figure 2.3: Radial-toroidal cut through TBM (status of 7/96)

Surface heating

A surface heat flux of 50 W/cm^2 was assumed for the present calculations. This is the maximum expected surface heat flux during the tests. With a FW projection area of 112.8 cm x 104.5 cm towards the plasma (according to Figures 2.2 and 2.3) the surface power results to 0.589 MW.

Volumetric heating

The nuclear power production in the TBM was assessed on the basis of the nuclear power density distribution obtained by three-dimensional Monte Carlo calculations performed with the MCNP-code [7]. Table 2.1 shows the toroidally averaged nuclear power density distribution inside the test module. Please note that the values given in Table 2.1 represent the state of the calculations of July 1996. The updated values corresponding to the current reference design can be found in [4]. The nuclear power production inside the TBM calculated with the power densities from Table 2.1 for the geometry shown in Figures 2.2 and 2.3 is compiled in Table 2.2.

The total volumetric power amounts to 1.514 MW. 12.3 % of the power is produced in the first wall, 72.1 % in the breeding zone, 2.2 % in the manifold region behind the breeding zone, and 13.4 % in the cover plates. 36.9 % of the volumetric power is generated in MANET, 34.3 % in Li_4SiO_4, 26.4 % in the beryllium of the breeding zone, and 2.4 % in the beryllium of the FW.

Table 2.1:
Power densities inside the HCPB TBM (status of 7/96).

	Nuclear power density (W/cm^3)			
Radial distance to first wall (cm)	MANET	Beryllium	Li_4SiO_4	Blanket region
0.5	–	7.60	–	
1.0	9.57	–	–	First
2.4	9.24	–	–	wall
3.0	8.56	–	–	
6.0	7.72	4.60	18.0	
9.0	6.49	3.85	14.7	
13.0	5.47	3.07	13.1	
18.0	4.28	2.35	11.9	
23.0	3.29	1.68	9.8	
28.0	2.45	1.22	7.9	Breeding
33.0	1.72	0.86	5.9	zone
38.0	1.41	0.60	4.7	
43.0	1.06	0.44	3.5	
48.0	0.78	0.32	2.7	
53.0	0.62	0.23	2.0	
57.3	0.49	0.17	1.7	
61.3	0.35	–	–	
78.3	0.26	–	–	Manifolds
100.5	0.17	–	–	

Total power

The total power load on the TBM equals the sum of surface power and volumetric power and amounts to 0.589 MW + 1.514 MW = 2.103 MW.

2.2.2 Decay Heat Power

The decay heat generation in the TBM after shutdown of the plasma originates from the nuclear decay heat of neutron-activated materials. Neutronic calculations of the activation and decay heat generation in the TBM were not available for the present report. Hence, as an approximation, the decay heat was estimated on the basis of decay heat power densities calculated for the HCPB DEMO blanket [8], [9]. The ratios of DEMO decay heat power density to nominal power density for MANET, beryllium, and Li_4SiO_4, at different times after shutdown and at different radial positions are shown in Tables 2.3 to 2.5. The nominal power densities for beryllium and Li_4SiO_4 were taken from [9], since only mean power densities for both pebble beds were given in [8].

Note that the ratios are based on an integral operation time of 20,000 hours at an

Table 2.2:
Power production inside the HCPB TBM.

Blanket region	Power (MW)
First wall: Beryllium	0.037
First wall: MANET	0.149
Breeding zone: Beryllium	0.400
Breeding zone: Li_4SiO_4	0.519
Breeding zone: MANET	0.172
Manifolds: MANET	0.034
Cover plates: MANET	0.203
Σ	1.514

average neutron wall loading of 2.2 MW/m^2 (DEMO specification). In contrast to that, the goal of ITER operation during the Basic Performance Phase (BPP) is to accumulate a few thousands of hours of full DT operation distributed over about 10 calendar years. Furthermore, the average neutron wall loading of ITER will be only 1.2 MW/m^2. These conditions will lead to lower specific decay heat values for the TBM in comparison with the DEMO blanket.

The extrapolated decay heat power values for the HCPB TBM, using the same ratios of decay heat densities to nominal power densities as obtained for DEMO (Tables 2.3 - 2.5) and the nominal power densities for the TBM according to Table 2.1, are shown in Table 2.6. The decay heat power in the first wall (including the beryllium coating) immediately after shutdown amounts to 4.0 % of the nominal power. In the breeding zone, the corresponding value amounts to 2.0 %, whereas for the manifold region and the cover plates the values are 3.5 % and 3.8 %, respectively. After one day, the decay heat equals 0.28 %, 0.06 %, 0.24 %, and 0.29 % of the nominal power in first wall, breeding zone, manifold region, and cover plates, respectively. The decay heat generation vs. time for the whole test module is depicted in Fig. 2.5 on page 13. Immediately after shutdown the decay heat in the whole TBM amounts to 1.8 % of the nominal total power or 2.5 % of the nominal volumetric power. After 1 day the decay heat has declined to 0.09 %/0.12 % of nominal total/volumetric power. Between 1 day and 1 month the decline in heat generation is very small, i.e. 1.0 % of the value at shutdown. The bulk of the decay heat is generated in MANET, while beryllium and Li_4SiO_4 contribute significantly to the decay heat only in the first minute after shutdown (see [10]).

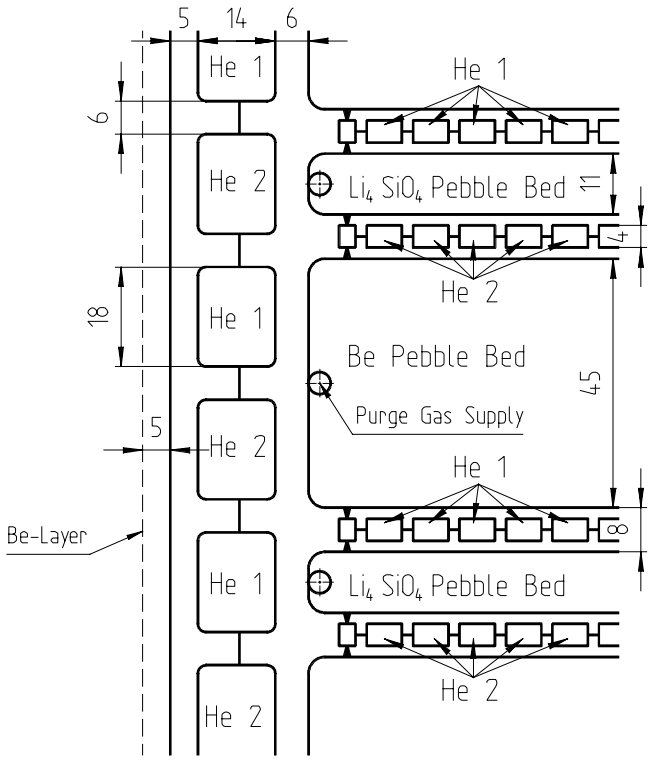

Figure 2.4: Detail of first wall and cooling plates (He 1 and He 2 refer to cooling loops 1 and 2, respectively).

Table 2.3:
Ratio of decay heat power density to nominal power density for DEMO MANET at torus equatorial plane.

MANET					
Decay heat power density/Nominal power density (%)					
Distance	Time after shutdown				
to FW (cm)	0 s	1 s	10 s	1 min	5 min
0.5	4.04	4.03	4.01	3.93	3.69
2.1	3.94	3.93	3.91	3.83	3.60
2.9	3.93	3.92	3.90	3.82	3.60
5.9	4.26	4.26	4.23	4.15	3.92
10.4	4.30	4.29	4.27	4.19	3.96
14.9	4.00	4.00	3.98	3.90	3.71
19.4	4.06	4.06	4.04	3.97	3.78
23.9	4.13	4.13	4.11	4.04	3.86
28.4	4.24	4.23	4.21	4.15	3.97
32.9	4.27	4.26	4.24	4.18	4.01
35.9	4.09	4.08	4.07	4.01	3.85
38.9	3.76	3.75	3.74	3.69	3.54
43.9	3.72	3.72	3.70	3.66	3.52
48.9	3.42	3.42	3.41	3.37	3.24
52.9	3.48	3.47	3.46	3.42	3.30
61.0	3.29	3.29	3.28	3.24	3.12
79.0	3.46	3.45	3.45	3.41	3.29
100.0	3.48	3.48	3.47	3.43	3.31
Distance	Time after shutdown				
to FW (cm)	10 min	1 h	5 h	1 day	1 month
0.5	3.53	2.85	1.21	0.36	0.30
2.1	3.45	2.78	1.18	0.35	0.29
2.9	3.45	2.78	1.17	0.34	0.28
5.9	3.76	3.03	1.28	0.37	0.30
10.4	3.81	3.07	1.29	0.37	0.30
14.9	3.57	2.87	1.20	0.34	0.27
19.4	3.64	2.93	1.22	0.34	0.27
23.9	3.72	3.00	1.24	0.34	0.27
28.4	3.83	3.09	1.28	0.34	0.26
32.9	3.87	3.12	1.28	0.33	0.26
35.9	3.72	3.00	1.23	0.31	0.24
38.9	3.43	2.76	1.13	0.29	0.22
43.9	3.40	2.74	1.12	0.28	0.22
48.9	3.14	2.52	1.03	0.25	0.19
52.9	3.19	2.57	1.04	0.25	0.19
61.0	3.02	2.43	0.99	0.25	0.18
79.0	3.18	2.55	1.03	0.25	0.18
100.0	3.21	2.57	1.04	0.24	0.17

Table 2.4:
Ratio of decay heat power density to nominal power density
for DEMO beryllium at torus equatorial plane.

BERYLLIUM					
Decay heat power density/Nominal power density (%)					
Distance	Time after shutdown				
to FW (cm)	0 s	1 s	10 s	1 min	5 min
5.9	0.19E+1	0.83E+0	0.21E−1	0.18E−1	0.15E−1
10.4	0.23E+1	0.98E+0	0.28E−1	0.24E−1	0.20E−1
14.9	0.25E+1	0.11E+1	0.35E−1	0.30E−1	0.25E−1
19.4	0.26E+1	0.11E+1	0.42E−1	0.36E−1	0.30E−1
23.9	0.27E+1	0.12E+1	0.48E−1	0.42E−1	0.35E−1
28.4	0.28E+1	0.12E+1	0.53E−1	0.46E−1	0.39E−1
32.9	0.29E+1	0.12E+1	0.53E−1	0.47E−1	0.40E−1
35.9	0.28E+1	0.12E+1	0.50E−1	0.44E−1	0.38E−1
38.9	0.28E+1	0.12E+1	0.43E−1	0.38E−1	0.33E−1
43.9	0.29E+1	0.12E+1	0.40E−1	0.36E−1	0.32E−1
48.9	0.27E+1	0.12E+1	0.37E−1	0.34E−1	0.30E−1
52.9	0.26E+1	0.11E+1	0.38E−1	0.35E−1	0.32E−1
Distance	Time after shutdown				
to FW (cm)	10 min	1 h	5 h	1 day	1 month
5.9	0.14E−1	0.10E−1	0.69E−2	0.39E−2	0.12E−2
10.4	0.19E−1	0.13E−1	0.86E−2	0.49E−2	0.15E−2
14.9	0.23E−1	0.16E−1	0.10E−1	0.59E−2	0.17E−2
19.4	0.28E−1	0.19E−1	0.12E−1	0.70E−2	0.19E−2
23.9	0.32E−1	0.22E−1	0.14E−1	0.79E−2	0.21E−2
28.4	0.35E−1	0.25E−1	0.15E−1	0.88E−2	0.22E−2
32.9	0.37E−1	0.26E−1	0.16E−1	0.93E−2	0.21E−2
35.9	0.35E−1	0.25E−1	0.15E−1	0.90E−2	0.20E−2
38.9	0.31E−1	0.22E−1	0.14E−1	0.80E−2	0.17E−2
43.9	0.30E−1	0.22E−1	0.13E−1	0.76E−2	0.16E−2
48.9	0.28E−1	0.21E−1	0.13E−1	0.73E−2	0.14E−2
52.9	0.30E−1	0.22E−1	0.13E−1	0.78E−2	0.15E−2

Table 2.5:
Ratio of decay heat power density to nominal power density
for DEMO Li_4SiO_4 at torus equatorial plane.

Li_4SiO_4					
Decay heat power density/Nominal power density (%)					
Distance	Time after shutdown				
to FW (cm)	0 s	1 s	10 s	1 min	5 min
5.9	0.17E+1	0.16E+1	0.95E+0	0.45E+0	0.15E+0
10.4	0.14E+1	0.12E+1	0.76E+0	0.36E+0	0.12E+0
14.9	0.10E+1	0.90E+0	0.55E+0	0.27E+0	0.90E−1
19.4	0.78E+0	0.69E+0	0.42E+0	0.21E+0	0.70E−1
23.9	0.62E+0	0.54E+0	0.33E+0	0.17E+0	0.58E−1
28.4	0.51E+0	0.44E+0	0.27E+0	0.14E+0	0.48E−1
32.9	0.44E+0	0.37E+0	0.23E+0	0.12E+0	0.42E−1
35.9	0.38E+0	0.33E+0	0.20E+0	0.11E+0	0.37E−1
38.9	0.33E+0	0.28E+0	0.18E+0	0.96E−1	0.33E−1
43.9	0.30E+0	0.26E+0	0.16E+0	0.90E−1	0.31E−1
48.9	0.26E+0	0.22E+0	0.14E+0	0.76E−1	0.27E−1
52.9	0.23E+0	0.20E+0	0.12E+0	0.68E−1	0.25E−1
Distance	Time after shutdown				
to FW (cm)	10 min	1 h	5 h	1 day	1 month
5.9	0.46E−1	0.11E−1	0.72E−2	0.26E−2	0.41E−4
10.4	0.38E−1	0.93E−2	0.59E−2	0.20E−2	0.36E−4
14.9	0.29E−1	0.80E−2	0.47E−2	0.14E−2	0.29E−4
19.4	0.24E−1	0.70E−2	0.40E−2	0.11E−2	0.23E−4
23.9	0.20E−1	0.64E−2	0.35E−2	0.95E−3	0.20E−4
28.4	0.17E−1	0.60E−2	0.32E−2	0.82E−3	0.17E−4
32.9	0.15E−1	0.57E−2	0.30E−2	0.74E−3	0.15E−4
35.9	0.14E−1	0.53E−2	0.28E−2	0.67E−3	0.14E−4
38.9	0.13E−1	0.50E−2	0.25E−2	0.59E−3	0.12E−4
43.9	0.12E−1	0.50E−2	0.25E−2	0.56E−3	0.12E−4
48.9	0.11E−1	0.48E−2	0.24E−2	0.51E−3	0.10E−4
52.9	0.10E−1	0.50E−2	0.24E−2	0.50E−3	0.93E−5

Table 2.6:
Decay heat power inside the HCPB TBM.

	Decay heat power (kW) in blanket region:				
Time after shutdown	First wall	Breeding zone	Manifolds	Cover plates	Entire TBM
0 s	7.33	22.00	1.18	7.64	38.15
1 s	6.52	16.00	1.18	7.62	31.32
10 s	5.90	10.37	1.18	7.60	25.05
1 min	5.78	9.02	1.16	7.50	23.46
5 min	5.43	7.84	1.14	7.22	21.63
10 min	5.20	7.30	1.08	6.98	20.56
1 h	4.19	5.80	0.88	5.62	16.49
5 h	1.78	2.44	0.34	2.30	6.86
1 day	0.52	0.69	0.08	0.58	1.87
1 month	0.43	0.55	0.06	0.46	1.50

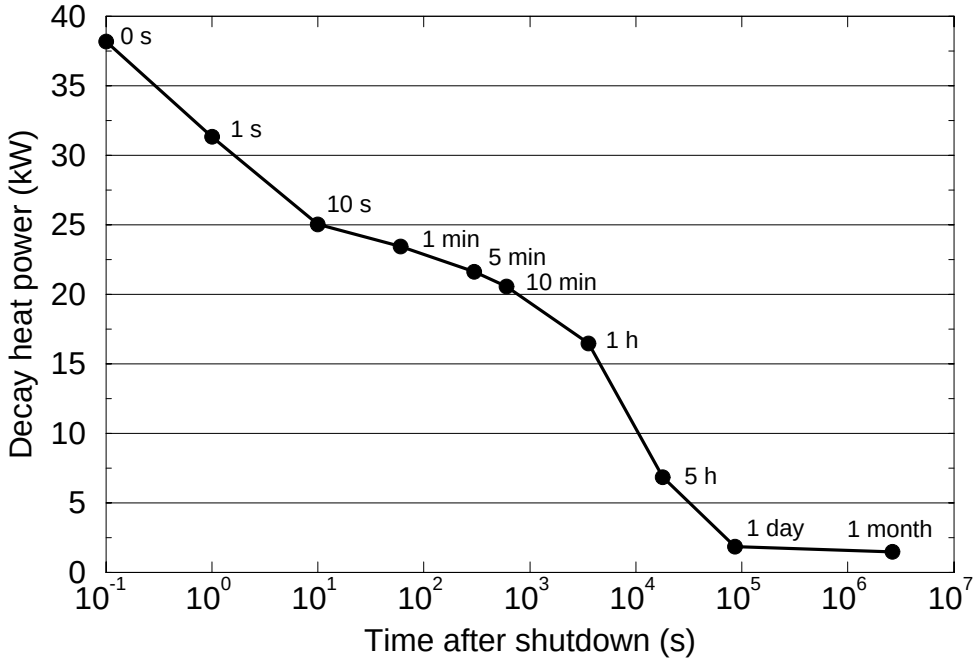

Figure 2.5: Decay heat power vs. time in HCPB TBM

Chapter 3

RELAP5/MOD3.1 Cooling System Model

The computer code RELAP5/MOD3.1 [5] has been developed for thermal-hydraulic transient simulation of light water reactor coolant systems. The code simulates the behaviour of the reactor coolant system during severe accidents like large and small break loss of coolant accidents, operational transients, loss of off-site power, loss of feed water, or loss of flow accidents. RELAP5 is a highly generic code that can be used for simulation of a wide variety of hydraulic and thermal transients in both nuclear and non-nuclear systems using a fluid that may be a mixture of steam, water, non-condensible gases, and a non-volatile solute (e.g. boron). In the present analysis, helium is the only component used as non-condensible gas with the other three components set to zero.

The hydrodynamic model is a one-dimensional, transient, non-homogeneous, non-equilibrium model for flow of a two-phase water mixture. The basic field equations consist of two-phase continuity equations, two-phase momentum equations, and two-phase energy equations. The system model is solved numerically using a semi-implicit or nearly implicit finite-difference technique, depending on the user's choice. So-called heat structures provided in RELAP5 permit calculation of the heat transferred across solid boundaries of hydrodynamic components, e.g. heat transfer across steam generator tubes or heat transfer from pipe and vessel walls. Heat structures are assumed to be represented by one-dimensional heat conduction in rectangular, cylindrical, or spherical geometry. Surface multipliers are used to convert the unit surface of the one-dimensional calculation to the actual surface of the heat structure. Temperature-dependent thermal conductivities and volumetric heat capacities are provided in tabular or functional form either from built-in or user-supplied data.

One out of two identical cooling loops of the HCPB TBM cooling system was modelled by RELAP5/MOD3.1 components. The model includes primary and secondary side pipework, helium circulator, heat exchanger, pressure control system, and temperature control system. It is based on the TBM cooling circuit layout described in [1]. The layout is based on the spatial arrangement of the TBM in ITER as shown in Fig. 3.1[1]. The nodalization scheme of the cooling loop as used for simulation of cyclic TBM operation and LOFAs is shown in Fig. 3.2. Detailed nodalization of the TBM is given in Fig. 3.3. The filled surfaces indicate RELAP5 heat structures. A description of the model components is provided below.

[1] In the meantime it has been decided to locate the heat transport system in the wedge-shaped room next to the cryostat which was formerly allocated to the tritium extraction system (TES).

Table 3.1:
Design parameters for different pipe components

Pipe number	Inside diam. (mm)	Outside diam. (mm)	Pipe length (m)	Average flow velocity (m/s)
1	148.3	168.3	10	15
3 (oc)	148.3	168.3	40	15
3 (ic)	98.3	114.3	10	33
6 (ic)	98.3	114.3	10	40
6 (oc)	148.3	168.3	40	18
9	148.3	168.3	40	18
11	70.0	82.5	10	–

Key: oc = outside cryostat, ic = inside cryostat.

3.1 Primary Side Piping

The primary side piping network of the model cooling loop consists of the following parts (the figures in brackets refer to the component numbers given in Fig. 3.2 on page 18):

Cold leg:

- Pipe from heat exchanger outlet to helium circulator (1).
- Pipe from helium circulator to TBM (3). This pipe is divided into a section outside the cryostat and a section inside the cryostat. Inside the cryostat the pipe diameter is smaller.

Hot leg:

- Pipe from TBM to dust filter (6). Similar to the cold leg, this pipe is divided into a small diameter section inside the cryostat and a large diameter section outside the cryostat.
- Pipe from dust filter to heat exchanger (9).

Bypass:

- Pipe from hot leg outlet to cold leg inlet (11).

In Table 3.1, the pipe inside and outside diameters, the pipe lengths, and the average flow velocities are displayed. The dust filter (8) was modelled as a single volume component with an inside diameter of 0.45 m and a length of 2.5 m, based on data given in [1]. The outside diameter was chosen as an equivalent diameter resulting from the given inside diameter and the total filter mass of 1324 kg to 0.54 m.

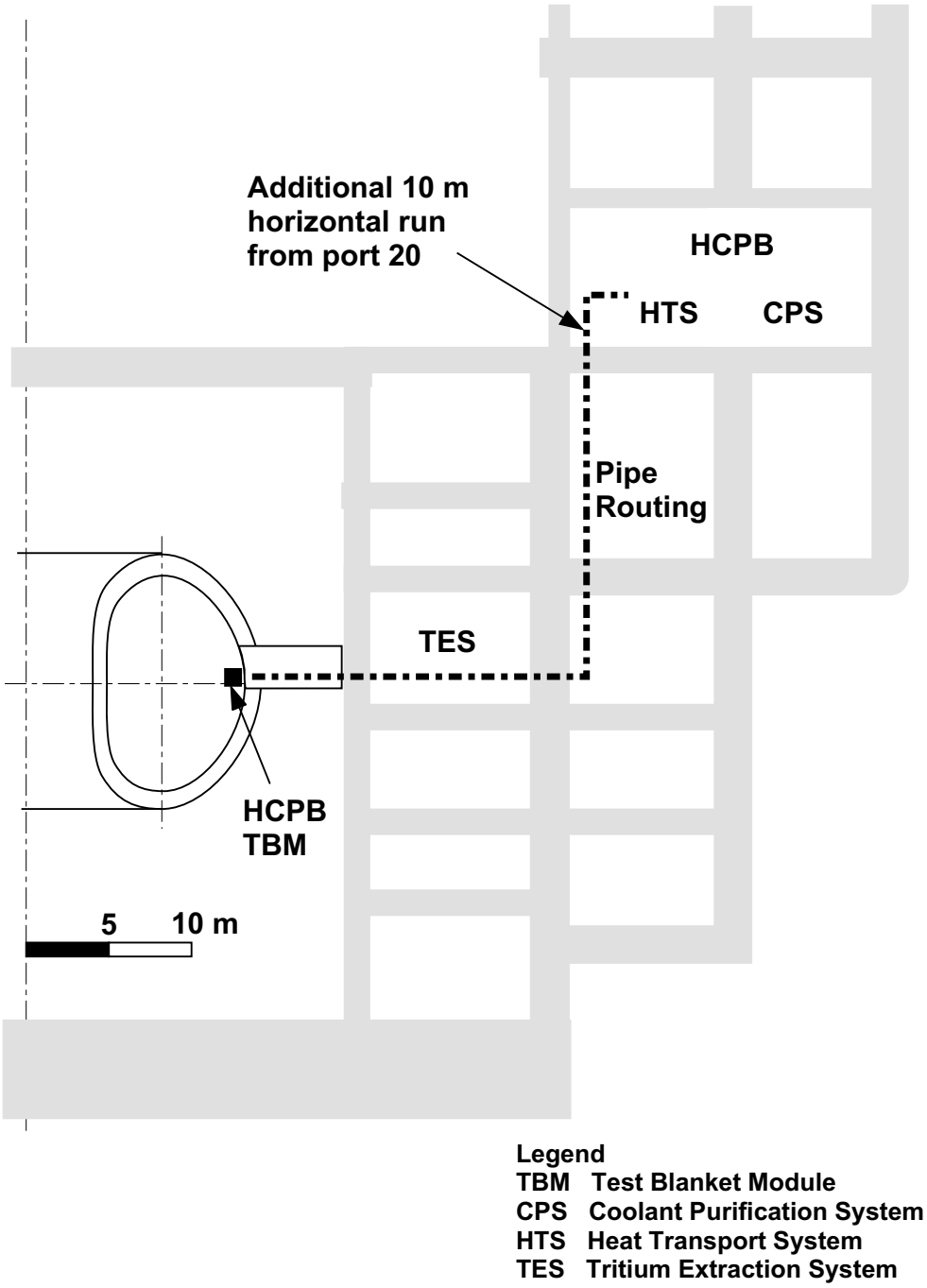

Figure 3.1: Location of the HCPB TBM in ITER and pipe routing (status of 7/96)

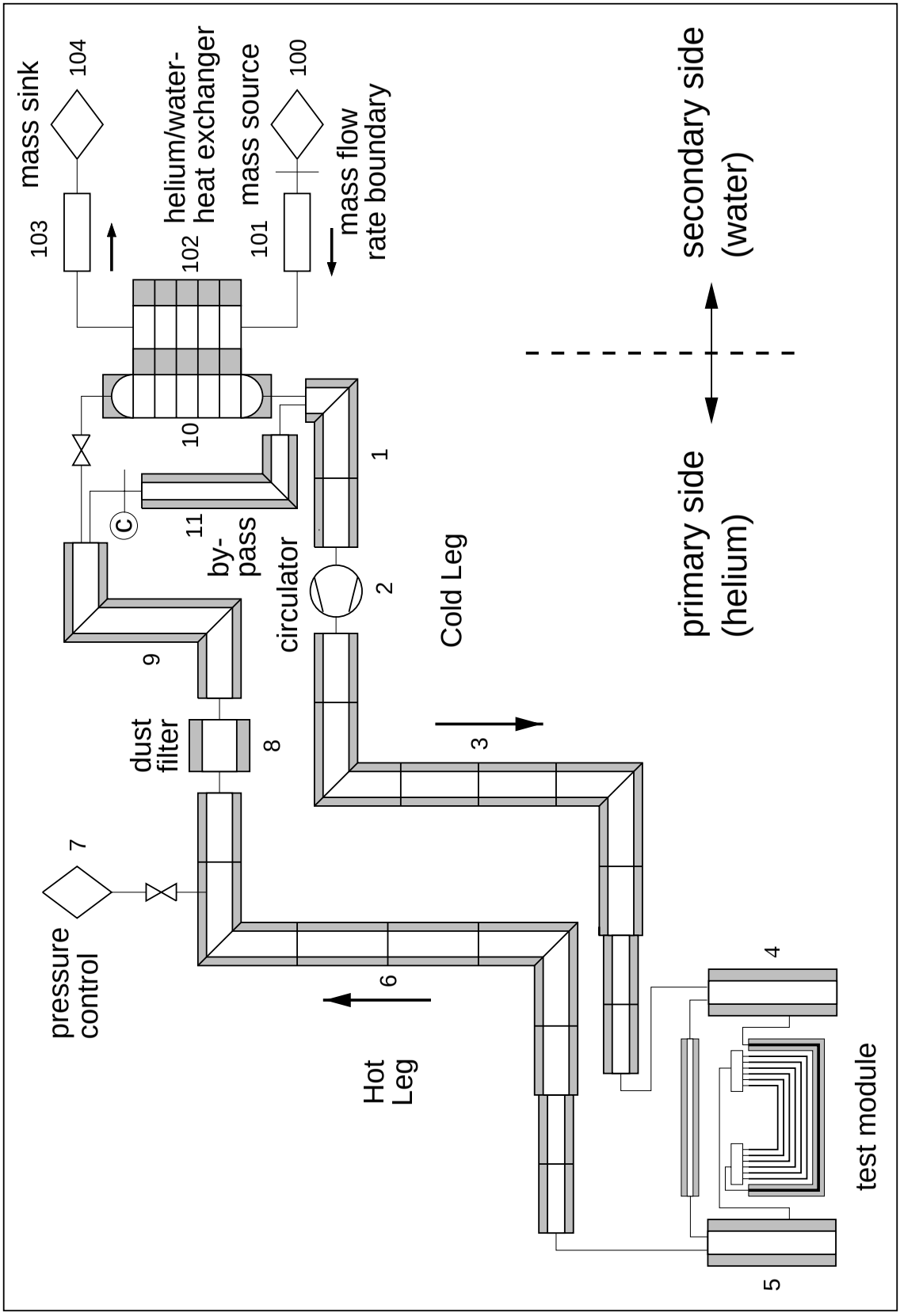

Figure 3.2: RELAP5/MOD3.1 nodalization of one cooling loop of the HCPB TBM cooling system.

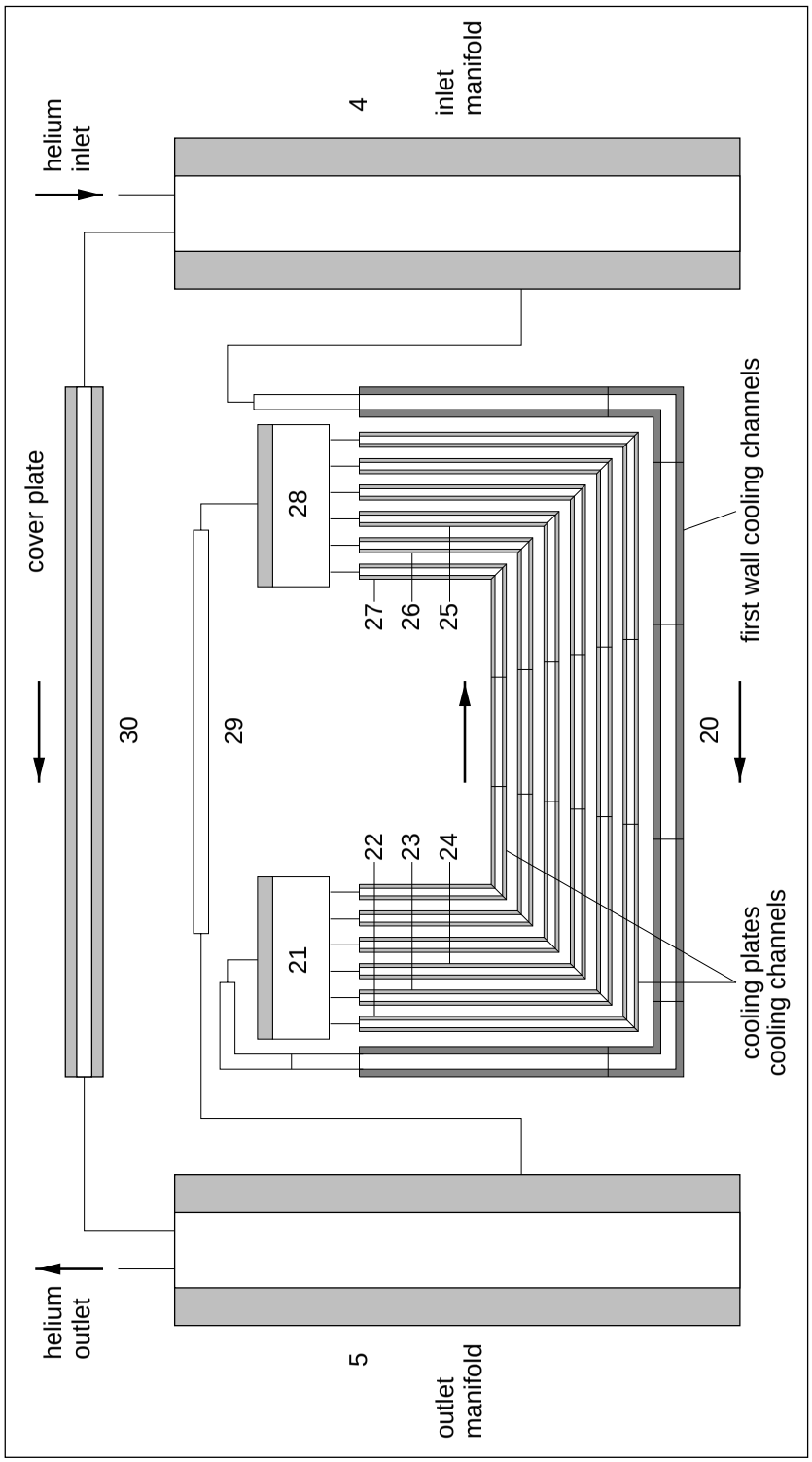

Figure 3.3: Detailed RELAP5/MOD3.1 nodalization of the HCPB TBM

The pipe walls of the cold leg piping, the hot leg piping, and of the bypass were considered in the RELAP5 model as cylindrical heat structures assigned to each pipe component. Austenitic stainless steel 316 L was assumed as pipe material.

Pressure losses

A surface roughness of $5 \cdot 10^{-5}$ m was assumed for all pipes and volume elements, which is a typical value for commercial pipes. In addition to the frictional pressure losses, losses due to bends, fittings, and abrupt area changes were considered. The number of bends and fittings in different loop sections were determined according to the cooling circuit layout given in [1]. The following numbers of bends and fittings at various loop sections were considered:

- Heat exchanger outlet to circulator: 3 bends
- Circulator to TBM: 13 bends
- TBM to dust filter: 13 bends
- Dust filter to heat exchanger: 3 bends, 1 valve

Energy loss coefficients (i.e. the pressure loss coefficient ζ in the flow resistance term $\zeta \frac{\rho}{2} v^2$) of 0.2 for one bend and 7.0 for one valve were applied [11]. For RELAP5 calculation of the pressure losses due to abrupt area changes the corresponding option was specified at the junctions connecting the model pipes.

The pressure loss in the dust filter is expected to be less than 0.03 MPa [1]. To achieve this pressure drop across the filter component (8), energy loss coefficients of 16.0 were applied at both the inlet and the outlet junction of the dust filter.

3.2 Test Module

One half of the test module, pertaining to one out of two cooling loops, was modelled by RELAP5 components. The whole test module is cooled by 34 FW cooling channels and 22 cooling plates. Therefore, 17 FW cooling channels and 11 cooling plates belong to one half of the test module. The modelling approach of the TBM cooling channels and structures is provided below.

3.2.1 Flow Channels

The hydrodynamic model of the TBM consists of the following parts (the numbers in brackets refer to the component numbers defined in Fig. 3.3 on page 19):

- Single volume (4) representing the inlet manifold.
- Pipe (20) representing the blanket box cooling channels and the connecting lines to the cooling plates distributors. Pipe (20) is divided into 10 volumes numbered in ascending order in flow direction. Volumes 1/2 and 8/9 represent the side walls of the blanket box, volumes 3 to 7 represent the FW, and volume 10 represents the connecting lines from the segment box to the cooling plates distributors. 17 blanket box cooling channels are lumped together in volumes 1 to 9, 11 connecting lines are lumped together in volume 10.
- Branch (21) representing the cooling plates distributors. 11 cooling plates distributors are lumped together in branch (21).

Table 3.2:
Division of cooling plates in six cooling zones (channel height = 4 mm).

Cooling zone	Radial extension in toroidal midplane (cm to FW)	Number of cooling channels	Channel width, side (mm)	Channel width, front (mm)
1	3.0 – 5.9	3	6.8	6.4
2	5.9 – 9.0	3	6.9	6.9
3	9.0 – 12.9	4	5.5	5.5
4	12.9 – 17.9	5	6.0	5.5
5	17.9 – 27.9	8	6.0	5.5
6A	27.9 – 36.3	8	6.0	5.5
6B	36.3 – 45.5	8	6.0	5.5
6C	45.5 – 56.8	8	6.0	5.5

- Pipes (22) to (27) representing the cooling plate channels. Each of the six pipes is divided into 5 volumes numbered in ascending order in flow direction. Each pipe simulates the flow in one out of 6 cooling zones of the breeding region. As indicated in Fig. 2.3 on page 6, the cooling zones are U-shaped with radially and toroidally running cooling channels. The first and the last volume of the pipes represent the radial flow path, whereas the middle volumes represent the toroidal flow path. The division of the breeding zone into six cooling zones of variable length follows the approach of the analyses carried out for the HCPB DEMO blanket [9]. The number of cooling channels pertaining to each cooling zone, the geometry of the cooling channels, and the radial extension of the cooling zones are summarised in Table 3.2. The flow channels of 11 cooling plates are lumped together in pipes (22) to (27).

- Branch (28) representing the cooling plates collectors. 11 cooling plates collectors are lumped together in branch (28).

- Single volume (29) representing the connecting lines from the cooling plates collectors to the outlet manifold.

- Single volume (5) representing the outlet manifold.

- Single volume (30) representing one cover plate. For the present analyses it was assumed, that each of the cover plates is cooled by one of the two cooling loops.

The main parameters of the hydrodynamic components of the TBM model are shown in Table 3.3 on page 38. The surface roughness specified in Table 3.3 is based on the values given in [9].

The dimensions, arrangement, and number of cooling channels in the cover plate have not yet been elaborated. However, from the overall dimensions of the cover plates (0.805 m radial depth x 1.198 m toroidal width x 0.05 m poloidal height per plate) and a steel fraction of 0.89 [12] the helium volume in one cover plate follows to 5304 cm^3. Assuming mainly toroidally running, parallel cooling channels with short radial supply lines, a mean

length of the cooling channels in the order of the toroidal width of the cover plates results. Thus, a length of 1.198 m and a volume of 5304 cm^3 were assigned to single volume (30).

Of the total mass flow rate of 1.85 kg/s in one cooling loop, 0.282 kg/s flow through the cover plate and 1.568 kg/s flow through the FW cooling channels and the cooling plate channels. To achieve the desired mass flow rate in the cover plate the helium flow was assumed to be throttled at the junction between the inlet manifold and the cover plate. This was accomplished by assigning a very small flow area of 2.5 cm^2 to this junction and by specifying the abrupt area change option for the junction. This causes a high pressure drop across the junction and yields the demanded mass flow rate division.

Pressure losses

The frictional pressure losses inside the TBM were calculated using the pipe lengths and surface roughnesses given in Table 3.3. The pressure losses due to bends and abrupt expansions and contractions were considered by energy loss coefficients (pressure loss coefficients) to junctions situated at locations causing pressure drops. The applied energy loss coefficients comply with the loss factors given in [9]. At the various TBM sections the following loss coefficients were applied:

- Connection between inlet manifold (4) and blanket box cooling channels (20): $\zeta = 0.10$.
- Blanket box cooling channels (20-1 to 20-9): 2 bends $\zeta = 2 \cdot 0.07$; blanket box outlet: $\zeta = 0.59$, inlet to connecting line to cooling plates distributors: $\zeta = 0.10$, connecting line (20-10): 1 bend $\zeta = 0.07$.
- Cooling plates distributors (21): Inlet $\zeta = 0.49$, outlets $\zeta = 0.25$.
- Cooling plate channels (22) - (26): 2 bends $\zeta = 2 \cdot 0.15$, cooling plate channels (27): 6 bends $\zeta = 6 \cdot 0.15$.
- Cooling plate collectors (28): Inlets $\zeta = 0.91$, outlet $\zeta = 0.10$.
- Connection between line from cooling plate collectors (29) and outlet manifold (5): $\zeta = 0.49$.

Orificing

Due to the strong decrease in heat generation in radial direction, the heat generated in the different cooling zones will vary considerably. To achieve equal outlet temperatures for all cooling zones, which is the current design target, the mass flow rates have to be adjusted for the different cooling zones. The flow rate in zone 1, with the highest power generation, has to be elevated, while the flow rates in the other zones have to be lowered, according to their power generation. Flow control can be accomplished by introduction of orifices at the inlets of the cooling plate channels.

In the RELAP5 loop model the orifices were simulated by input of energy loss coefficients of varying magnitude at the outlet junctions of branch (21), see Fig. 3.4 on page 23. The values of the energy loss coefficients needed to achieve equal temperatures at the channel outlets were determined by trial and error in steady-state RELAP5 runs. These values correspond to certain ratios of the channel flow areas to the orifice areas. For a sharp-edge orifice as shown in Fig. 3.5, the loss coefficient is defined as [13]:

$$\zeta = \left(\frac{A_1}{A_2 \cdot \psi} - 1 \right)^2$$

with

$$\psi = 0.63 + 0.37 \cdot \left(\frac{A_1}{A_2}\right)^3,$$

where A_1 is the channel flow area and A_2 is the orifice flow area. The pressure loss Δp across the orifice follows to:

$$\Delta p = \zeta \frac{\rho}{2} v^2,$$

where ρ is the fluid density and v is the fluid velocity in the flow channel with area A_1.

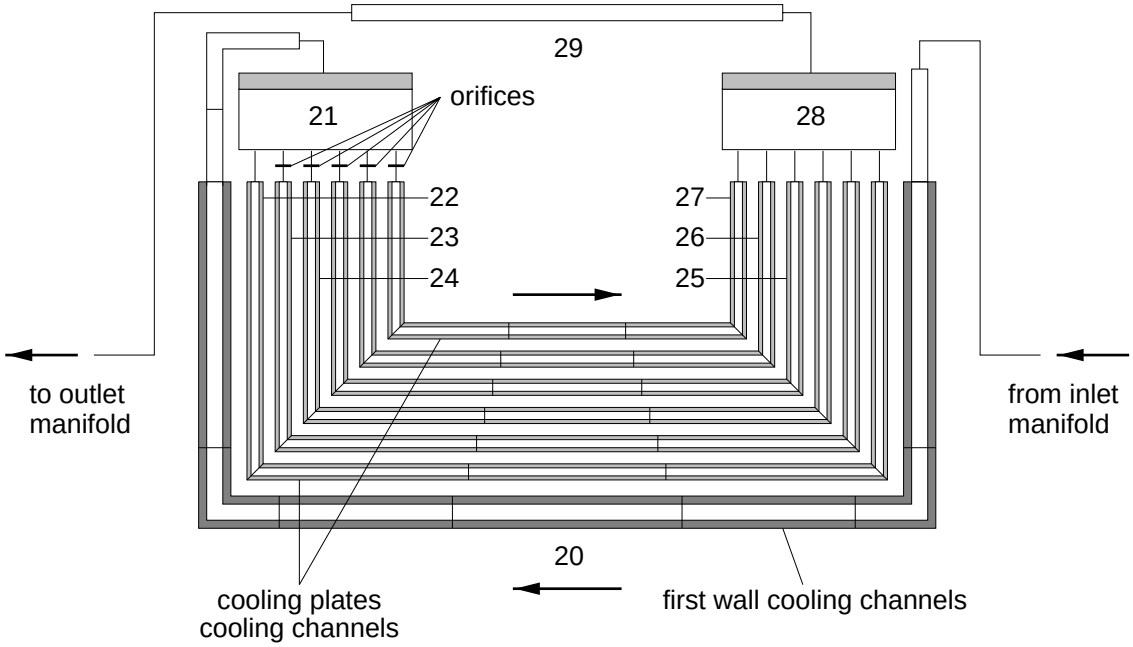

Figure 3.4: Location of orifices in TBM model

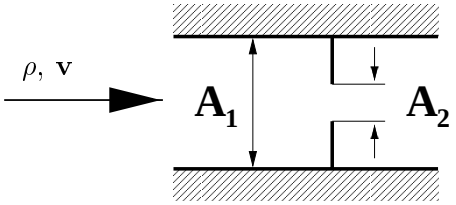

Figure 3.5: Sharp-edge orifice, ρ = fluid density, v = fluid velocity, A_1 = channel flow area, A_2 = orifice flow area.

The energy loss coefficients used in the RELAP5 model and the pertaining area ratios, channel areas, and orifice areas for the six zones are shown in Table 3.4 on page 39.

Note: The small orifice openings at the cooling channels in the rear part of the TBM are susceptible to plugging by possibly entrained particles in the helium stream. This

could lead to local overheating of the test module due to insufficient cooling.

3.2.2 Structure

The modelling capabilities of RELAP5 allow for only one-dimensional calculation of heat conduction in simple geometries like rectangular plates, cylindrical shells, or spherical shells. Hence, the complicated shape of the TBM was modelled by equivalent rectangular and cylindrical heat structures.

According to RELAP5 conventions each heat structure has two sides, denoted as left side and a right side, at which boundary conditions have to be specified by the user. If only one of the two boundaries communicates energy with a hydrodynamic volume, usually the left side of the heat structure is associated with the fluid volume. In this case, a convective boundary condition with heat transfer coefficients obtained from RELAP5/MOD3.1 Heat Transfer Package 1 or with user-supplied heat transfer coefficients is used at the left side and either an insulated boundary condition, a temperature boundary condition, or a heat flux boundary condition is used at the right side. When both boundaries communicate energy with different hydrodynamic volumes, convective boundary conditions are used at both the left and the right side of the heat structure.

Blanket box

The structure of the blanket box, of which the plasma facing part constitutes the FW, was modelled by rectangular heat structures in such a way that the heat flux in radial direction in the FW area was simulated properly. The thicknesses of the heat structures in radial direction and the total volumes of the heat structures are identical to the actual wall thicknesses and the actual volumes. Actual and modelled cross section of the FW are shown in Fig. 3.6. Heat structure 1 models the part of the FW between the plasma and the coolant. It consists of a 5 mm beryllium layer and a 5 mm MANET layer. At one side of the heat structure a convective boundary condition is used where the heat transfer coefficient is obtained from RELAP5/MOD3.1 Heat Transfer Package 1. The sink temperature is the temperature of the helium in the hydrodynamic volume of pipe (20) which is connected to the heat structure. At the other side of the heat structure the surface heat flux from the plasma is used as boundary condition. To account for the volumetric power generation, an internal heat source with a characteristic radial power distribution is applied to the heat structure.

Heat structure 2 in Fig. 3.6 models the remainder structure of the FW (that is, the 6 mm thick rear plate and the ribs between the cooling channels) and constitutes an enlarged 6 mm MANET layer. Similar to heat structure 1, a convective boundary condition is used at one side of the heat structure. At the other side of the structure an adiabatic boundary condition is used. This means, that the heat transfer between the blanket box and the breeding zone is neglected for the present analyses. An internal heat source is assigned to heat structure 2 to account for the volumetric power generation.

Near the cover plates the amount of structural material pertaining to one cooling channel is larger than in the rest of the blanket box. This is expressed by the total poloidal height of the FW, which is equal to 0.845 m, in comparison to the height of 0.816 m, which results from the number of cooling channels, 34, multiplied by the structure height of 24 mm apportioned to one cooling channel (see Fig. 3.6). Consideration of this additional structural material leads to the corrected heat structure heights of 24.85 mm and 40.84 mm in contrast to 24 mm and 38 mm for heat structures 1 and 2, respectively.

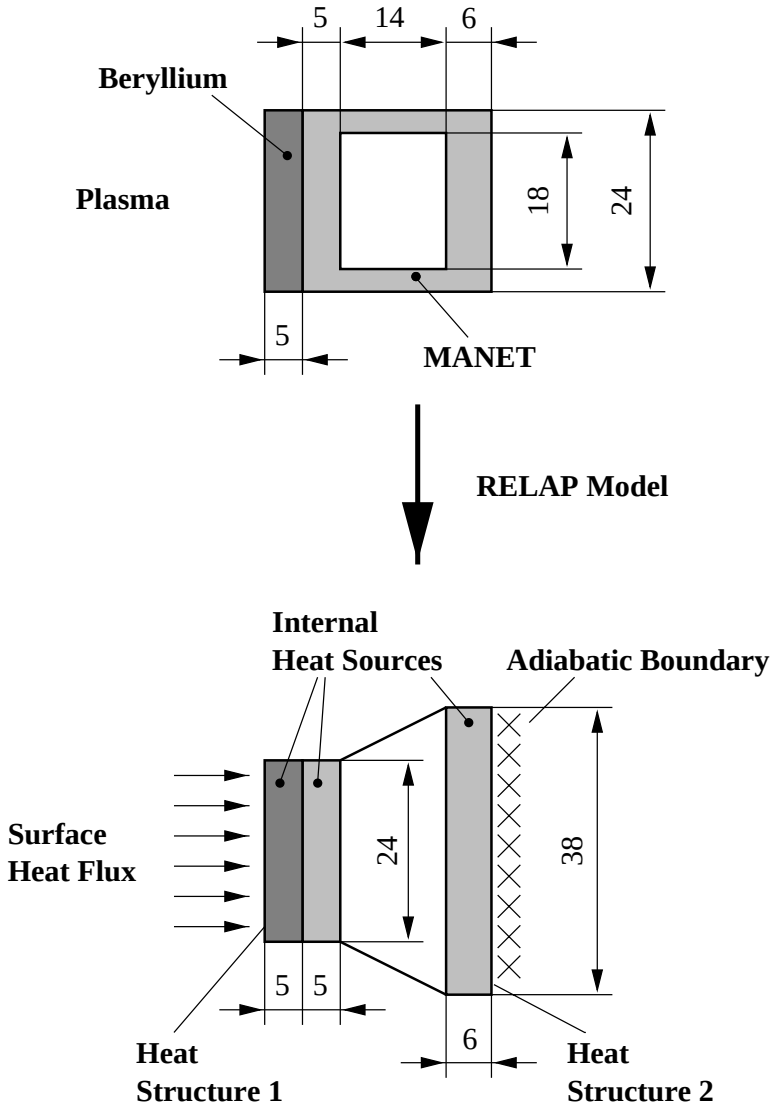

Figure 3.6: Modelling of first wall with RELAP5 heat structures (dimensions in mm). Top: real unit cell, bottom: modelled unit cell.

The heat transfer areas of the heat structures result from the corrected heat structure heights times 17 FW cooling channels for one cooling loop times the lengths of the heat structures. The lengths of the heat structures correspond to the lengths of volumes 2 to 8 of pipe (20). The heat structures assigned to volumes 2 and 8 represent the side walls of the blanket box, the structures assigned to volumes 3 and 7 represent the corners of the blanket box, and the structures assigned to volumes 4 to 6 represent the plasma facing part of the blanket box. With the volume lengths given in Table 3.3 heat transfer areas of 0.187 m^2, 0.070 m^2, and 0.130 m^2 result for volumes 2/8, 3/7, and 4/5/6, respectively. The corresponding heat transfer areas for heat structure 2 are equal to 0.308 m^2, 0.094 m^2, and 0.213 m^2, respectively.

The volumes of the heat structures are equal to the heat transfer areas times the heat structure thicknesses.

Breeding zone

The solid structure of the breeding zone including the cooling plates, the beryllium pebble beds, and the Li_4SiO_4 pebble beds, were modelled by rectangular heat structures. They were arranged such that the heat flux in poloidal direction was modelled. The thicknesses of the pebble beds in the RELAP5 model and the volumes of the heat structures are identical to their actual size. The thicknesses of the MANET layers in the RELAP5 model was computed such that the total MANET volume in the heat structure is equal to the actual MANET volume. Actual and modelled cross section of a part of the breeding zone are shown in Fig. 3.7. The breeding zone was modelled by two heat structures for each volume of pipes (22) to (27). The first heat structure models the part of the breeding zone from the middle of the Li_4SiO_4 pebble bed to the coolant. It consists of a MANET layer, the equivalent thickness of which varies with the cooling zone, and of a 5.5 mm Li_4SiO_4 bed layer. At one side of the heat structure (bottom side in Fig. 3.7, facing the coolant channel) a convective boundary condition is used. The sink temperature is the temperature of the helium in the pipe volume connected to that heat structure. At the other side of the heat structure (top side in Fig. 3.7) an adiabatic boundary condition is applied (assuming the boundary as a plane of symmetry). The second heat structure models the part of the breeding zone from the middle of the beryllium pebble bed to the coolant. It consists of a MANET layer of variable thickness and of a 22.5 mm beryllium bed layer. Equally to the first heat structure, a convective boundary condition is used at one side and an adiabatic boundary condition is used at the other side of the heat structure.

The heat transfer areas of the heat structures result from the widths of the cooling zones times the lengths of the heat structures times 11 cooling plates served by one cooling loop. The lengths of the heat structures correspond to the lengths of the volumes of pipes (22) to (27). The heat transfer areas of the breeding zone heat structures are compiled in Table 3.5 on page 39.

The volumes of the heat structures are equal to the heat transfer areas times the heat structure thicknesses.

Correction of heat transfer equivalent diameter

The described modelling approach for the blanket box and the breeding zone leads to similar wall thicknesses in the direction of the heat flux, and to similar volumes for the RELAP5 model and the actual structure. In contrast to that, the third important parameter for calculation of heat transfer phenomena, the heat transfer area , is different in the RELAP5 model geometry and in the actual geometry. This is a result of the one-

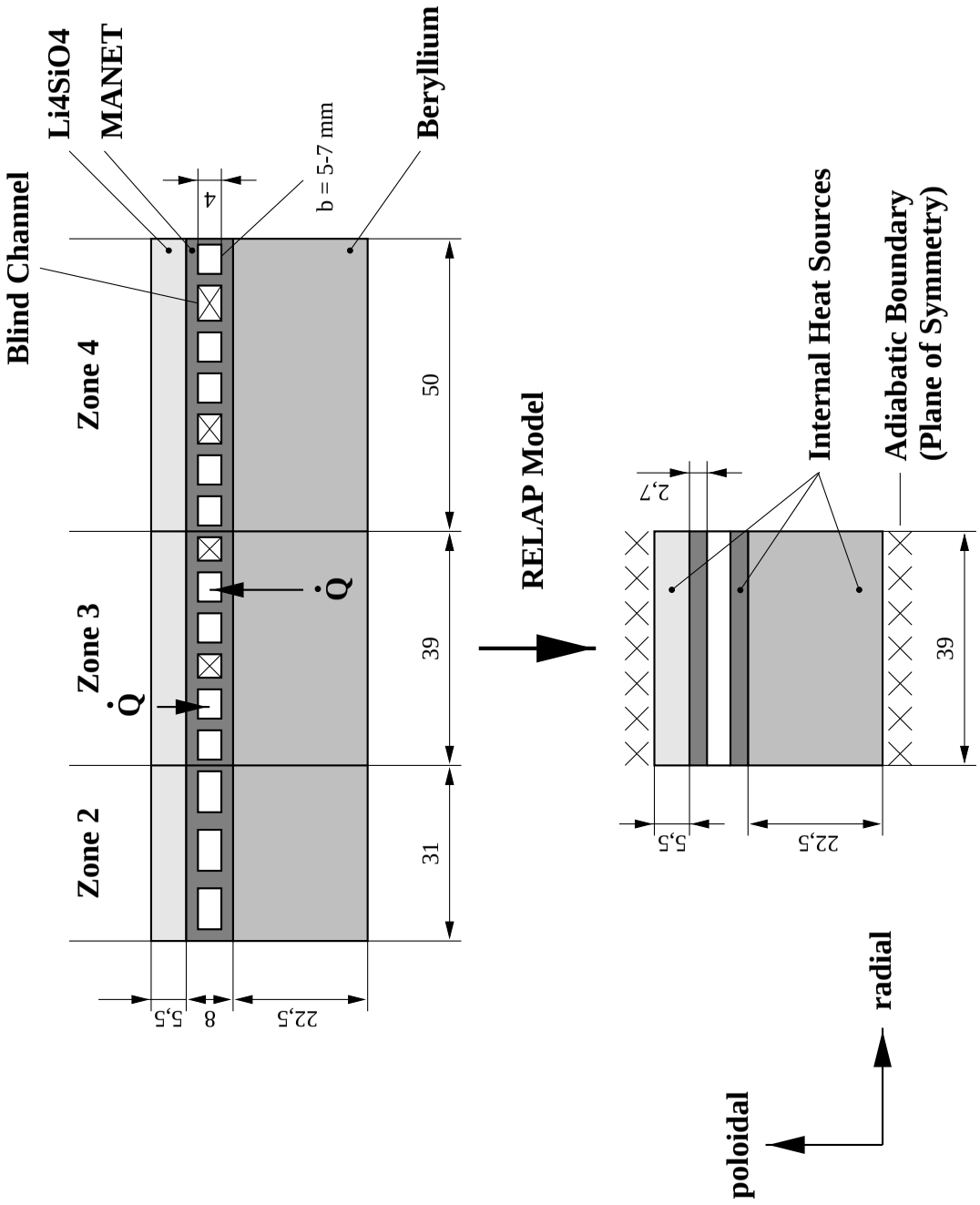

Figure 3.7: Modelling of breeding zone with RELAP5 heat structures (dimensions in mm).

dimensional modelling of a two-dimensional heat transfer problem. To compensate for the unreal heat transfer areas, the equivalent diameters of the heat structures, which are used by RELAP5 for computation of the heat transfer coefficients, was adjusted such that the correct heat transfer rates from the structures to the coolant result.

For single-phase forced convection RELAP5 calculates the heat transfer coefficient according to the Dittus-Boelter correlation [5]:

$$\alpha = 0.023 \frac{\lambda}{D_e} Re^{0.8} Pr^{0.4}$$

where the terms are:

α (W/m^{2}K)	=	heat transfer coefficient
λ (W/mK)	=	thermal conductivity of the fluid
D_e (m)	=	equivalent diameter
Re	=	Reynolds number $= v \cdot D_e/\nu$
		(v (m/s) = velocity, ν (m^2/s) = kinematic viscosity)
Pr	=	Prandtl number.

The heat transfer rate from the wall to the coolant is equal to:

$$\dot{Q} = \alpha A \Delta T$$

where

$\dot{Q}$ (W)	=	heat transfer rate
A (m^2)	=	heat transfer area
ΔT (K)	=	temperature difference between wall and coolant.

From the above correlations the following dependency of the heat transfer rate on the heat transfer area and on the equivalent diameter follows:

$$\dot{Q} \sim \frac{A}{D_e^{0.2}}.$$

To achieve identical heat transfer rates in the RELAP5 model (index mod) and in the real test module (index real), the following condition has to be fulfilled:

$$\dot{Q}_{mod} = \dot{Q}_{real} \quad \Rightarrow \quad \frac{A_{mod}}{D_{e,mod}^{0.2}} = \frac{A_{real}}{D_{e,real}^{0.2}}.$$

Hence, the equivalent diameter for the RELAP5 model heat structures follows to:

$$D_{e,mod} = \left(\frac{A_{mod}}{A_{real}}\right)^5 \cdot D_{e,real}.$$

For the blanket box cooling channels and the RELAP5 heat structures, the heat transfer area is equal to the wetted perimeter times the channel length and structure length, respectively. The following equivalent diameters for the heat structures result (compare Fig. 3.7):

- Heat structure 1: Model wetted perimeter (corrected) = 24.85 mm, real wetted perimeter = 18 mm, real equivalent diameter = 15.75 mm
  $\Rightarrow D_{e,mod} = (24.85/18)^5 \cdot 15.75$ mm = 78.83 mm.

- Heat structure 2: Model wetted perimeter (corrected) = 40.84 mm, real wetted perimeter = 46 mm, real equivalent diameter = 15.75 mm
  $\Rightarrow D_{e,mod} = (40.84/46)^5 \cdot 15.75$ mm = 8.70 mm.

The model's wetted perimeter of heat structure 1 is 38 % higher than the real wetted perimeter of the pertaining part of the cooling channel. Therefore, a considerably higher equivalent diameter has to be input for heat structure 1, compared to the real equivalent diameter. On the contrary, the model's wetted perimeter of heat structure 2 is 11 % smaller than the real wetted perimeter, which demands the input of a smaller equivalent diameter.

For the cooling plate channels in the six cooling zones the heat transfer area is equal to the total wetted perimeter of the cooling channels in the respective zone times the channel length. For the RELAP5 heat structures, the heat transfer area is equal to the width of the respective cooling zone times the structure length, which is equal to the real channel length. Thus, for one heat structure, the ratio of the model heat transfer area to the real heat transfer area is equal to the zone width divided by the half of the total perimeter of the cooling channels in the considered cooling zone. The resulting equivalent diameters for the breeding zone heat structures are compiled in Table 3.6 on page 40 (for geometry of cooling channels and heat structures see Tables 3.2 and 3.5, respectively).

In the rear part of the breeding zone the ratio between the model heat transfer area and the real heat transfer area is larger than in the front part because of the increasing number of blind channels in the cooling plates (see Fig. 3.7). The blind channels were introduced into the blanket design to provide for lower helium throughputs in the blanket sections with low heat generation.

Steel plate at the back of the breeding zone

The breeding zone is closed by a 4 cm MANET steel plate with a toroidal width of 115.2 cm and a poloidal height of 84.5 cm. The cooling plates distributors and collectors are integrated into the steel plate. With an assumed steel fraction of 50 % the total volume of the steel plate follows to 19469 cm^3. In the RELAP5 model the structure of the steel plate was considered by two cylindrical heat structures assigned to volumes (21) and (28) with structure lengths of 6.028 m (11 distributors/collectors x 0.548 m) and inside/outside diameters of 18/36.8 mm. According to the symmetry of the RELAP5 model, the heat structures make up one half of the steel plate structure.

Manifold region

The blanket box is closed by a 23 cm MANET steel block housing the main coolant feed lines and exhaust lines. The average toroidal width of the steel block is equal to 118 cm at a poloidal height of 84.5 cm. The total steel volume of the block equals 0.1614 m^3, which is equivalent to a steel fraction of 70.4 %. In the RELAP5 model the structure of the steel block was considered by two cylindrical heat structures assigned to volumes (4) and (5) with structure lengths of 0.845 m and inside/outside diameters of 160/294 mm. According to the symmetry of the RELAP5 model, the heat structures make up one half of the steel block structure.

Cover plate

Each of the two MANET cover plates has a steel volume of 0.0429 m^3. In the RELAP5 model the structure of one cover plate was modelled by a cylindrical heat structure assigned to volume (30). The inside diameters of the cover plate channels were estimated on basis of a helium flow velocity of 55 m/s, which is similar to the flow velocity in the FW cooling

channels. With a mass flow rate of 0.282 kg/s per cover plate and an average helium density of 6.8 kg/m^3 the equivalent inside diameters of the cooling channels follow to 31 mm. With a helium volume of 0.0053 m^3 per cover plate the total length of all cooling channels follows to 7.03 m. This length was adopted for the model heat structure. The inside/outside diameters of the heat structure follow to 31/93.4 mm.

To simplify the modelling of the cover plate, the mass of the 5 mm beryllium coating on the plasma facing part of the cover plate was neglected for the present analyses. Since it is very small compared to the bulk of the cover plate, this seems to be justified.

3.2.3 Power Generation

Blanket box

The nominal power load on the blanket box consists of surface heating and volumetric heating. With a surface heat flux of 50 W/cm^2 and a projection area of 112.8 cm x 42.25 cm for one half of the FW towards the plasma, the surface heating per cooling loop amounts to 238.29 kW. In the RELAP5 model the surface heat flux of 50 W/cm^2 was applied as boundary condition at the heat structures of pipe volumes 20-4/5/6 (heat structure 1). At pipe volumes 20-3 and 20-7, representing the corners of the blanket box, a surface heat flux of 0.663 x 50 W/cm^2 = 33.15 W/cm^2 was applied. The factor 0.663 originates from the conversion of the oblique corner areas with curvature angles of 86.25° relative to the front surface.

The internal heat sources of the two different heat structures of the model pipe (20) were deduced from the power density values given in Table 2.1. At the corners of the blanket box (i.e. structures of pipe volumes 20-3 and 20-7), again, a factor of 0.663 was applied to obtain the corner power densities from the power densities in the front part of the blanket box. The MANET power densities for heat structure 1 of pipe volumes 20-2/8, 20-3/7, and 20-4/5/6 follow to 1.99 W/cm^3, 6.34 W/cm^3, and 9.57 W/cm^3, respectively. The corresponding values for heat structure 2 follow to 1.99 W/cm^3, 5.85 W/cm^3, and 8.82 W/cm^3, respectively.

With the geometry of the heat structures described above, MANET power values of 1.86 kW/3.67 kW, 2.22 kW/3.30 kW, and 6.21 kW/11.29 kW, respectively, result for heat structures 1/2 of pipe volumes 20-2/8, 20-3/7, and 20-4/5/6.

The beryllium layer power densities for heat structure 1 of pipe volumes 20-3/7 and 20-4/5/6 are equal to 0.663 x 7.60 W/cm^3 = 5.04 W/cm^3 and 7.60 W/cm^3, respectively. The resulting beryllium power values of pipe volumes 20-3/7 and 20-4/5/6 are equal to 1.76 kW and 4.93 kW, respectively.

The total volumetric power in heat structure 1 of pipe (20), including the beryllium layer, amounts to 45.12 kW. In heat structure 2, a total power of 47.82 kW is generated.

The history of the decay heat power in the blanket box MANET was calculated according to the DEMO MANET ratios of the decay heat power density to the nominal power density in the torus equatorial plane and at the radius of 0.5 cm to the FW for heat structure 1, and at the radius of 2.1 cm to the FW for heat structure 2 (see Table 2.3). The resulting decay heat power values are compiled in Table 3.7 on page 40.

Since decay heat values for irradiated pure beryllium were not available, the history of the decay heat power in the blanket box beryllium coating was calculated according to the DEMO beryllium pebble bed ratios of the decay heat power density to the nominal power density at the radius of 5.9 cm to the FW (see Table 2.4). The resulting decay heat power values, which refer to heat structure 1, are given in Table 3.8 on page 41.

Breeding zone

For the determination of the power generation in the six cooling zones of the TBM breeding zone the local power densities given in Table 2.1 were converted into mean power densities for the six cooling zones. This was accomplished by considering the extension of the TBM in radial direction, the different cross section areas of the cooling channels, and the different number of blind channels in the six cooling zones. The calculated power densities for the three blanket components, MANET, beryllium, and Li_4SiO_4, and the distribution of the power densities on the model pipe components are shown in Table 3.9 on page 41. The resulting internal heat sources in the heat structures pertaining to model pipes (22) to (27) are compiled in Table 3.10.

The history of decay heat power generation in the breeding zone was estimated on basis of the local ratios of the decay heat power density to the nominal power density in the torus equatorial plane calculated for the HCPB DEMO blanket. The total decay heat values for the heat structures of the model pipes are shown in Tables 3.11 and 3.12 beginning on page 43. As mentioned above, beryllium and Li_4SiO_4 contribute significantly to the decay heat power only in the first minute after shutdown. Afterwards, the power generation is dominated solely by the cooling plates' material MANET.

Steel plate at the back of the breeding zone

The nominal power density in the steel plate closing the breeding zone is equal to 0.351 W/cm^3 (see Table 2.1), yielding a volumetric power of 3.42 kW per cooling loop. Consequently, the internal heat sources of the heat structures pertaining to volumes (21) and (28) were set equal to 1.71 kW.

The decay heat power was calculated according to the DEMO MANET ratios of the decay heat power density to the nominal power density at the radius of 61 cm to the FW in the torus equatorial plane (see Table 2.3). The power values at times of 0 s, 1 s, 10 s, 1 min, 5 min, 10 min, 1 h, 5 h, and 1 day are equal to 112.8 W, 112.8 W, 112.6 W, 111.2 W, 107.0 W, 103.6 W, 83.2 W, 34.0 W, and 8.4 W, respectively. The power values were distributed equally onto the heat structures of volumes (21) and (28).

Manifold region

The nominal power density in the manifold region is 0.17 W/cm^3 (see Table 2.1 on page 7), yielding a volumetric power of 13.72 kW per cooling loop. Consequently, the internal heat sources of the heat structures pertaining to volumes (4) and (5) were set equal to 6.86 kW.

The decay heat power was calculated according to the ratios of the decay heat power density to the nominal power density at the radius of 100 cm to the FW in the torus equatorial plane (see Table 2.3). The power values at times of 0 s, 1 s, 10 s, 1 min, 5 min, 10 min, 1 h, 5 h, and 1 day are equal to 481.6 W, 480.2 W, 478.8 W, 474.8 W, 458.2 W, 443.2 W, 355.4 W, 144.0 W, and 33.4 W, respectively. The power values were distributed equally on the heat structures of volumes (4) and (5).

Cover plate

The nominal power load on the cover plate consists of surface heating and volumetric heating. With a surface heat flux of 50 W/cm^2 and a projection area of 112.8 cm x 10 cm per plate towards the plasma the surface heating amounts to 56.4 kW. The volumetric heat sources in the upper and lower cover plate are equal to 107.0 kW and 96.3 kW, respectively [7]. The surface power and the mean volumetric power per cover plate of 101.65 kW were added together for input as single internal heat source of 158.08 kW for

the heat structure pertaining to volume (30).

The history of decay heat power generation in the cover plate was estimated on basis of the DEMO MANET ratios of the decay heat power density to the nominal power density at the radius of 38.9 cm to the FW in the torus equatorial plane (see Table 2.3). The chosen interval marks approximately the middle of the cover plate in radial direction. The decay heat power generation in the beryllium coating on the plasma facing part of the cover plate was neglected for the present analyses. The volumetric heating at times of 0 s, 1 s, 10 s, 1 min, 5 min, 10 min, 1 h, 5 h, and 1 day follows to 3.82 kW, 3.81 kW, 3.80 kW, 3.75 kW, 3.61 kW, 3.49 kW, 2.81 kW, 1.15 kW, and 0.29 kW, respectively.

3.3 Circulator

The helium circulator is identified by pump component (2) in Fig. 3.2 on page 18. The hydrodynamic model consists of one volume and two associated junctions (suction junction and discharge junction). Interaction of the circulator and the fluid is described by characteristic curves relating the circulator head and torque to the volumetric flow and angular velocity. Characteristic curves for the type of helium circulator planned for the TBM cooling loops are not yet available. Instead, the characteristic curves of the helium circulators developed for the German Thorium High Temperature Reactor (THTR-300) were used for modelling the TBM circulators [14]. The pressure head vs. volumetric flow curve and the pumping power vs. volumetric flow curve for this type of circulator at a speed of 5250 rev/min are shown in Fig. 3.8. The curves are extrapolated in the ranges from 0 to 7 m^3/s and from 18 to 20 m^3/s. The rated data for the THTR-300 circulator are:

Rated flow rate: 14.0 m^3/s
Rated head: 11000 mm water column
Rated power: 1780 kW.
Rated speed: 5440 rev/min.

The nominal pressure at the suction junction is 3.82 MPa, the nominal inlet temperature is 250 °C. The characteristic curves for speeds other than 5250 rev/min are congruent to those shown in Fig. 3.8. They can be computed by the following similarities:

$$\Delta p \sim N^2, \qquad P \sim N^3, \qquad Q \sim N$$

where Δp represents the pressure head, P is the power, Q is the volumetric flow rate, and N is the speed. For example, a decrease in speed from 5250 rev/min to 4200 rev/min shifts the operating point at $Q = 13$ m^3/s, $\Delta p = 10450$ mm water column, $P = 1610$ kW to the operating point $Q = 0.8 \cdot 13 = 10.4$ m^3/s, $\Delta p = 0.8^2 \cdot 10450 = 6688$ mm water column, $P = 0.8^3 \cdot 1610 = 824$ kW. At both points, the proportions $\Delta p/N^2$, P/N^3, and Q/N are equal. Therefore, the knowledge of the dependence of $\Delta p/N^2$ on Q/N and P/N^3 on Q/N is sufficient to characterise the circulator performance in the whole range of operation, provided the laws of similarity are valid.

RELAP5 demands the input of the above dependencies in a special dimensionless form. This is accomplished in two steps. First, all data are made dimensionless by using the rated head, H_R, flow, Q_R, speed, N_R, and torque, M_R, to form the corresponding dimensionless parameters $h = \Delta p/\Delta p_R = H/H_R$, $v = Q/Q_R$, $\alpha = N/N_R$, and $\beta = P/P_R \cdot N_R/N = M/M_R$, respectively. The torque ratio β results from the relation $P = M\omega = M2\pi N$, where M is the torque and ω is the angular velocity. (From this relation, the similarity

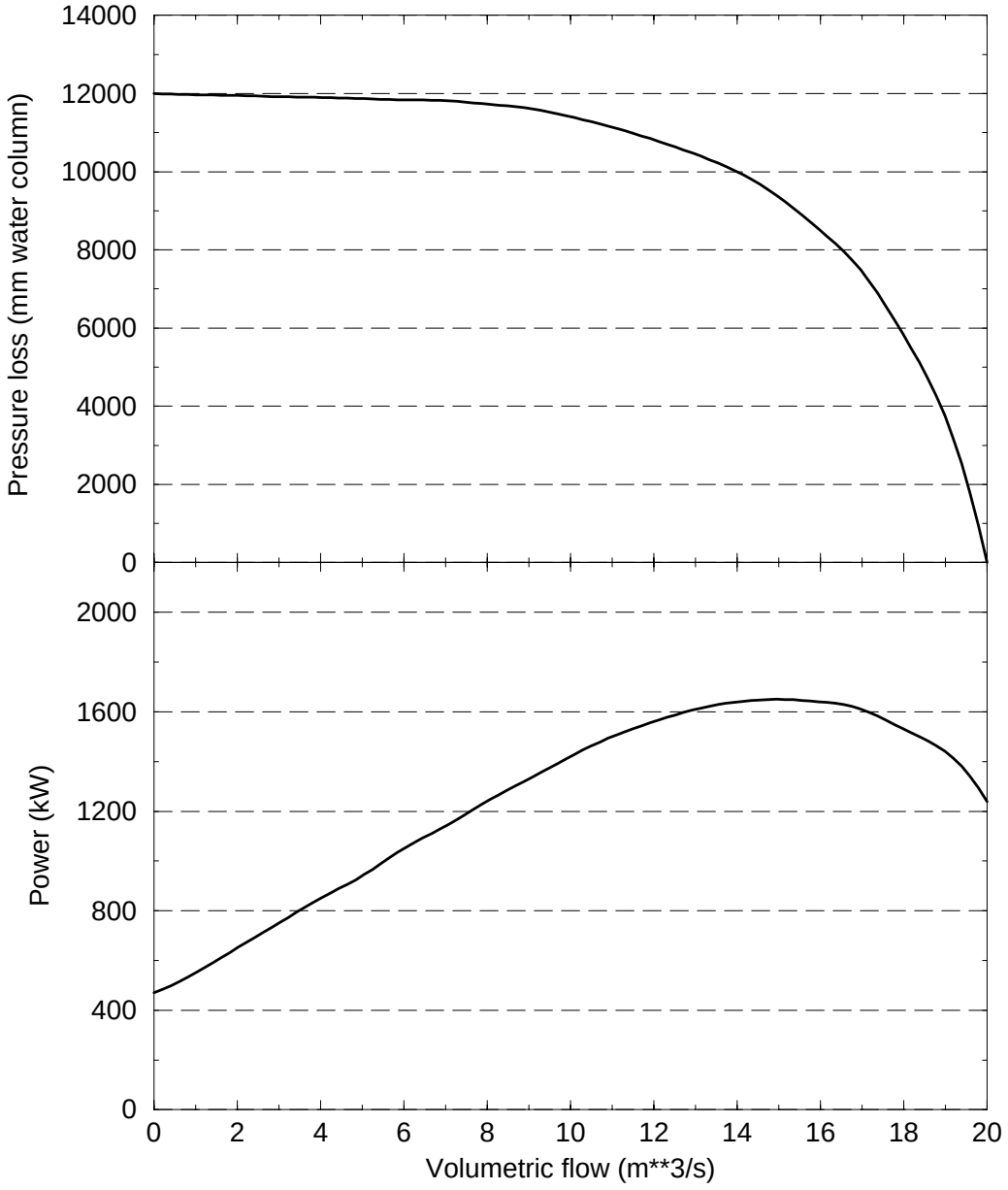

Figure 3.8: Characteristic curves of the helium circulator designed for the German THTR-300 Reactor (speed N = 5250 rev/min). Curves are extrapolated for volumetric flows of $< 7\ m^3/s$ and $> 18\ m^3/s$.

$M \sim N^2$ follows). Second, the so-called homologous parameters h/α^2 and β/α^2 are plotted as functions of v/α; and h/v^2 and β/v^2 are plotted as functions of α/v. The different curve types correspond to different octants in the circulator performance diagram. The choice is made such that the values v/α and α/v are bounded, i.e. lie in an interval between ± 1.0.

The above procedure applied to the curves in Fig. 3.8 delivers the data shown in Table 3.13 on page 45. These data and the rated operating values of the TBM circulator were used to simulate the circulator performance. A rated speed of $N_R = 6000$ rev/min was assumed for the TBM circulator, which is similar to the rated speed of the THTR-300 circulator. This speed is equivalent to an angular velocity of $\omega_R = 628.3$ rad/s. With an anticipated pressure drop of $\Delta p = 0.27$ MPa in the cooling loop [1] and an average helium pressure of 8 MPa in the circuit, the pressure at the circulator inlet results to $p_i = 8$ MPa – 0.27 MPa/2 = 7.865 MPa. Taking into account the helium temperature rise of approx. 10 K across the circulator, the helium inlet temperature will be approx. 240 °C, yielding the desired helium temperature of 250 °C at the TBM inlet. The corresponding density at the circulator inlet follows to $\rho_i = 7.38$ kg/m^3. With a nominal throughput of $\dot{m}_R = 1.85$ kg/s in one cooling loop and a total circulator efficiency of $\eta = 0.75$ the following rated values result for the TBM circulator (g represents the gravitational acceleration):

Rated flow rate: $Q_R = \dot{m}_R/\rho_i = 0.25$ m^3/s
Rated head: $H_R = \Delta p/(\rho_i g) = 3730$ m
Rated power: $P_R = Q_R \Delta p/\eta = 90$ kW
Rated torque: $M_R = P_R/\omega_R = 143.2$ Nm.

The total moment of inertia of the circulator, which is responsible for the coast-down behaviour of the circulator in case of a loss of electrical power, was found by determining the time $T_{1/2}$ during which the circulator slows down to half speed. Transient RELAP5 runs delivered moments of inertia of 0.55 kgm^2 and 1.50 kgm^2 for time constants of 2 s and 6 s, respectively.

For the circulator component (2) a length of 1.8 m and a volume of 0.025 m^3 was estimated. The stainless steel structure of the circulator, for which a volume of 0.0286 m^3 has been assessed, was modelled by a cylindrical heat structure of 0.25 m length with inside/outside diameters of 0.45/0.59 m.

3.4 Heat Exchanger

The helium/water heat exchanger (HX) was modelled as a counterflow heat exchanger employing straight tubes. The primary helium flows downward inside the tubes and the secondary water flows upward outside the tubes. The helium flow path is represented by pipe component (10) on the primary side and the water flow path by pipe component (102) on the secondary side (see Fig. 3.2 on page 18). Primary and secondary side are connected via two-sided RELAP5 heat structures. As structural material INCOLOY 800 was assumed for the tube walls and stainless steel 316 L for the remainder of the HX.

Primary side

The nominal inlet/outlet temperatures of the helium are 350/250 °C at a mass flow rate of 1.85 kg/s. The HX consists of two end domes with inside diameters of 0.31 m and of 96 straight tubes with lengths of 1.2 m and inside/outside diameters of 14/18 mm. The overall height of the HX is 2.2 m.

Pipe component (10) is divided into 7 volumes. Volumes 1 and 7 represent the end

domes with flow areas of 0.0755 m^2 and lengths of 0.5 m, volumes 2 to 6 represent the 96 tubes lumped together to single volumes with flow areas of 0.01478 m^2 and lengths of 0.24 m. The hydraulic diameter of the volumes was set to the real tubes inside diameter of 14 mm.

Only frictional pressure losses were considered inside the HX. A surface roughness of $5 \cdot 10^{-5}$ m was applied to the HX tubes.

The solid structure of 1 m of the HX shell, of the tube plate, the flanges, and the end caps, making up a volume of 0.041 m^3, was lumped together to give two equivalent cylindrical heat structures for volumes 10-1 and 10-7 with lengths of 0.5 m and inside/outside diameters of 0.31/0.385 m.

The HX tube walls were modelled by two-sided cylindrical heat structures, with primary side pipe (10) connected to the left side and secondary side pipe (102) connected to the right side of the heat structures. At both sides convective boundary conditions, where the heat transfer coefficient is obtained from RELAP5/MOD3.1 Heat Transfer Package 1, were used. The heated equivalent diameter, which is used for computation of the heat transfer coefficient, was set to 14 mm at the left boundary and to 18 mm at the right boundary. The structure of the 96 HX tubes was lumped together to 5 cylindrical heat structures for volumes 10-2 to 10-6 with lengths of 23.04 m ($96 \cdot 1.2\ m/5$) and inside/outside diameters of 14/18 mm.

Secondary side

The nominal inlet/outlet temperatures of the cooling water are 35/75 °C at a mass flow rate of 6.9 kg/s. The water pressure is 1 MPa.

Pipe component (102) is divided into 5 volumes with flow areas of 0.0328 m^2 and lengths of 0.24 m. The flow areas result from the cross sectional area of the HX tube bundle, which has a diameter of 0.27 m, minus the area occupied by the 96 tubes.

For computation of frictional pressure losses a surface roughness of $5 \cdot 10^{-5}$ m was applied. The hydraulic diameter of the volumes was set to the real tube outside diameter of 18 mm.

The solid structure of 1.2 m of the HX shell, which has a volume of 0.0249 m^3, was modelled by 5 cylindrical heat structures for volumes 102-1 to 102-5 with lengths of 0.24 m and inside/outside diameters of 0.31/0.35 m.

3.5 Pressure Control System

The helium pressure control system consists mainly of dump tanks for accommodation of the helium in case of loop overpressurization, and of a buffer tank to feed helium into the loop in case the loop pressure gets too low. The control system was modelled with a time dependent volume (7) and a valve junction connecting the time dependent volume with the hot leg. The time dependent volume is filled with helium at the conditions prevailing in the junction volume (6-9) at steady state conditions, i.e. 7.91 MPa, 350 °C. It represents an infinitely large reservoir and thus serves as a constant boundary condition. Any deviation from the nominal pressure in volume (6-9) leads to an inflow from volume (7) into the loop or reverse.

The valve junction can be opened or closed by user defined instructions, thereby the pressure control can be switched on or off.

The above simplified pressure control was used for steady state runs and accidents other than LOCAs. During these runs, the valve position was always open.

For LOCA runs, the time dependent volume (7) was substituted by a single volume representing the buffer tank. This was accomplished at restart of the problem from steady state. The buffer tank has a volume of 0.26 m^3 and a length of 1.3 m. It contains helium at 14 MPa and 50 °C.

3.6 Temperature Control System

To keep the helium temperature at the TBM inlet at a constant value of 250 °C during normal operation, i.e. during an ITER cycle with 50 s power ramp-up, 1000 s burn, 100 s power ramp-down, and 1050 s dwell time, a temperature control system is envisaged for the helium cooling system. The control system will be realised by partition of the helium flow to the HX and a bypass to the HX, while the helium circulator operates at nominal speed. If the TBM inlet temperature falls below 250 °C, a certain amount of the helium will be diverted from the HX to the bypass until the reference value is reached. During the ITER burn times, practically all of the helium will flow through the HX.

RELAP5 provides the possibility of simulating control systems. The control system capability consists of several types of control components, each type of component defining a control variable as a specific function of time-dependent quantities. They include quantities of hydrodynamic volumes, junctions, heat structures, and other specialised components. The control components perform algebraic operations such as addition, subtraction, multiplication, division, exponentiation, and others. Complex expressions can be developed by combination of different control components. A simple example would be the computation of differential pressures of hydrodynamic volumes as auxiliary output quantities for plot requests.

The TBM temperature control system was simulated by a heat exchanger bypass (pipe (11) in Fig. 3.2 on page 18), a time dependent junction located between the hot leg outlet and the bypass inlet (indicated by (C) in Fig. 3.2), and several control variables. The bypass mass flow rate was determined by an enthalpy balance at the HX outlet, where the helium from the bypass and the HX merge. A schematic of this node is shown in Fig. 3.9. The enthalpy balance reads:

$$\dot{m}_{11}\, c_p\, \vartheta_{11} + \dot{m}_{10}\, c_p\, \vartheta_{10} = \dot{m}_1\, c_p\, \vartheta_1.$$

With the mass balance,

$$\dot{m}_{11} + \dot{m}_{10} = \dot{m}_1,$$

and a constant value of 240 °C for the controlled variable ϑ_1 (accounting for a steady state temperature increase across the circulator of approx. 10 °C), the mass flow rate in the bypass follows to:

$$\dot{m}_{11} = \left(\frac{240\,°C - \vartheta_{10}}{\vartheta_{11} - \vartheta_{10}} \right) \cdot \dot{m}_1.$$

The above expression was evaluated in RELAP by 5 control variables: one for the numerator, one for the denominator, one for the fraction, one for calculation of $\dot{m}_1$, and one for the product of the fraction and $\dot{m}_1$. To eliminate the influence of oscillations in the mass flow rate at the cold leg inlet, the mass flow rate $\dot{m}_1$, which represents the total mass flow rate in the loop, was calculated as mean value of the mass flow rates at four different locations in the loop, namely, cold leg inlet (1-1), cold leg outlet (3-10), hot leg inlet (6-1), and hot leg outlet (9-3).

For the control system output to become effective in controlling the flow partition in the two branches, the control variable representing $\dot{m}_{11}$ was used as search variable (instead of the time) for the time dependent junction (C) at the bypass inlet.

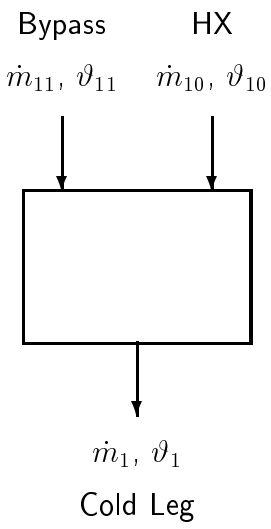

Figure 3.9: Mixing of bypass and HX flow

3.7 Secondary Side Piping

The secondary side cooling loop consists of two so-called time dependent volumes (100) and (104), two single volumes (101) and (103), and one pipe component (102). The time dependent volumes serve as mass source and mass sink. They contain water at a pressure of 1 MPa and at temperatures of 35 °C and 75 °C for volume (100) and (104), respectively.

The two single volumes have lengths of 5 m and flow areas of 0.0328 m^2. This is the same flow area as applied to the heat exchanger pipe (102).

The mass flow rate on the secondary side is adjusted by a so-called time dependent junction which serves as mass flow rate boundary. It is situated between volumes (100) and (101) and provides a constant mass flow rate of 6.9 kg/s.

Table 3.3:
Main parameters of TBM model hydrodynamic components.

Component number	Flow area (cm^2)	Length (cm)	Hydraulic diameter (mm)	Surface roughness (μm)	No. of channels lumped together
4/5	201.1	74.7	160.0	20	1
20-1	42.84	41.2	15.75	8	17
20-2/8	42.84	44.3	15.75	8	17
20-3/7	42.84	16.6	15.75	8	17
20-4/5/6	42.84	30.7	15.75	8	17
20-9	42.84	15.2	15.75	8	17
20-10	27.99	21.0	18.0	20	11
21/28	27.99	54.8	18.0	–	11
22-1/5	8.98	49.5	5.04	5	3 x 11
22-2/3/4	8.45	33.6	4.92	5	3 x 11
23-1/5	9.11	47.1	5.06	16	3 x 11
23-2/3/4	9.11	31.8	5.06	16	3 x 11
24-1/5	9.68	44.0	4.63	25	4 x 11
24-2/3/4	9.68	29.5	4.63	25	4 x 11
25-1/5	13.20	39.2	4.80	25	5 x 11
25-2/3/4	12.10	26.9	4.63	25	5 x 11
26-1/5	21.12	33.1	4.80	25	8 x 11
26-2/3/4	19.36	24.2	4.63	25	8 x 11
27-1/5	21.12	23.5	4.80	25	8 x 11
27-2/3/4	19.36	57.8	4.63	25	8 x 11
29	27.99	28.0	18.0	20	11
30	44.27	119.8	unknown	unknown	unknown

Table 3.4:
Energy loss coefficients and geometry of actual orifices.

Cooling zone	Loss coefficient ζ	Channel flow area A_1 (mm^2)	Area ratio A_1/A_2	Orifice area A_2 (mm^2)
1	0	27.2	1	27.2
2	6	27.6	2.28	12.11
3	9	22.0	2.60	8.46
4	33	24.0	4.28	5.61
5	70	24.0	5.92	4.05
6	110	24.0	7.25	3.31

Table 3.5:
Heat transfer areas of breeding zone heat structures.

Heat structures pertaining to component no.	Structure length (cm)	Structure width (cm)	Surface area (cm^2)
22-1/5	49.5	2.9	1579
22-2/3/4	33.6	2.9	1073
23-1/5	47.1	3.1	1606
23-2/3/4	31.8	3.1	1084
24-1/5	44.0	3.9	1888
24-2/3/4	29.5	3.9	1264
25-1/5	39.2	5.0	2156
25-2/3/4	26.9	5.0	1481
26-1/5	33.1	10.0	3641
26-2/3/4	24.2	10.0	2666
27-1/5	23.5	9.63	2489
27-2/3/4	57.8	9.63	6126

Table 3.6:
Heat transfer equivalent diameters
of breeding zone heat structures.

Heat structures pertaining to component no.	A_{mod}/A_{real} (–)	$D_{e,real}$ (mm)	$D_{e,mod}$ (mm)
22-1/5	0.90	5.04	2.98
22-2/3/4	0.93	4.92	3.42
23-1/5	0.95	5.06	3.92
23-2/3/4	0.95	5.06	3.92
24-1/5	1.03	4.63	5.37
24-2/3/4	1.03	4.63	5.37
25-1/5	1.00	4.80	4.80
25-2/3/4	1.05	4.63	5.91
26-1/5	1.25	4.80	14.65
26-2/3/4	1.32	4.63	18.55
27-1/5	1.20	4.80	11.94
27-2/3/4	1.27	4.63	15.30

Table 3.7:
Decay heat power generation in blanket box MANET.

Time after shutdown	Decay heat power (W)						
	Heat structure 1 of pipe number			Heat structure 2 of pipe number			
	20-2/8	20-3/7	20-4/5/6	20-2/8	20-3/7	20-4/5/6	Total
0 s	75.1	123.6	345.6	144.6	130.0	444.8	3317.8
1 s	75.0	104.1	290.9	144.2	129.7	443.7	3109.8
10 s	74.6	89.4	249.7	143.5	129.1	441.4	2946.5
1 min	73.1	87.7	245.2	140.6	126.3	432.4	2888.2
5 min	68.6	82.2	229.6	132.1	118.8	406.4	2711.4
10 min	65.7	78.6	219.6	126.6	113.8	389.5	2596.7
1 h	52.8	63.4	177.2	102.0	91.7	313.9	2093.1
5 h	22.5	27.0	75.6	43.3	38.9	133.2	889.8
1 day	6.6	7.9	22.3	12.7	11.4	39.1	261.4

Table 3.8:
Decay heat power generation
in blanket box beryllium coating.

Time after shutdown	Decay heat power (W)		
	Pipe number		
	20-3/7	20-4/5/6	Total
0 s	33.55	93.97	349.01
1 s	14.47	40.52	150.50
10 s	0.37	1.04	3.86
1 min	0.32	0.89	3.31
5 min	0.26	0.74	2.74
10 min	0.25	0.69	2.57
1 h	0.18	0.49	1.83
5 h	0.12	0.35	1.29
1 day	0.07	0.20	0.74

Table 3.9:
Nominal power densities in the six cooling zones
of the TBM breeding zone model.

Cooling zone	Nominal power density (W/cm^3)			Pipe number
	MANET	Beryllium	Li_4SiO_4	
1	7.72	4.60	18.00	22-2/3/4
2	6.53	3.87	14.85	23-2/3/4
3	5.47	3.07	13.10	24-2/3/4
4	4.30	2.36	11.92	25-2/3/4
5	2.89	1.46	8.89	26-2/3/4
6	1.04	0.45	3.50	27-1/2/3/4/5, 26-1/5
$\overline{2-6}$	2.40	1.25	6.81	22-1/5
$\overline{3-6}$	2.13	1.07	6.29	23-1/5
$\overline{4-6}$	1.83	0.90	5.69	24-1/5
$\overline{5-6}$	1.52	0.71	4.89	25-1/5

Key: $\overline{i-j}$ = weighted average value of zones i to j
(weighted by cooling zone radial widths taken from Table 3.2)

Table 3.10:
Nominal power generation in breeding zone structures.

Pipe number	Nominal power (kW)			
	Heat structure 1		Heat structure 2	
	Beryllium	MANET	Li_4SiO_4	MANET
22-1/5	4.44	0.99	5.91	0.99
22-2/3/4	11.10	2.24	10.62	2.24
23-1/5	3.87	0.92	5.56	0.92
23-2/3/4	9.44	1.91	8.86	1.91
24-1/5	3.82	0.79	5.91	0.79
24-2/3/4	8.73	1.59	9.11	1.59
25-1/5	3.44	0.75	5.80	0.75
25-2/3/4	7.87	1.59	9.71	1.59
26-1/5	3.69	0.91	7.01	0.91
26-2/3/4	8.76	2.00	13.03	2.00
27-1/5	2.52	0.65	4.79	0.65
27-2/3/4	6.20	1.66	11.79	1.66
Total	199.86	42.99	259.32	42.99

Table 3.11:
Decay heat power vs. time in breeding zone heat structure 1.

Heat Structure 1 (Beryllium + MANET)									
	Decay heat power (W)								
Pipe	Time after shutdown								
number	0 s	1 s	10 s	1 min	5 min	10 min	1 h	5 h	1 day
22- 1/5	1.5479e+2	9.6213e+1	5.2737e+1	5.1615e+1	4.8867e+1	4.6962e+1	3.7732e+1	1.5941e+1	4.5850 e+0
22- 2/3/4	3.0287e+2	1.7901e+2	8.7184e+1	8.5153e+1	8.0090e+1	7.6722e+1	6.1688e+1	2.6312e+1	7.82 59e+0
23- 1/5	1.4043e+2	8.7915e+1	4.8934e+1	4.7908e+1	4.5404e+1	4.3655e+1	3.5074e+1	1.4797e+1	4.2328 e+0
23- 2/3/4	2.9057e+2	1.6991e+2	8.0484e+1	7.8628e+1	7.4158e+1	7.1144e+1	5.7178e+1	2.4326e+1	7.16 72e+0
24- 1/5	1.3503e+2	8.1193e+1	4.1271e+1	4.0391e+1	3.8313e+1	3.6854e+1	2.9585e+1	1.2482e+1	3.5647 e+0
24- 2/3/4	2.7156e+2	1.5350e+2	6.6035e+1	6.4463e+1	6.0854e+1	5.8413e+1	4.6898e+1	1.9966e+1	5.88 56e+0
25- 1/5	1.2480e+2	7.4156e+1	3.6612e+1	3.5845e+1	3.4064e+1	3.2796e+1	2.6311e+1	1.1075e+1	3.1290 e+0
25- 2/3/4	2.6464e+2	1.5146e+2	6.7588e+1	6.6014e+1	6.2489e+1	6.0063e+1	4.8190e+1	2.0432e+1	5.93 61e+0
26- 1/5	1.3946e+2	8.2184e+1	3.9741e+1	3.8945e+1	3.7094e+1	3.5750e+1	2.8662e+1	1.2020e+1	3.3402 e+0
26- 2/3/4	3.2162e+2	1.8610e+2	8.5651e+1	8.3772e+1	7.9585e+1	7.6622e+1	6.1413e+1	2.5878e+1	7.33 04e+0
27- 1/5	9.5917e+1	5.5278e+1	2.5203e+1	2.4752e+1	2.3664e+1	2.2843e+1	1.8296e+1	7.6252e+0	2.0575 e+0
27- 2/3/4	2.3837e+2	1.3838e+2	6.4369e+1	6.3228e+1	6.0460e+1	5.8365e+1	4.6756e+1	1.9474e+1	5.24 29e+0
Total	6.6497+3	3.8890+3	1.8430+3	1.8027+3	1.7077+3	1.6417+3	1.3177+3	5.5704+2	1.5998+2

Table 3.12:
Decay heat power vs. time in breeding zone heat structure 2.

Heat Structure 2 (Li_4SiO_4 + MANET)									
Decay heat power (W)									
Pipe number	Time after shutdown								
	0 s	1 s	10 s	1 min	5 min	10 min	1 h	5 h	1 day
22- 1/5	1.0765e+2	1.0301e+2	8.8977e+1	7.7030e+1	6.6499e+1	6.1753e+1	4.9141e+1	2.0615e+1	5.7538 e+0
22- 2/3/4	2.9383e+2	2.7771e+2	2.1602e+2	1.6373e+2	1.2709e+2	1.1264e+2	8.8132e+1	3.7443e+1	1.08 74e+1
23- 1/5	9.8029e+1	9.3911e+1	8.1871e+1	7.1627e+1	6.2323e+1	5.8063e+1	4.6253e+1	1.9374e+1	5.3768 e+0
23- 2/3/4	2.1500e+2	2.0306e+2	1.5985e+2	1.2335e+2	9.6828e+1	8.6313e+1	6.7676e+1	2.8633e+1	8.19 50e+0
24- 1/5	8.7105e+1	8.2956e+1	7.1396e+1	6.1776e+1	5.3185e+1	4.9354e+1	3.9250e+1	1.6408e+1	4.5065 e+0
24- 2/3/4	1.8075e+2	1.6985e+2	1.3248e+2	1.0125e+2	7.8394e+1	6.9461e+1	5.4332e+1	2.2948e+1	6.50 83e+0
25- 1/5	7.5731e+1	7.1954e+1	6.2109e+1	5.4057e+1	4.6703e+1	4.3411e+1	3.4530e+1	1.4382e+1	3.8845 e+0
25- 2/3/4	1.5935e+2	1.4975e+2	1.2004e+2	9.5519e+1	7.6457e+1	6.8806e+1	5.4125e+1	2.2734e+1	6.32 39e+0
26- 1/5	7.9909e+1	7.5746e+1	6.5669e+1	5.7606e+1	5.0026e+1	4.6608e+1	3.7082e+1	1.5369e+1	4.0557 e+0
26- 2/3/4	1.6786e+2	1.5738e+2	1.2957e+2	1.0735e+2	8.8744e+1	8.1024e+1	6.4030e+1	2.6678e+1	7.17 36e+0
27- 1/5	4.2015e+1	3.9582e+1	3.4235e+1	3.0117e+1	2.6127e+1	2.4340e+1	1.9345e+1	7.9491e+0	2.0100 e+0
27- 2/3/4	1.0594e+2	9.9949e+1	8.6783e+1	7.6616e+1	6.6700e+1	6.2224e+1	4.9476e+1	2.0328e+1	5.14 04e+0
Total	4.3491+3	4.1074+3	3.3427+3	2.7079+3	2.2124+3	2.0085+3	1.5845+3	6.6449+2	1.8382+2

Table 3.13:
Homologous parameters of helium circulator.

Q (m^3/s)	v/α	h/α^2	β/α^2	α/v	h/v^2	β/v^2
0	0	1.172	0.294			
1	0.074	1.168	0.344			
2	0.148	1.166	0.406			
3	0.222	1.164	0.469			
4	0.296	1.162	0.532			
5	0.370	1.160	0.587			
6	0.445	1.155	0.656			
7	0.518	1.154	0.713			
8	0.592	1.145	0.775			
9	0.666	1.134	0.831			
10	0.740	1.114	0.888			
11	0.815	1.088	0.937			
12	0.888	1.057	0.975			
13	0.963	1.020	1.006			
14				0.965	0.909	0.955
15				0.901	0.742	0.838
16				0.845	0.592	0.731
17				0.795	0.459	0.636
18				0.750	0.320	0.539
19				0.711	0.185	0.455
20				0.675	0	0.354

Chapter 4

Normal Operation Analyses

ITER is supposed to operate in a pulsed mode with typically 1000 s burn time followed by 1000 s dwell time. In a later stage, attempts may be made to prolong the burn cycles of ITER, leading in terms of thermo-dynamics to almost steady state conditions. Hence, both operating modes (steady state and pulsed) are investigated here. The steady state mode delivers at the same time the initial conditions needed for the accident analyses described in chapter 5.

4.1 Steady State Analysis

The steady state conditions were computed with the RELAP5 model explained in chapter 3. They serve as starting point for the transient accident simulations.

Pressure distribution

To match the circulator characteristics with the plant characteristics at the desired mass flow rate of 1.85 kg/s, the speed of the circulator was increased by a factor 1.04 from the rated speed of 628.3 rad/s to the initial speed of 653.4 rad/s. An overall pressure drop of 0.298 MPa in the cooling loop was observed, which is 11 % higher than the design value of 0.268 MPa. The pressure loss in the TBM amounts to 0.220 MPa, which is 74 % of the total pressure loss.

To evaluate the influence of the orifices (see subsection 3.2.1) at the inlets of the breeding zone cooling channels on the pressure loss in the TBM, a steady state calculation without orifices was conducted. A pressure loss of 0.154 MPa in the TBM was observed, which is 30 % less than the pressure loss with throttles.

Helium temperatures

The calculated steady state helium temperatures refer to the situation with closed HX bypass, that is to 100 % helium throughput through the HX. TBM inlet and outlet temperatures of 254 °C and 360 °C, respectively, were observed, which equals a temperature rise of 106 °C across the TBM. The outlet temperature of the HX is 243 °C, implying a temperature rise of 11 °C across the circulator. In the blanket box, the helium heats up by 40 °C, followed by a temperature increase of further 66 °C in the breeding zone. Due to the adjusted mass flow rates at the inlet to the cooling plates the helium temperature rises in the six cooling zones are uniform. Without orifices, temperature rises of 110 °C, 92 °C, 88 °C, 61 °C, 43 °C, and 45 °C in cooling zones one through six, respectively, would result.

Table 4.1:
Steady state structural temperatures.

Mesh point	Temperature (°C) FIDAP	RELAP5
FW1: beryllium plasma side	540	581
FW1: interface beryllium/MANET	510	555
FW1: interface MANET/helium	410	448
FW2: MANET breeding zone side	344	296
BZ: beryllium, hottest node	450	479
BZ: Li_4SiO_4, hottest node	630	643

Key: FW1/2 = part of FW modelled by RELAP5 heat structure 1/2, BZ = breeding zone.

Structural temperatures

The calculated structural temperatures were compared against the temperatures obtained by 3D calculations with the finite element code FIDAP [15]. The result is shown in Table 4.1 for various nodes of the TBM first wall and breeding zone. The FW RELAP5 temperatures refer to the heat structures of pipe volume (20-5), which marks the toroidal middle of the TBM. The heat structure temperatures in the nodes upstream (20-4) and downstream (20-6) are approximately 10 °C lower and higher, respectively. This temperature distribution is caused by the lack of the second cooling loop of the TBM in the RELAP5 model, which, due to its opposite flow direction, provides actuallly for a uniform toroidal temperature distribution in the FW and the breeding zone. Therefore, the heat structure temperatures pertaining to the middle volumes of the FW and the breeding zone cooling channels were used as reference temperatures. The maximum breeding zone temperatures in Table 4.1 obtained with RELAP5 refer to cooling zone 1 (pipe volume (22-3)).

The RELAP5 temperatures in heat structure 1, which models the 10 mm layer of the FW between the plasma and the coolant, are $\approx$ 40 $°C$ higher than the corresponding FIDAP temperatures, whereas the RELAP5 temperature at the back of heat structure 2, which models the 6 mm layer between the coolant and the breeding zone plus the ribs between the two layers, is $\approx$ 50 $°C$ lower than the corresponding FIDAP temperature. This can be put down to the fact that the RELAP5 1D heat transfer model allows for only heat transfer between the front and the back part of the FW via the coolant, whereas in the FIDAP 3D heat transfer model the heat transfer via heat conduction in the ribs between the front part and the back part is considered, too. Furthermore, the RELAP5 model does not account for the thermal coupling between the FW and the breeding zone as does the FIDAP model. The coupling tends to raise the temperature at the back of the FW (mesh point FW2 in Table 4.1). The temperature gradient across the 10 mm layer of the FW on the plasma side, which equals 130 °C, however, is similar in the RELAP5 and FIDAP calculations.

The maximum and minimum breeding zone temperatures in the RELAP5 model appear in cooling zone 1 and 6 (pipe (22) and (27)), respectively. Radial differential temperatures within the pebble beds of 122 °C for the beryllium pebble bed and 237 °C for the Li_4SiO_4 pebble bed were observed.

Table 4.2:
Steady state heat transfer coefficients.

Location (front part)	Heat transfer coefficient (W/m^2K)	
	Design value	RELAP5
First wall	4484	4851
Breeding zone:		
Cooling zone 1	5607	6117
Cooling zone 2	4750	5008
Cooling zone 3	4532	4701
Cooling zone 4	3457	3861
Cooling zone 5	2525	3104
Cooling zone 6	2153	2583

Heat transfer coefficients

The calculated heat transfer coefficients were compared against the values used for the thermal-hydraulic layout of the test module [16]. The result is shown in Table 4.2. The RELAP5 values in the table refer to volume 5 of pipe (20) and to volume 3 of pipes (22) to (27). The agreement between the two groups of values is satisfying.

Note: The heat transfer coefficients stated for the RELAP5 calculations are the corrected values which result if the true heat transfer equivalent diameters are used in the RELAP5 model (see subsection 3.2.2).

4.2 Pulsed Operation Analysis

The experimental reactor ITER will operate in a pulsed mode. One power pulse comprises a 50 s power ramp-up period, a 1000 s full power period, and a 100 s power ramp-down period. Between the power pulses, a dwell time of 1050 s is planned, making up a repetition time of 2200 s for the whole cycle [17].

Before the first power cycle and after maintenance or repair periods, the whole test module will be baked at 240 °C, which is the temperature envisaged for outgassing the surfaces of the vacuum vessel prior to generation of the plasma. The power needed to heat up the system from ambient temperature to the baking temperature is provided by a 100 kW electrical heater located in the HX bypass. During the system heat up it is assumed that the HX is isolated from the system and that the circulator operates at reduced speed. The time needed for heating the TBM and the external loop components from 20 °C to 240 °C at a power of 100 kW (the circulator power at low speeds can be neglected, since $P \sim N^3$) was estimated at $\approx$ 6 h (heat up rate of 0.01 K/s or 36 K/h). After the baking period the temperature at the TBM inlet is adjusted to 250 °C by means of the temperature control system as described in section 3.6. This is the starting point for the transient simulations.

In the RELAP5 model the power of the electrical heater was simulated as internal heat source in the heat structures of pipe (11) in Fig. 3.2. The initial condition was calculated with the internal heat source of pipe (11) as the only heat source in the loop and temperature control by flow partition to HX and bypass.

The course of the structural temperatures in the FW and the breeding zone in the toroidal midplane of the TBM over two power cycles is shown in Fig. 4.1. At the end of the 1000 s full power period the temperatures in the FW and breeding zone have reached nearly steady state. In fact thay are smaller than the calculated steady state temperatures, namely, 4 to 5 °C in the FW, 3 to 6 °C in the beryllium pebble beds of the six cooling zones, and 4 to 5 °C in the Li_4SiO_4 pebble beds of the six zones. If one takes into account the lower helium temperature at the TBM inlet of 250 °C compared to the value of 254 °C obtained from the steady state calculations, the structural temperatures at the end of the burn time are very close to the steady state values. During dwell time, the controlled initial temperature of 250 °C is reached rapidly in the FW, whereas in the pebble beds a uniform temperature in all cooling zones is reached only at the end of the zero power period.

As is evident from Fig. 4.1, the TBM can follow the power cycles. Regarding the remaining components of the cooling loop, the most critical region is the hot leg, where the helium temperature is not controlled and where the pipe walls have high heat capacity. The situation is depicted in Fig. 4.2, top frame. At the end of the second power cycle the temperature near the end of the hot leg, i.e., at a distance of 60.5 m to the TBM, the wall temperature is 0.5 °C higher than at the end of the first power cycle. This would result in a certain drift of a few tens of °C with increasing cycle numbers, until a saturation is reached. However, since the TBM inlet temperature is kept constant by HX bypass control, this will not have consequences on the structural temperatures inside the test module.

Characteristic helium temperatures in the cooling loop are shown in Fig. 4.2, middle. The temperatures at the cold leg inlet and outlet remain constant during the power cycles, as a result of the temperature control mechanism. The cold leg temperature rise of 11 °C is caused by the circulator. The temperature at the hot leg inlet (TBM outlet) increases steadily during the heating period and reaches a value of 352 °C before power ramp-down.

The resulting 102 °C temperature increase of the helium across the TBM is 4 °C below the steady state temperature increase of 106 °C.

To illustrate the operation of the temperature control system, the mass flow rates in the HX, the bypass, and the main loop during the two power cycles are plotted in Fig. 4.2, bottom. During the burn periods the bulk of the helium flows through the HX, whereas during the zero power periods, most flows through the HX bypass. The sum of the mass flow rates in the HX and the bypass always equals the total mass flow rate in the cooling loop.

To analyse the system behaviour without temperature control computations over five power cycles with the HX bypass closed were performed. Since the conditions on the HX secondary side, i.e. water inlet temperature (35 °C) and mass flow rate stay constant during the power cycles, the helium cools down below the design value of 240 °C at the HX outlet when full power conditions are not fulfilled. This concerns both the power ramp-up periods and the power ramp-down periods, as well as especially the zero power periods, where the primary HX outlet temperature sinks to a temperature of $\approx$ 100 °C (see Fig. 4.3). During the burn pulses the test module is cooled down by the cold helium, ensuing initial structural temperatures significantly below the design value of 250 °C. As a consequence, the temperatures in the FW and the breeding zone never reach steady state conditions during the full power periods (Fig. 4.4 on page 55). With increasing number of cycles, the temperatures in the test module will decrease steadily. Therefore, a temperature control system is mandatory for the TBM cooling system to ensure reasonable operation of the test module in ITER.

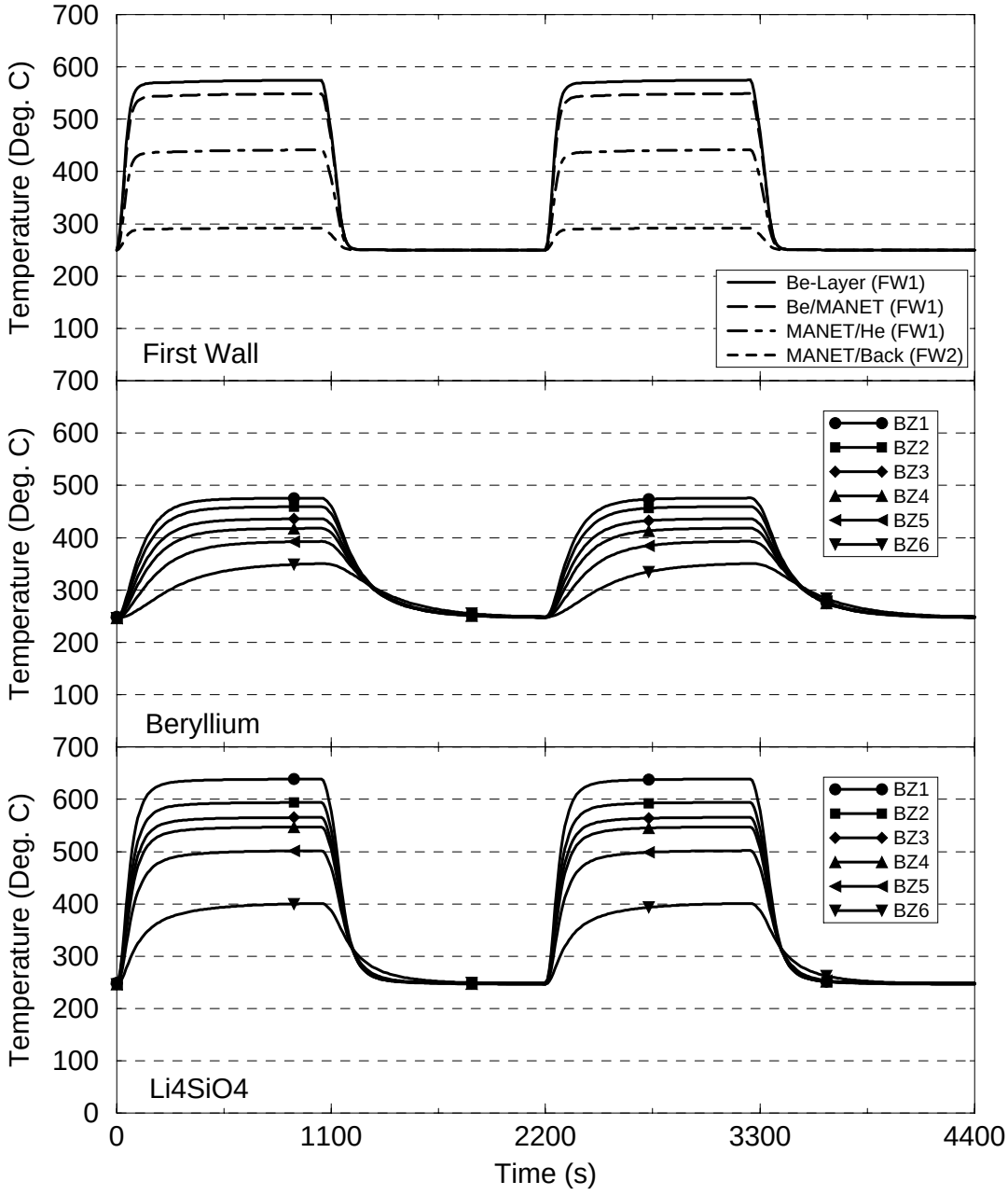

Figure 4.1: ITER pulsed operation: Structural temperature vs. time in toroidal midplane (FW1/2 = part of FW modelled by RELAP5 heat structure 1/2, BZ i = cooling zone i of breeding zone).

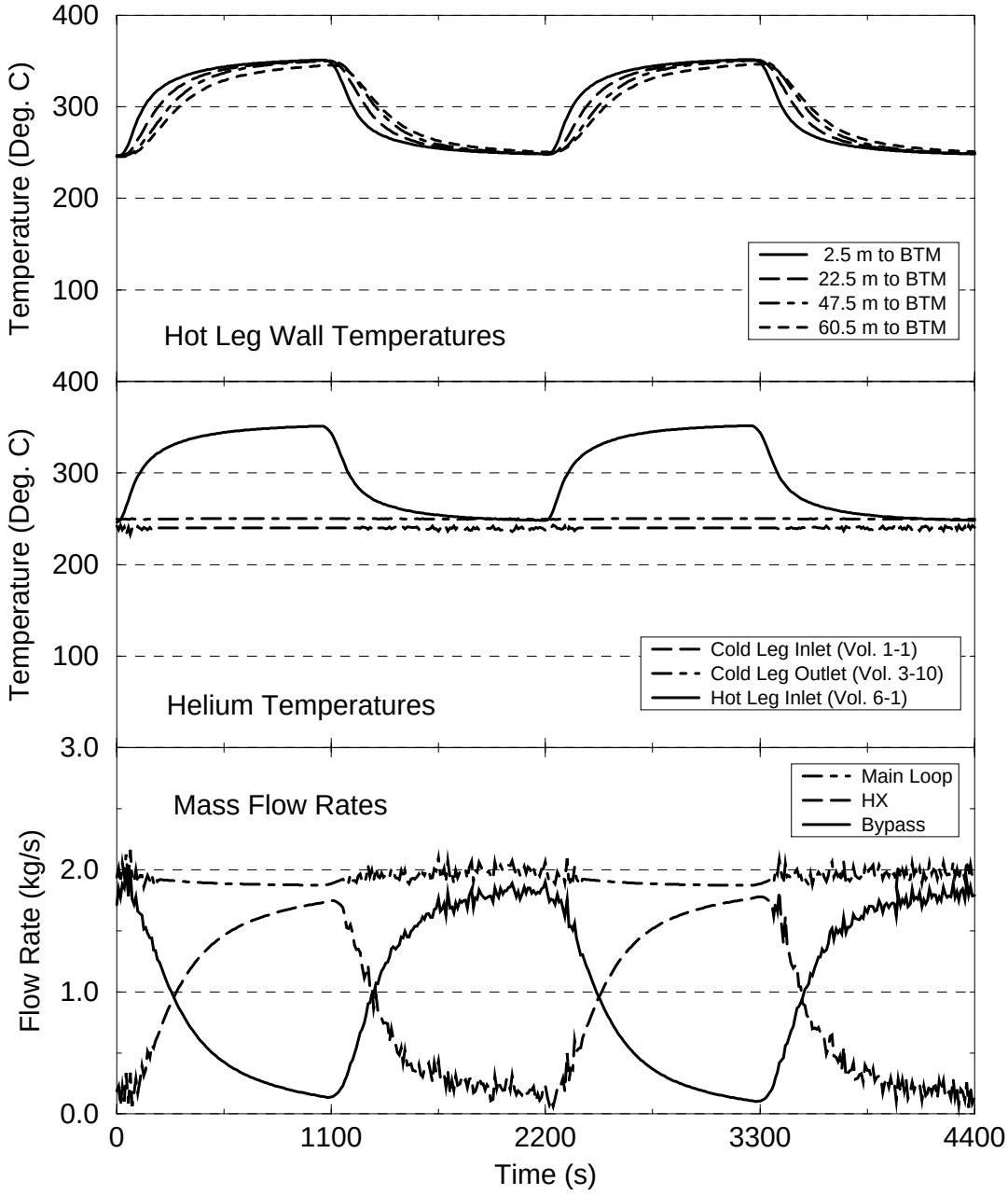

Figure 4.2: ITER pulsed operation: Hot leg wall temperatures, helium temperatures, and mass flow rates vs. time.

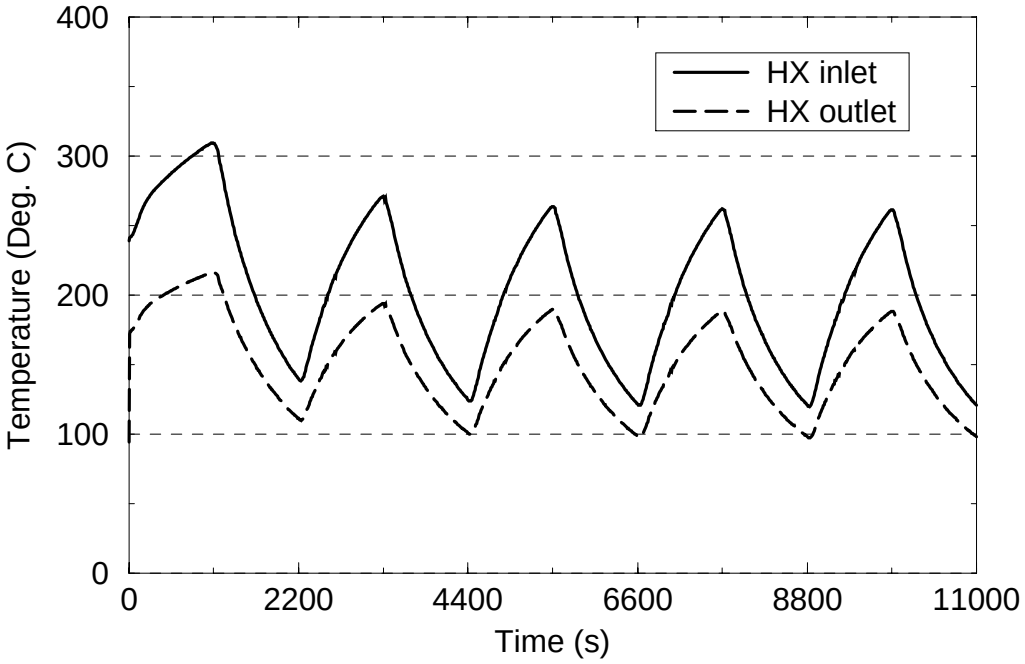

Figure 4.3: ITER pulsed operation without active temperature control: Helium temperature at HX inlet and outlet vs. time.

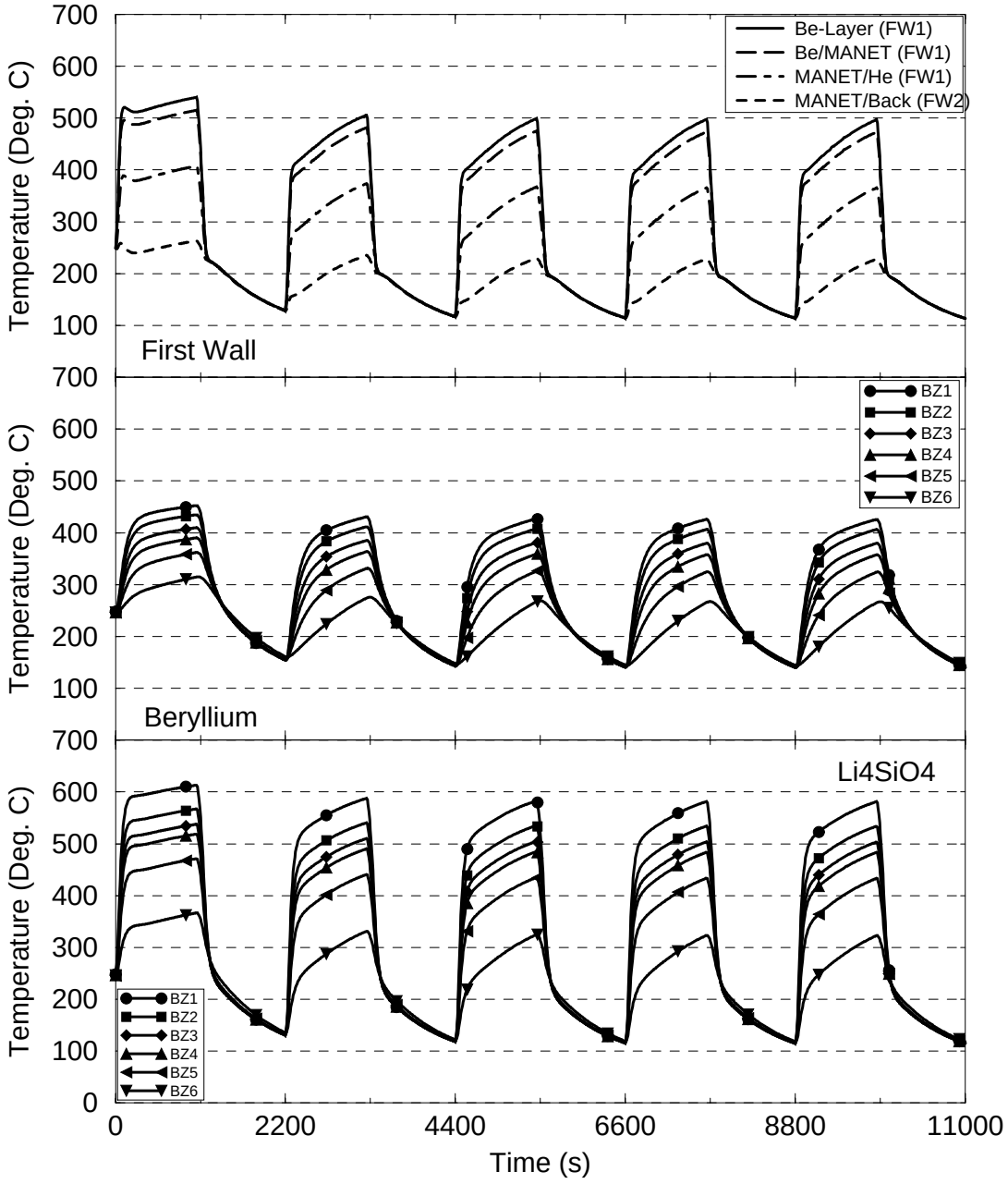

Figure 4.4: ITER pulsed operation without HX bypass: Structural temperatures in toroidal midplane vs. time. (FW1/2 = part of FW modelled by RELAP5 heat structure 1/2, BZ i = cooling zone i of breeding zone).

Chapter 5

Accident Analyses

The transient behaviour of the test module during postulated accidents was analysed. Four groups of accidents were investigated: loss of flow accidents (LOFA), loss of coolant accidents (LOCA), leak inside test module accidents (LEAK), and loss of heat sink accidents (LOHS). For all accidents analysed, except for the LOHS, unchanged conditions on the secondary side, i.e., constant secondary side flow rate and HX inlet temperature, were assumed. The methods and results of the analyses are outlined in the following sections. Main results of the investigated accidents are compiled in Table 5.3 on page 100.

5.1 Loss of Flow Accidents

Loss of flow accidents following a loss of electrical power of the circulators in both cooling loops (denoted as LOFA2, where the 2 indicates that both loops are affected), and an inadvertent valve closure in both cooling loops (LOFA2A) were analysed. The analyses were performed with the RELAP5 model of the TBM cooling loop shown in Fig. 3.2 on page 18.

5.1.1 Loss of Electrical Power of Circulators (LOFA2)

Accident description

The accident is characterised by a loss of forced flow in both TBM cooling loops due to loss of electrical power of the circulators, coast-down of the circulators (ruled by the circulators' moment of inertia), and transition from forced flow to buoyancy-driven natural circulation flow (ruled by the level difference between heat source and heat sink and by the time-dependent helium densities in the cold leg and hot leg).

Cases investigated

Nine transients under various boundary conditions were investigated, shown in Table 5.1. The key parameters varied are: a) the plasma shutdown scenario after detection of the accident, b) the delay time between detection of the accident and initiation of the plasma shutdown, c) the level difference between the heat exchanger and the TBM, and d) the time constant $T_{1/2}$ of the circulator which gives the time during which the circulator slows down to half speed.

The so-called normal shutdown scenario complies with the scheduled power ramp-down at the end of an ITER power pulse. Therefore, it is characterised by a linear decrease of the surface power from its nominal value to zero within 100 s and by a linear decrease of the volumetric power from its nominal value to the decay heat power level within 100 s.

Table 5.1:
Investigated LOFAs - loss of electrical power.

Case	Shutdown scenario	Delay time (s)	Level difference TBM - HX (m)	$T_{1/2}$ circulator (s)
I	No shutdown	inf.	22	2
II	Normal shutdown	10	22	2
III	Normal shutdown	1	22	2
IV	Normal shutdown	10	22	6
V	Normal shutdown	1	22	6
VI	Fast shutdown	1	22	2
VII	Fast shutdown	1	22	6
VIII	Normal shutdown	10	3	2
IX	Normal shutdown	10	0.5	2

The fast shutdown scenario is defined as follows: linear decrease of the surface power from its nominal value to zero within 20 s and immediate (millisecond-range) decline of the volumetric power from its nominal value to the decay heat power level.

Results

i) Coast-down behaviour:

The coast-down behaviour of the circulator after loss of the power supply is shown in Fig. 5.1. The depicted course of the circulator speed holds for a total moment of inertia of 1.50 kgm^2 of the circulator and all directly coupled components. The speed decreases exponentially, showing a 50 % decline within the first 6 s.

ii) Temperature transients without plasma shutdown (case I):

Without plasma shutdown (case I in Table 5.1) a steep temperature increase in the FW is observed, see Fig. 5.2. The maximum temperature in FW MANET (at the interface to the beryllium protection layer, curve Be/MANET, FW1) rises at a rate of 7 K/s at the beginning of the transient and at a rate of 5 K/s after 300 s. The temperatures in the breeder material and in the beryllium multiplier increase at rates of 2 K/s and 1 K/s, respectively, at a problem time of $\approx 120\ s$. Also depicted in Fig.5.2 are the temperature histories in the beryllium protection layer on the plasma side (curve Be-Layer, FW1) and at the back side of the FW at the interface to the breeding zone (curve MANET/Back, FW2).

Failure of the FW is expected to occur at a temperature level of $\approx 700 - 800\ °C$, which is reached approximately 30 s after start of the accident. An in-vessel loss of coolant with succeeding quench of the plasma would be the consequence. In the hypothetical case of no FW failure, the FW MANET would reach its melting point at 120 s into the transient, whereas the breeder and multiplier would reach their melting points approximately at 380 s and 620 s into the transient, respectively.

iii) Temperature transients with plasma shutdown (cases II to VII):

Histories of the maximum FW MANET temperature for cases II-VII (level difference TBM - HX $\Delta H_{TBM/HX} = 22$ m) with plasma shutdown are shown in Fig. 5.3. The

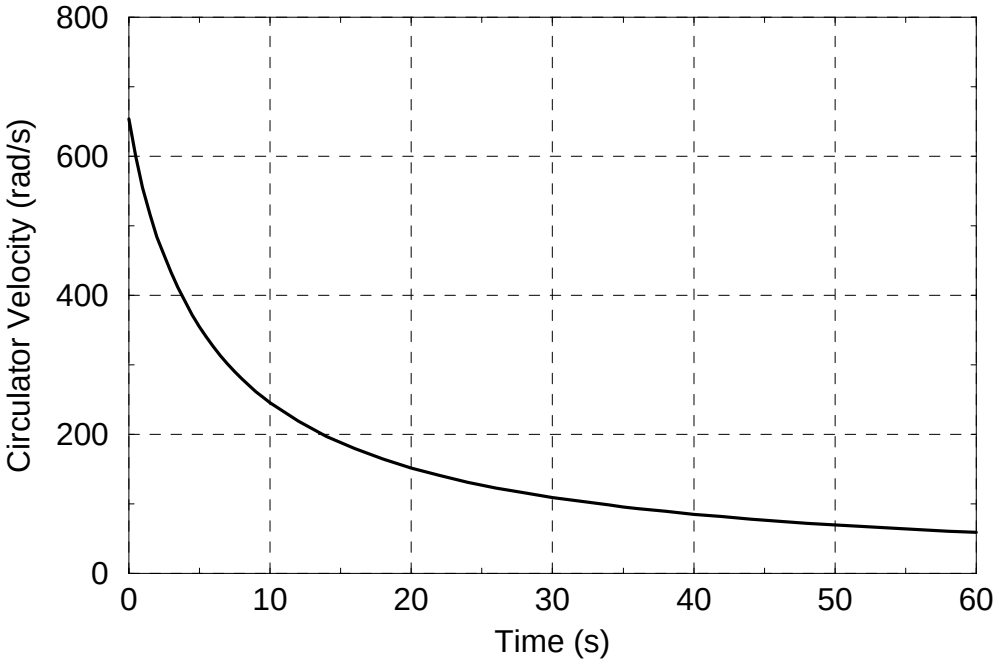

Figure 5.1: LOFA2: circulator coast-down behaviour (moment of inertia = 1.50 kgm^2).

temperature overshoot in cases with normal plasma shutdown shows a strong dependence on the shutdown delay time and on the circulators' moment of inertia. At a delay time of 10 s and a circulator coast- down time constant of $T_{1/2} = 2$ s a temperature overshoot of 325 °C at 100 s into the transient is observed. A decrease of the delay time from 10 s to 1 s reduces the overshoot by 60 °C, whereas an increase of the time constant $T_{1/2}$ from 2 s to 6 s reduces the overshoot by 110 °C. At a delay time of 1 s and a time constant of $T_{1/2} = 6$ s the maximum overshoot is 165 °C above the steady state value.

The situation is different if a fast plasma shutdown is executed. In this case, the temperature overshoot at $T_{1/2} = 2$ s reduces to 15 °C. With a higher moment of inertia ($T_{1/2} = 6$ s), temperatures are continuously decreasing during the accident.

Temperature histories at various points of the FW and at the hottest nodes of the breeder and multiplier pebble beds are shown in Figures 5.4 through 5.8 for different boundary conditions. With normal shutdown, 10 s delay time, and $T_{1/2}$ (circulator) = 2 s (Fig. 5.4), the peak RELAP5 temperature in FW MANET goes up to 880 °C at about 100 s into the transient, declining fast afterwards. The breeder pebble beds experience a negligible temperature overshoot, whereas the beryllium pebble beds stay near the steady state temperature level. The temperature in the Be-layer on the plasma side is very close to the MANET temperature at the interface of the two materials. This holds especially for the period after the shutdown process when the surface heat flux has turned to zero and the temperature distribution in the FW is dominated by the decay heat generation, which is significantly higher in MANET compared to beryllium. The maximum temperature difference across the FW (solid line minus dash-dotted line in Fig. 5.4) increases from 285 °C (RELAP5 steady state) to 470 °C at 100 s and then declines gradually. In the later phase of the transient the FW temperatures converge. The temperature at the

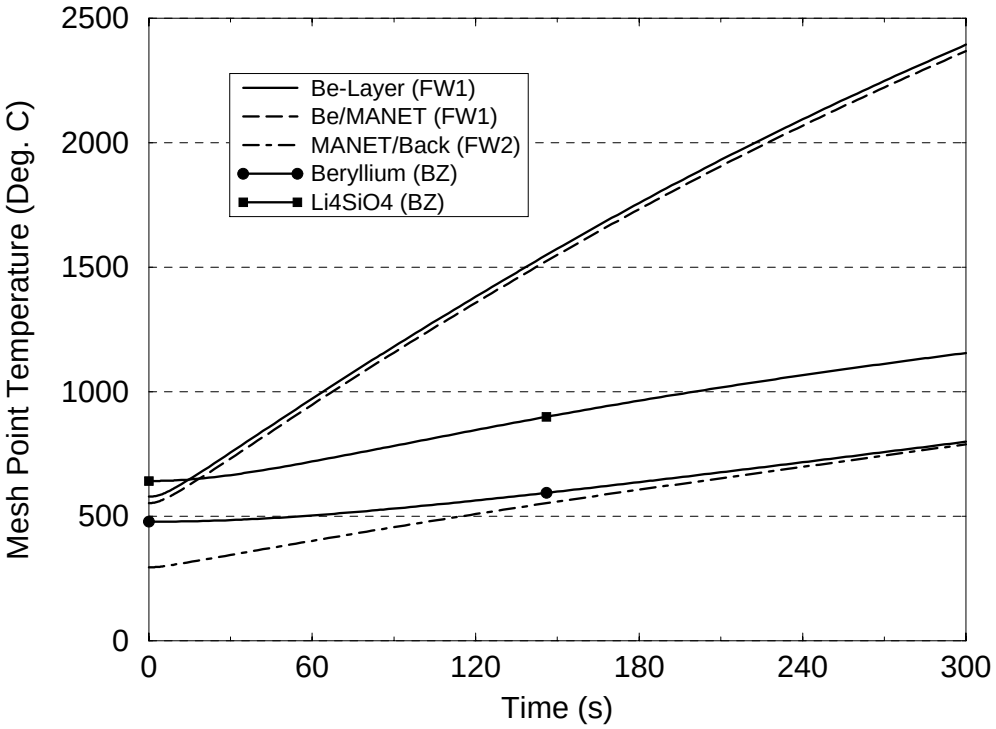

Figure 5.2: LOFA2 case I: maximum structural temperatures vs. time (no plasma shutdown, $\Delta H_{TBM/HX} = 22$ m, $T_{1/2}$ (circulator) = 2 s).

back side of the FW is of interest with regard to the welds connecting the blanket box with the cooling plates. Generally, the temperature excursions in the back of the FW are less pronounced than in the front part.

iv) The effect of bypass flow control:

The results shown in Fig. 5.3 were obtained with closed HX bypass, that is, with 100 % throughput through the heat exchanger. A comparison of the results obtained with and without flow control is shown in Figures 5.9 and 5.10 for short term and long term, respectively. In the early phase of the transient, particularly at the point of the maximum temperature overshoot, the control system has no impact on the temperature evolution. The reason is that the flow rate in the circuit at that time is still ruled by the circulator coast-down. However, at the 24 h scale, there is a strong influence on the development of the maximum temperature in the FW. With controlled flow through the bypass this temperature will stabilise at 250 °C, whereas with all the flow passing the HX (and assuming the secondary side operating at nominal conditions) the FW temperature will go down to almost the secondary cooling water inlet temperature of 35 °C (Fig. 5.10).

Mass flow rates for the case of controlled temperatures are displayed in Fig. 5.11. Immediately after loss of the power supply the total mass flow rate in the circuit decreases very fast, i.e., within 20 s to approximately 10 % of the nominal value of 1.85 kg/s. After 120 s the flow rate has diminished to 0.05 kg/s or 2.7 % of nominal. At 300 s into the transient 40 % of the total flow passes the HX and 60 % is directed across the bypass.

The evolution of the corrected heat transfer coefficients (calculated with the corrected equivalent diameters, see correlations in subsection 3.2.2) in the FW cooling channels and the breeding zone cooling channels near the FW (cooling zone 1) for different circulator

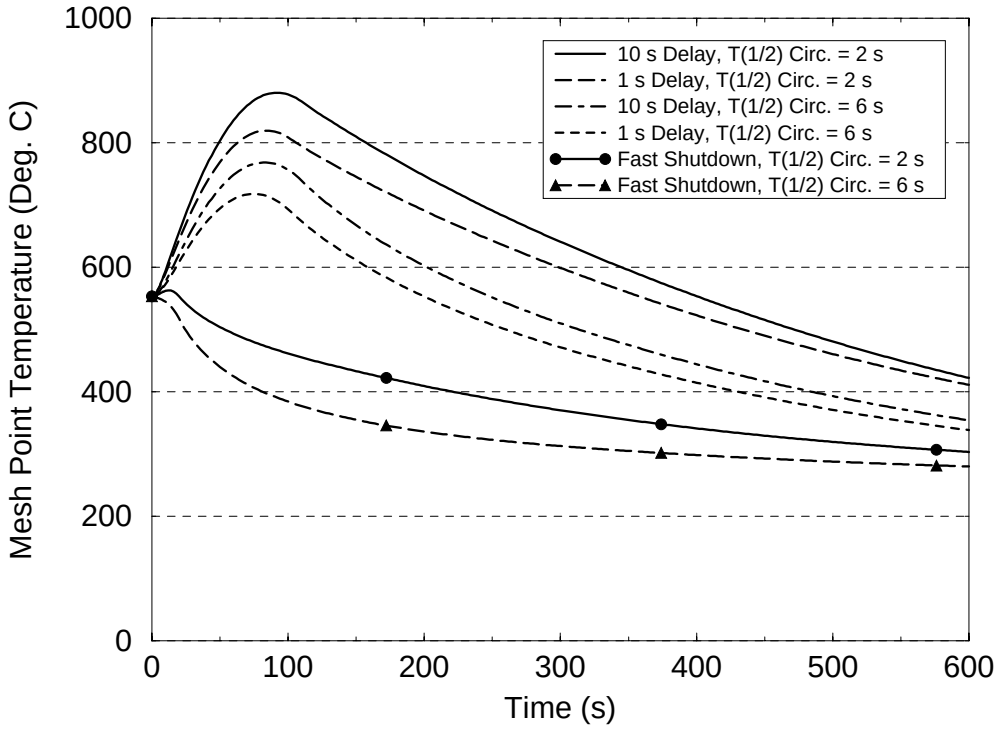

Figure 5.3: LOFA2 cases II to VII: maximum FW MANET temperature vs. time ($\Delta H_{TBM/HX}$ = 22 m, different shutdown scenarios and circulator coast-down time constants).

time constants is shown in Fig. 5.12. Since

$$\alpha \sim Re^{0.8} \sim \dot{m}^{0.8}$$

(α = heat transfer coefficient, Re = Reynolds number, $\dot{m}$ = mass flow rate), the strong decrease of the mass flow rate ensues a strong decrease of the heat transfer coefficient. The influence of the coast-down time constant (6 s versus 2 s) is about a factor of 2 in the first 100 s. Later in the transient, when the transition from forced flow to natural circulation flow has taken place, the influence diminishes.

v) The effect of varying the HX geodetic height:

The effect of varying the geodetic height between heat sink (HX) and heat source (TBM) in the situation with closed HX bypass is shown in Figures 5.13 to 5.15. After 24 h the mass flow rates in both affected cooling loops of the TBM have reduced to 1.7 %, 1.0 %, and 0.6 % of nominal at level differences of 22 m, 3 m, and 0.5 m, respectively (Fig. 5.13). The comparatively strong natural circulation at low geodetic level differences is a result of the high differential density between the cold leg and the hot leg, which results from the low helium flow velocity inside the blanket and the heat exchanger. Furthermore, one has to take into account, that the level difference between the thermal centres of the TBM and the HX is larger than the geodetic level difference.

The maximum temperature overshoots during the LOFAs with circulator coastdown are nearly independent of the TBM-HX level difference. However, the medium term temperatures are affected. After 1 h into the transient, maximum RELAP5 Be-layer temperatures in the toroidal middle of the FW of 182 °C, 261 °C, and 315 °C result for level

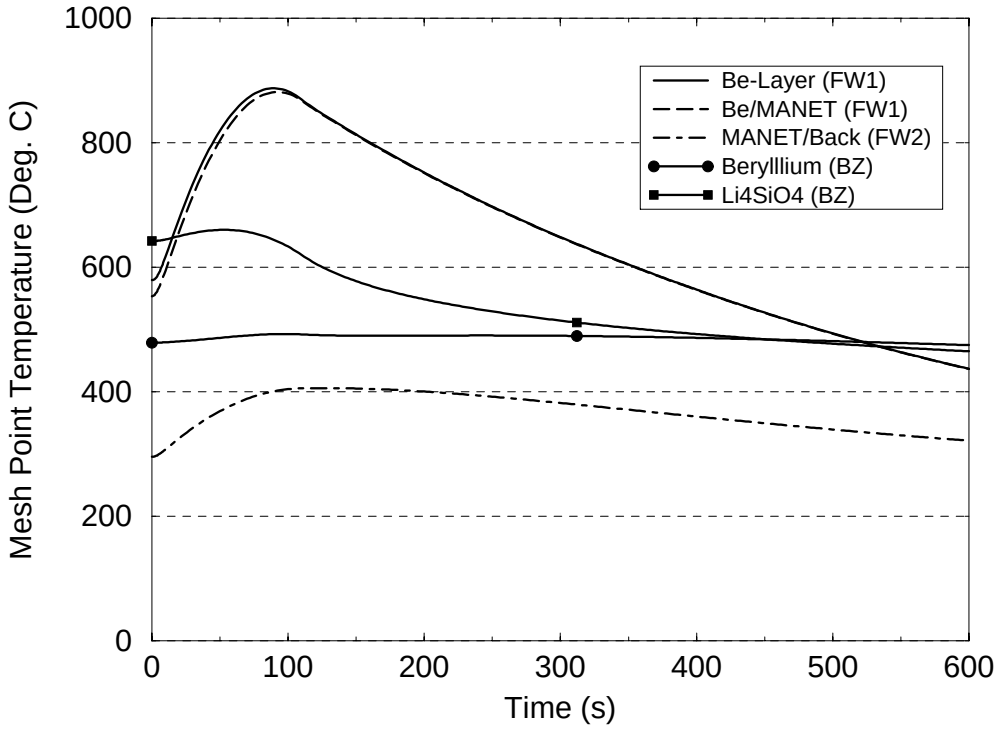

Figure 5.4: LOFA2 case II: maximum structural temperature vs. time ($\Delta H_{TBM/HX}$ = 22 m, $T_{1/2}$ (circulator) = 2 s, with HX bypass, normal shutdown after 10 s delay).

differences of 22 m, 3 m, and 0.5 m, respectively (Fig. 5.14). The long term thermal behaviour of the test module is characterised by a temperature evolution towards the secondary side HX inlet temperature of 35 °C.

vi) The effect of thermal inertia of the pipework:

There is a strong influence of the thermal inertia of the pipe walls on the helium temperature at the TBM inlet. Due to the very low helium velocity after the circulator has tripped and the low heat capacity of the gas, the helium temperature in the cold leg assumes almost the temperature of the pipe walls. This is illustrated in Fig. 5.16 for a LOFA according to case II. The pipe walls at the cold leg inlet (near the HX outlet) are cooled down fast by the cold helium leaving the heat exchanger (curve Vol. 1-1), whereas the walls further away from the HX are cooled down with a certain delay, since the helium is heated up on its way through the pipework. At the cold leg outlet, i.e. more than 60 m away from the HX, the delay is most pronounced (curve Vol. 3-10). Thus, even without active temperature control, the helium inlet temperature to the test module will remain close to 250 °C for about 1000 s into the accident and will stay above 200 °C for at least 2400 s.

Please note, that insulation losses from pipe and component walls have been ignored in the present analysis, but are significant.

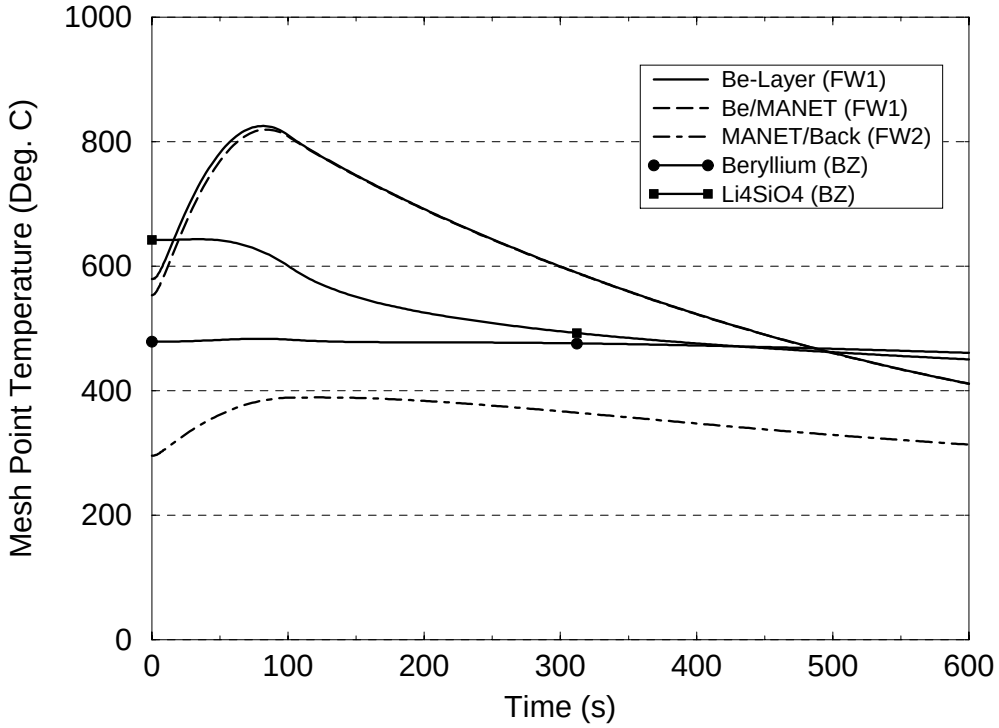

Figure 5.5: LOFA2 case III: maximum structural temperature vs. time ($\Delta H_{TBM/HX}$ = 22 m, $T_{1/2}$ (circulator) = 2 s, with HX bypass, normal shutdown after 1 s delay).

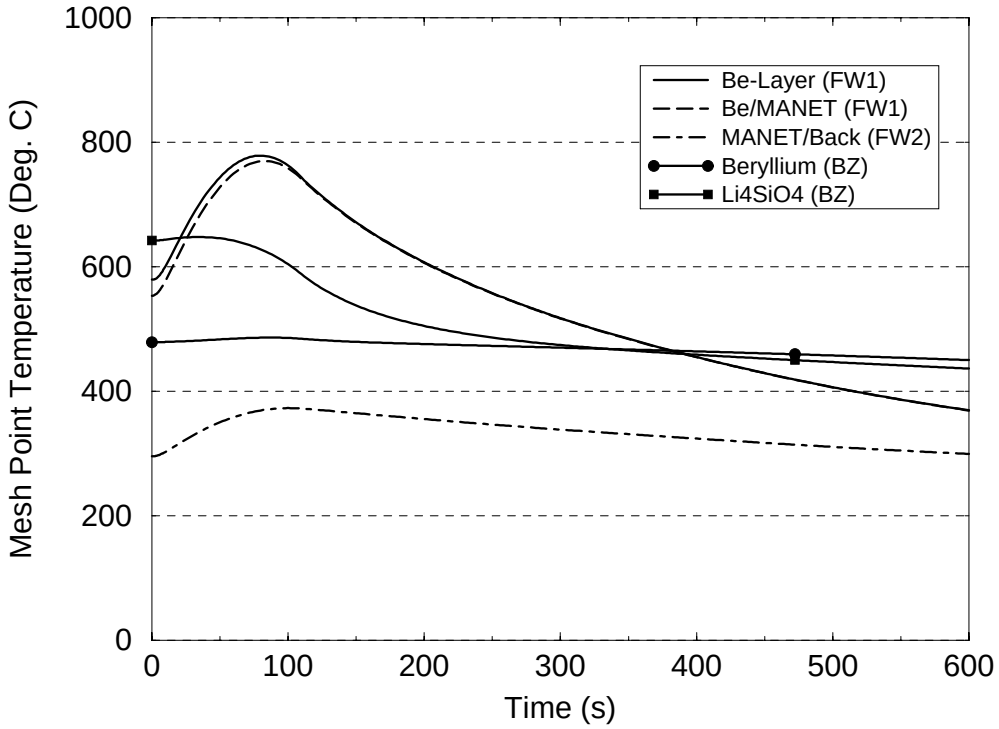

Figure 5.6: LOFA2 case IV: maximum structural temperature vs. time ($\Delta H_{TBM/HX}$ = 22 m, $T_{1/2}$ (circulator) = 6 s, with HX bypass, normal shutdown after 10 s delay).

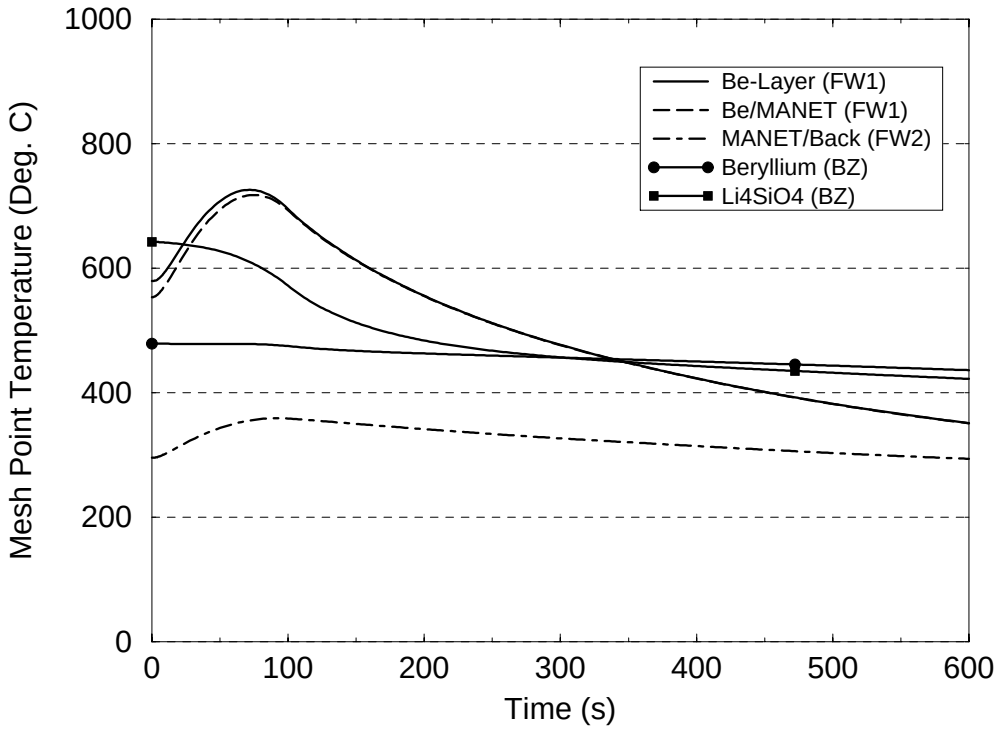

Figure 5.7: LOFA2 case V: maximum structural temperature vs. time ($\Delta H_{TBM/HX}$ = 22 m, $T_{1/2}$ (circulator) = 6 s, with HX bypass, normal shutdown after 1 s delay).

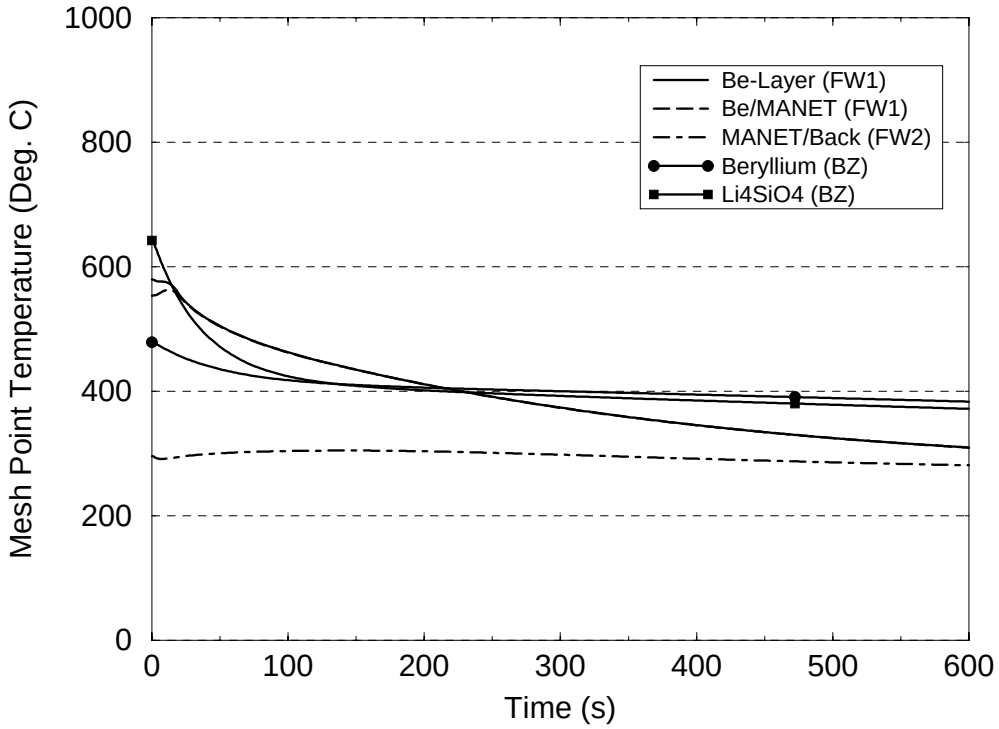

Figure 5.8: LOFA2 case VI: maximum structural temperature vs. time ($\Delta H_{TBM/HX}$ = 22 m, $T_{1/2}$ (circulator) = 2 s, with HX bypass, fast shutdown after 1 s delay).

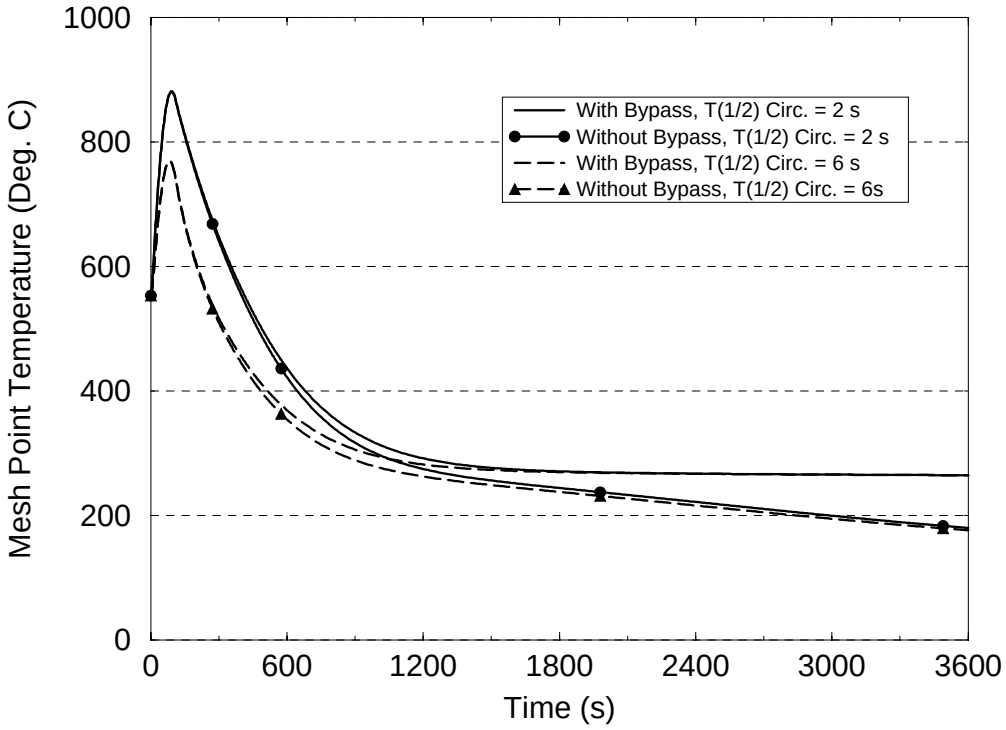

Figure 5.9: LOFA2: maximum FW MANET temperature vs. time during the first hour ($\Delta H_{TBM/HX}$ = 22 m, $T_{1/2}$ (circ.) = 2/6 s, with/without HX bypass, normal shutdown after 10 s delay).

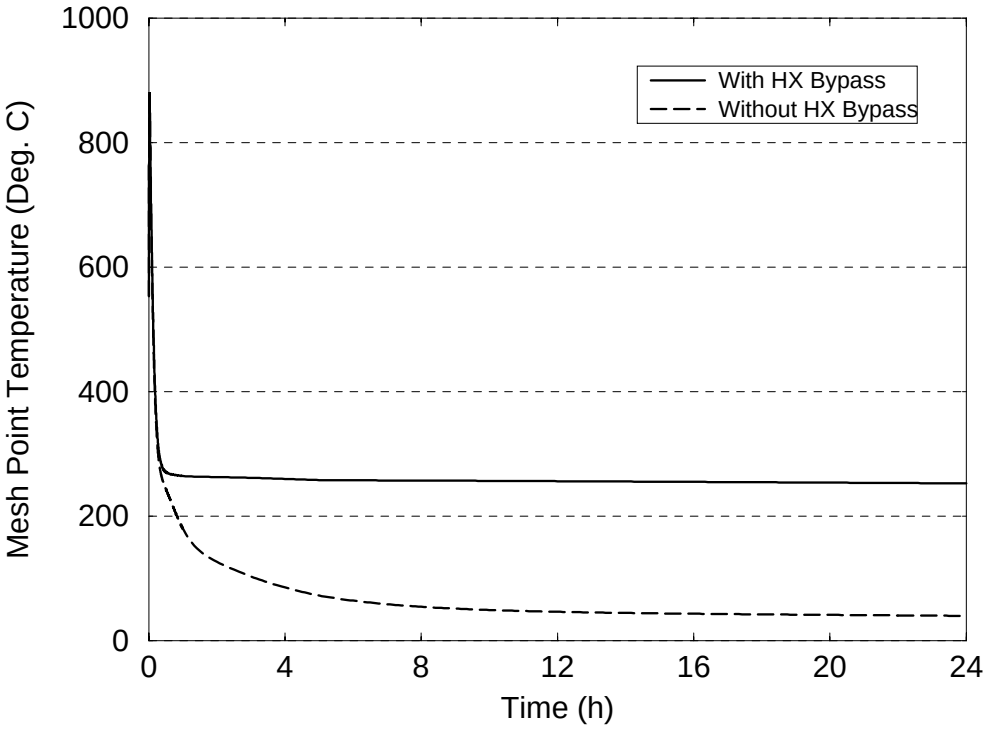

Figure 5.10: LOFA2: maximum FW MANET temperature vs. time during the first day ($\Delta H_{TBM/HX}$ = 22 m, $T_{1/2}$ (circ.) = 2 s, with/without HX bypass, normal shutdown after 10 s delay).

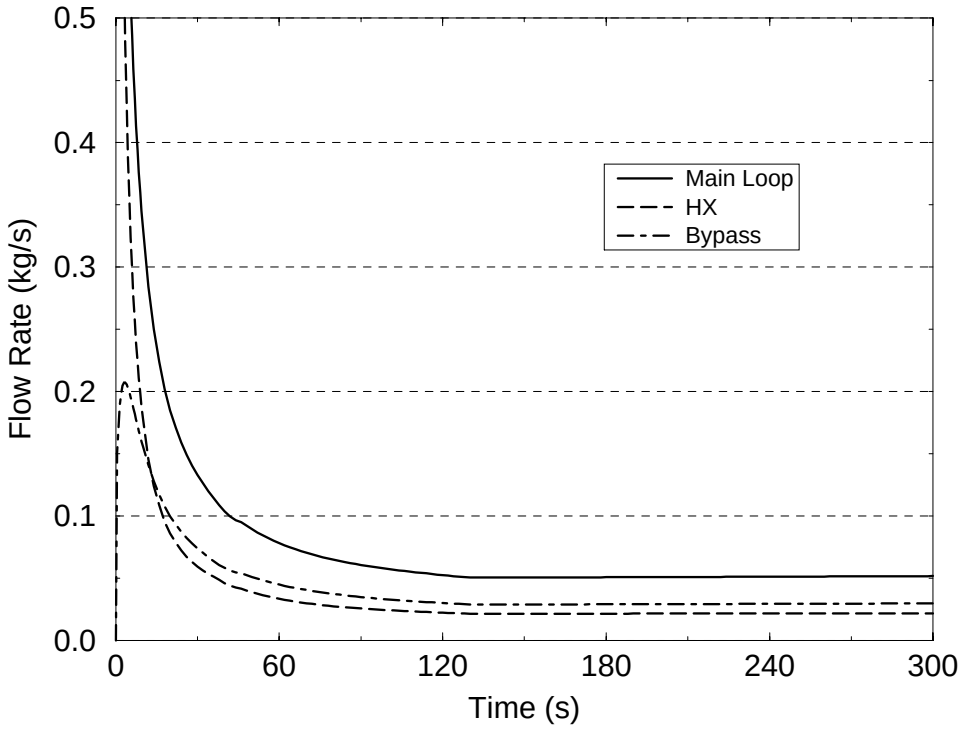

Figure 5.11: LOFA2: controlled mass flow rates vs. time ($\Delta H_{TBM/HX}$ = 22 m, $T_{1/2}$ (circulator) = 2 s, with HX bypass, normal shutdown after 10 s delay).

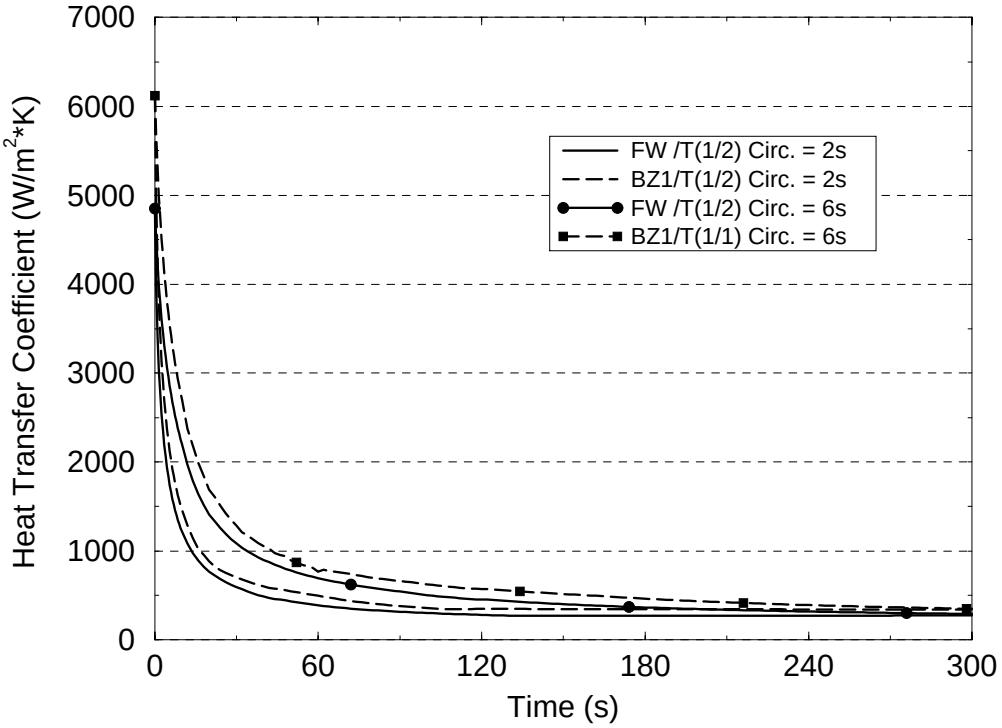

Figure 5.12: LOFA2: corrected heat transfer coefficients vs. time ($\Delta H_{TBM/HX}$ = 22 m, $T_{1/2}$ (circulator) = 2 s, with HX bypass, normal shutdown after 10 s delay).

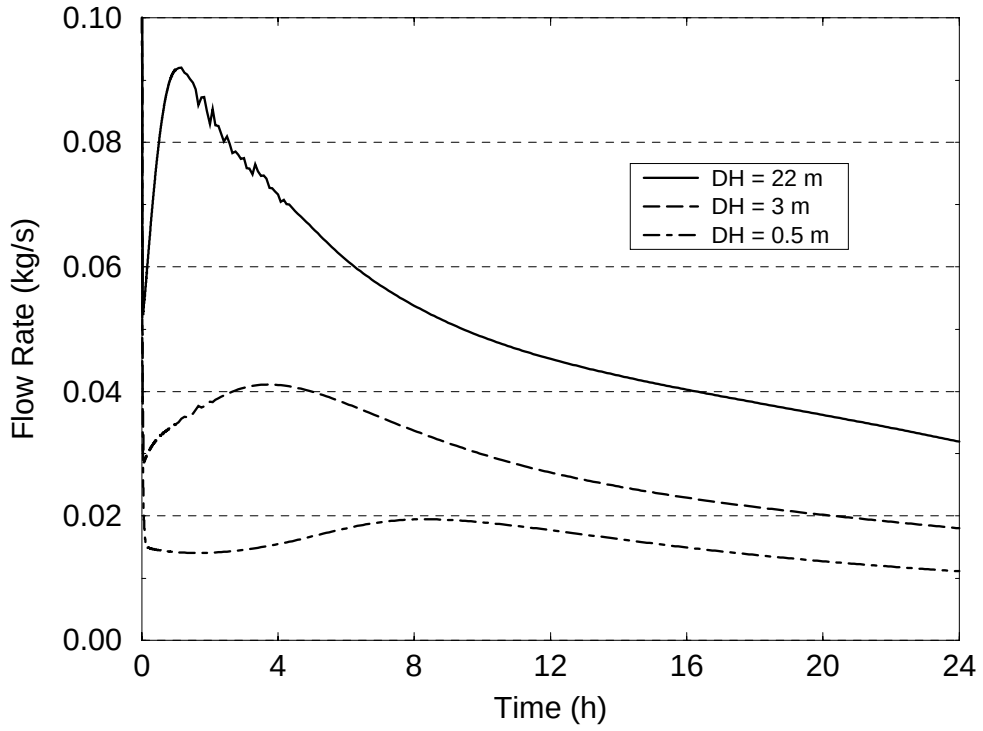

Figure 5.13: LOFA2: main loop flow rates vs. time ($\dot{m}$(0s)=1.85 kg/s, $\Delta H_{TBM/HX}$ = 22/ 3/ 0.5 m, $T_{1/2}$ circ. = 2 s, no HX bypass, normal shutdown after 10 s delay).

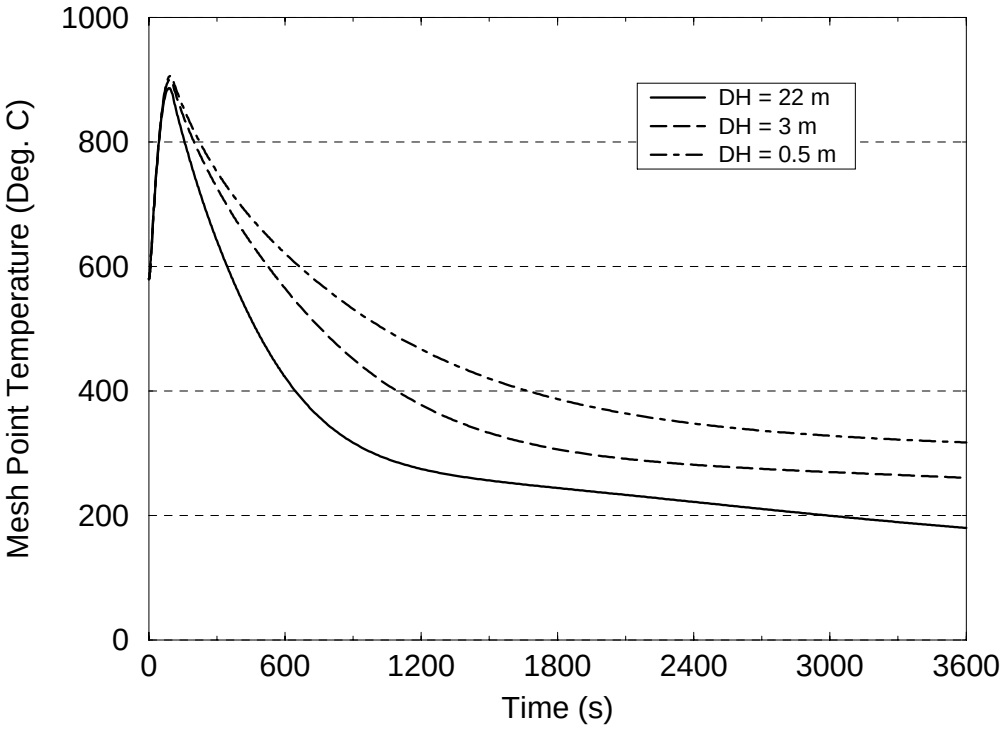

Figure 5.14: LOFA2: maximum FW beryllium temperature vs. time during the first hour ($\Delta H_{TBM/HX} = 22/3/0.5$ m, $T_{1/2}$ (circulator) = 2 s, without HX bypass, normal shutdown after 10 s delay).

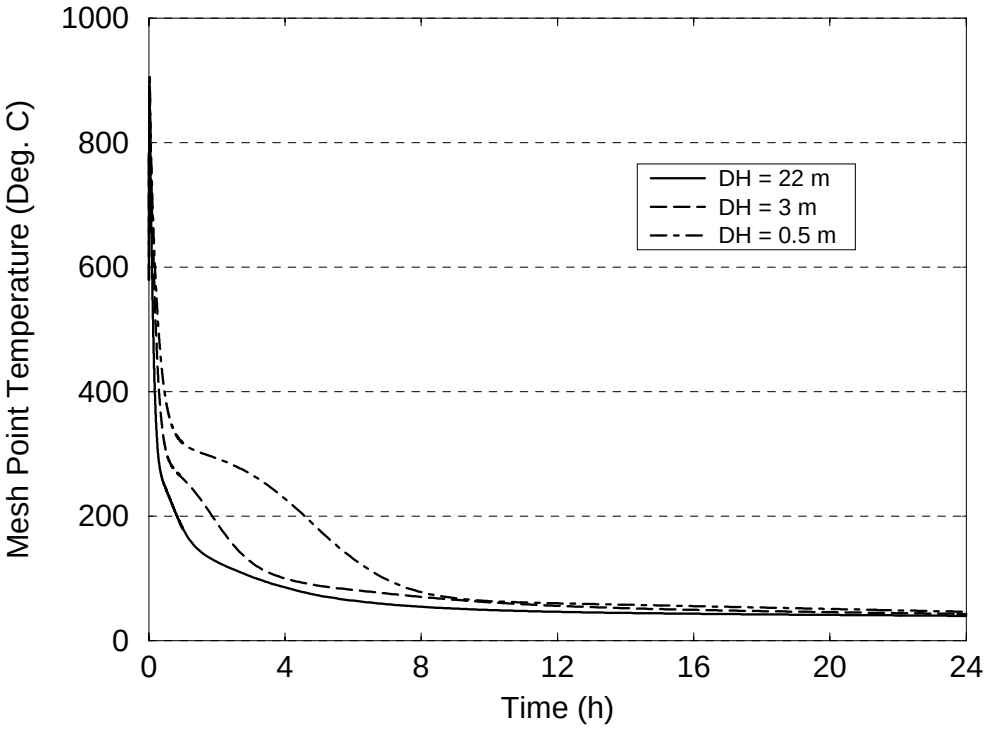

Figure 5.15: LOFA2, maximum FW beryllium temperature vs. time during the first day ($\Delta H_{TBM/HX} = 22/3/0.5$ m, $T_{1/2}$ (circulator) = 2 s, without HX bypass, normal shutdown after 10 s delay).

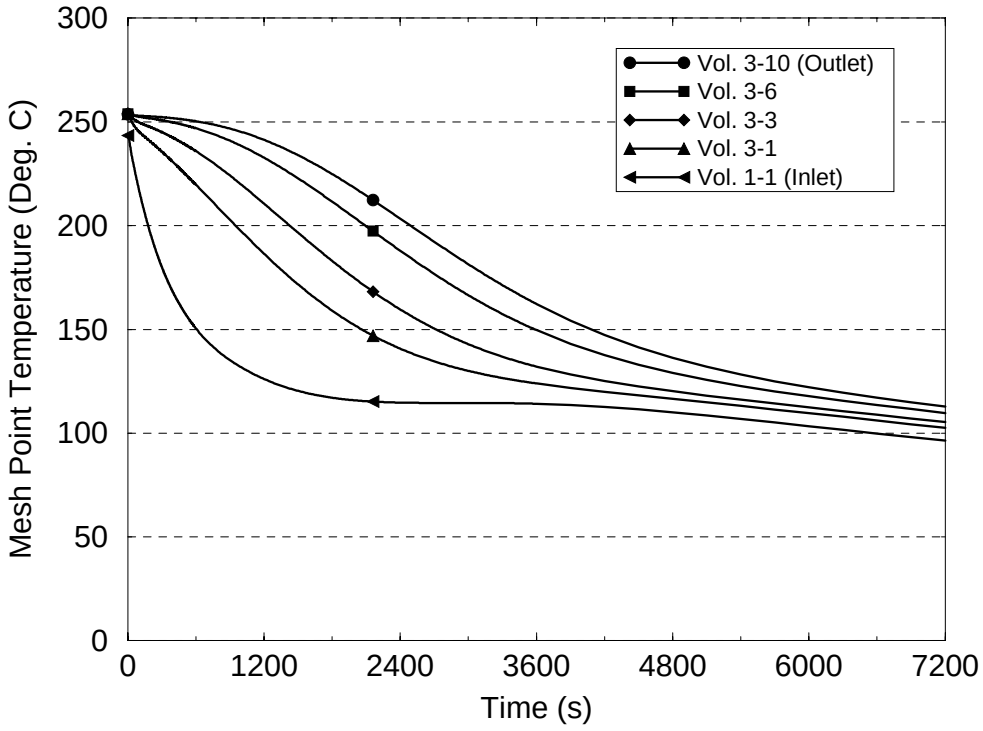

Figure 5.16: LOFA2, cold leg wall temperature vs. time ($\Delta H_{TBM/HX} = 22$ m, $T_{1/2}$ (circulator) = 2 s, without HX bypass, normal shutdown after 10 s delay).

5.1.2 Inadvertent valve closure (LOFA2A)

Accident description

The accident is characterised by a total loss of flow in both TBM cooling loops due to coherent inadvertent valve closures. The valve closures are assumed to occur within 3 s. In the RELAP5 model the initiating event was simulated by a motor valve component with a prescribed closing time constant of 0.333 1/s. The motor valve was introduced into the model between the hot leg outlet and the HX inlet at restart of the problem from steady state. Further, the circulator component (2) was substituted by a single junction component at restart of the problem to avoid complications with the RELAP5 circulator model at zero flow.

Cases investigated

Three cases with (I) normal shutdown after 1 s delay, (II) normal shutdown after 10 s delay, and (III) fast shutdown after 1 s delay were investigated.

Results

Case I: Short and long term temperature evolution

The temperature evolution at the hottest nodes of the TBM in the case of normal shutdown after 1 s delay is depicted in Fig. 5.17 for the first hour of the accident. Immediately after initiation of the accident the plasma facing part of the FW experiences a steep temperature increase which is expected to lead to failure of the FW. Assuming an intact FW for the further course of the accident, a peak FW temperature of 980 °C would be reached after 90 s, which is equivalent to a temperature overshoot of 420 °C. The temperature at the back of the FW adjacent to the breeding zone increases degressively, reaching the 800 °C temperature level after 3000 s. The Li_4SiO_4 pebble beds show a small temperature overshoot of $20°C$, 60 s after start of the transient, whereas the beryllium pebble beds show no overshoot but a slow and steady increase in temperature towards 550 °C. The long term temperature evolution is characterised by an unlimited temperature increase in the test module, as outlined in Fig. 5.18. After one day the FW hypothetically would have reached a temperature of more than 1200 °C, whereas the breeding zone would have reached 800 °C. Generally, the FW and the breeding zone tend to equalise their temperatures. As visualised in Fig. 5.17, the temperatures in the FW converge within one hour and the temperatures in the pebble beds even within 15 minutes. In the actual test module, temperature equalization between the FW and the breeding zone will be enhanced by heat conduction. Therefore, the mean temperature curves for the TBM will lie between the curves presented for the FW and the breeding zone in Figures 5.17 and 5.18.

Note: In the present RELAP5 model thermal coupling between the FW and the breeding zone is not included, since the multi-dimensional heat transport can not be modelled properly by one-dimensional RELAP5 heat structures. A further restriction of the underlying RELAP5 model is that no heat rejection due to radiation from the TBM side walls to the TBM support frame and from the surface of the FW towards the opposite inboard blanket is considered. This mechanism will lead to effective cooling of the test module at high temperature levels as additional 1-D analyses showed [4]. However, the steep temperature increase in the FW in the early phase of the accident won't be mitigated considerably by heat radiation.

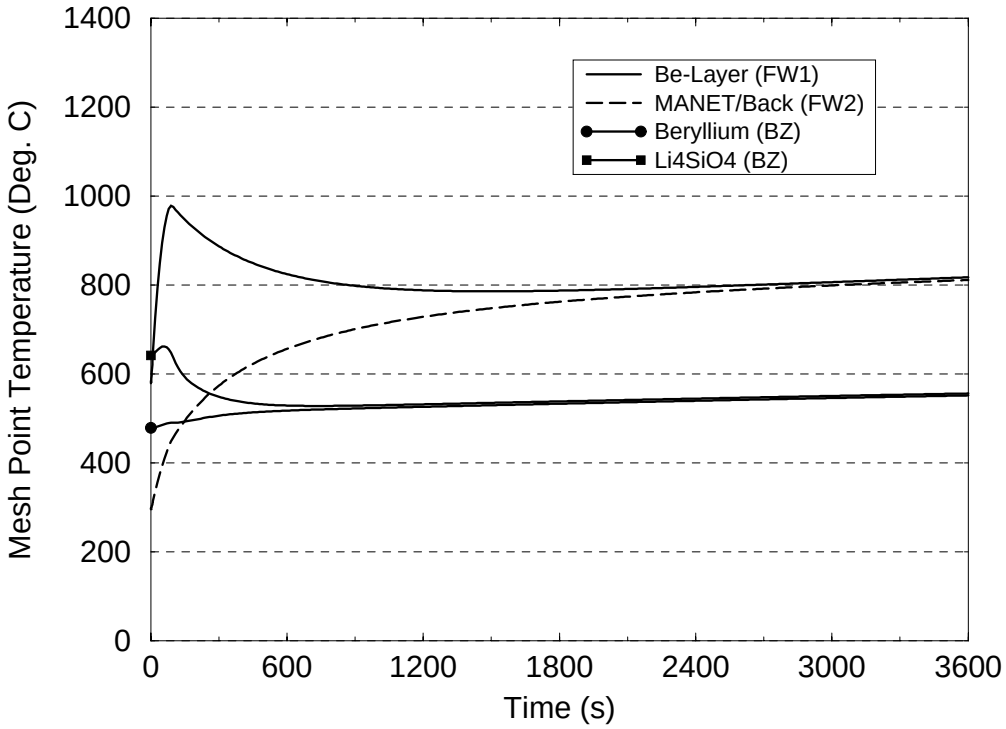

Figure 5.17: LOFA2A case I: maximum structural temperatures vs. time during the first hour (normal shutdown after 1 s delay).

Cases I to III: The effect of shutdown parameters:

A comparison of the temperature evolution in FW MANET at the hottest node for different shutdown scenarios is given in Fig. 5.19. The normal shutdown scenario after 1 s delay provides only for a small time delay in the temperature evolution, compared to the normal shutdown scenario after 10 s delay. In contrast to that, the fast shutdown procedure avoids the large temperature overshoot in the first 100 s and provides for a considerable time delay in the long term temperature development. Detailed information on the maximum temperatures and differential temperatures in the TBM for all three investigated cases can be found in Table 5.3.

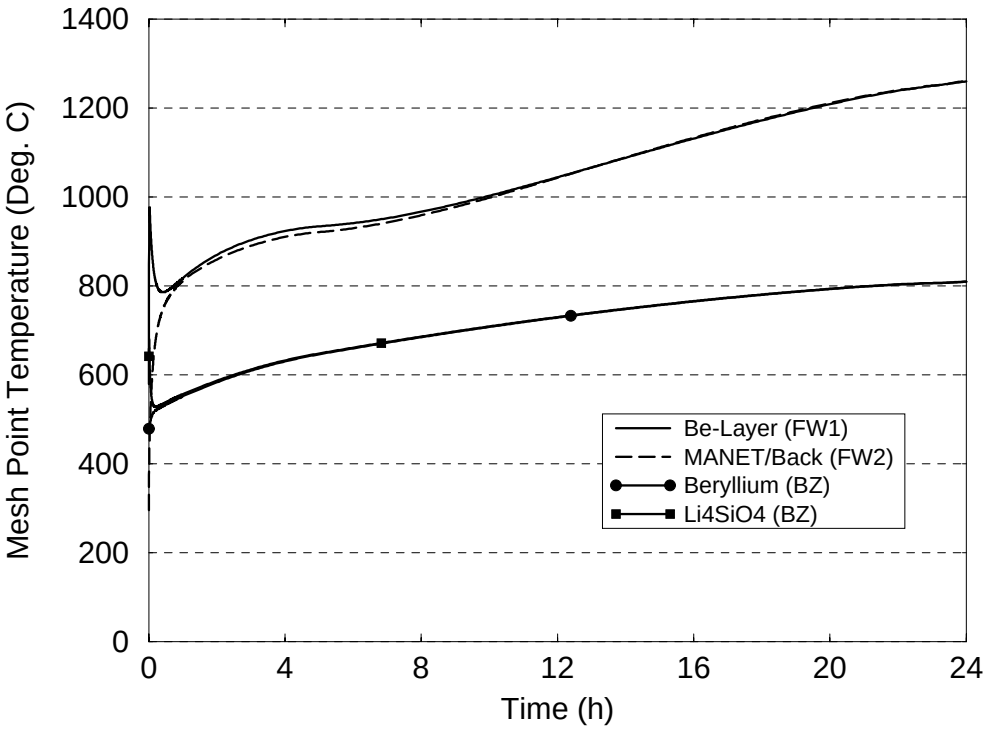

Figure 5.18: LOFA2A case I: maximum structural temperatures vs. time during the first day (normal shutdown after 1 s delay).

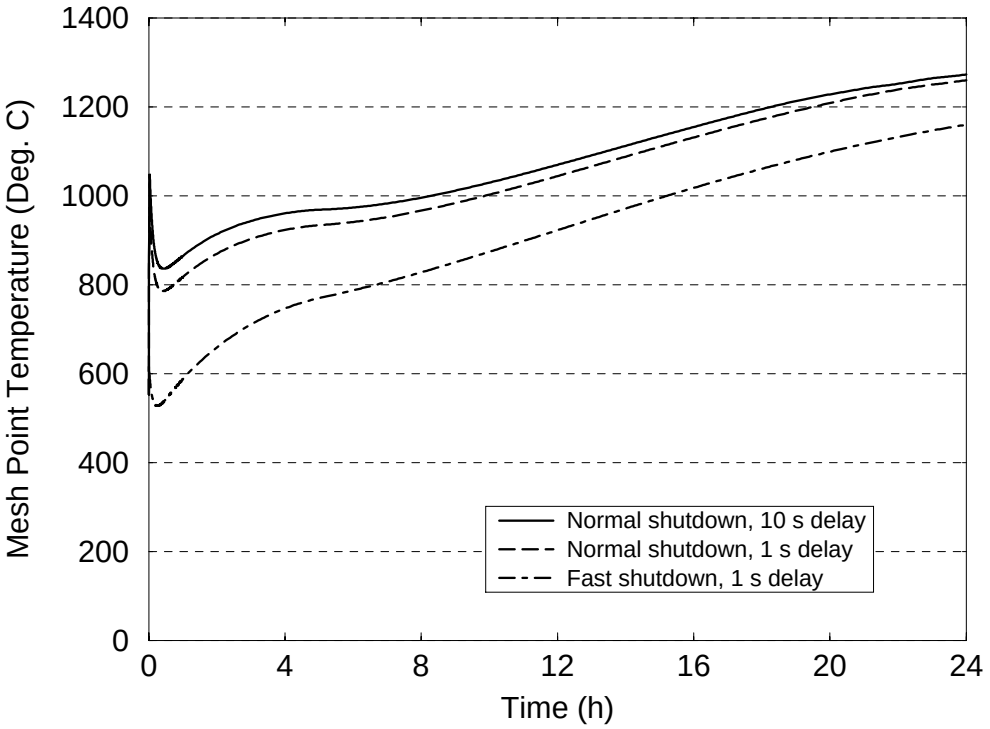

Figure 5.19: LOFA2A cases I-III: maximum FW MANET temperature vs. time (different shutdown scenarios).

5.2 Loss of Coolant Accidents

5.2.1 Ex-vessel Loss of Coolant (LOCA2EX)

Accident description

The event is characterised by simultaneous guillotine-breaks in the hot legs of both TBM cooling loops. No plasma shutdown, no circulator trip, and no HX bypass control are supposed. The calculations were performed with the RELAP5 nodalization of the TBM cooling loop shown in Fig. 5.20. The break is located in the hot leg at half distance between the TBM and the HX. Two time-dependent volumes (13) and (14) filled with helium at ambient conditions (0.1 MPa, 20 °C) serve as mass sinks, simulating the reactor building as an infinitely large reservoir. A further change to the steady state cooling loop model (Fig. 3.2) is the explicit nodalization of the helium buffer tank (7), which will be emptied during the accident, too. The buffer tank was modelled by a single volume component filled with helium at 14 MPa and 50 °C (compare section 3.5). It is connected to the hot leg via a valve junction which opens when the pressure in the connecting volume falls below its steady state value of 7.91 MPa.

Case investigated

Only the case (case I) of double-ended breaks of the large-diameter pipes in the hot legs of both TBM cooling loops without plasma shutdown was investigated. The probability of occurrence for a simultaneous break in both loops is in the hypothetical category, but the present RELAP5 model does not allow to simulate a failure in a single loop.

Remarks

Results for the present case are only available for the first 1.81 s of the accident. At this time RELAP5 terminated the calculation due to an error which is related to the very low coolant temperatures occurring during the accident, and to the water/non-condensible gas mixture model used in RELAP5. (Please recall that it is not possible in RELAP5 to specify helium as primary fluid). Former loss of coolant calculations indicated that this leads to failure in determining the kinematic viscosity of the mixture, because the temperature goes out of range of the temperature-viscosity table specified for the water component. (No numerical oscillations were observed.) Nevertheless, the following results covering the decisive period of the accident, namely the rapid depressurization of the cooling system in the beginning of the transient, are regarded as meaningful.

Results

Case I:
Immediately after rupture of the hot leg pipe the cooling system drains very fast, i.e., within approximately 2 s (Fig. 5.21, top). While the test module outlet header near the break location is depressurised within some tenths of a second, the depressurization in the buffer tank lasts for about 2 s.

Critical outflow in the break orifices with the helium flowing at the local speed of sound prevails for $\approx 0.7\ s$ (Fig. 5.21, middle). The mass flow rate of the helium goes up to 48 kg/s per break side immediately after start of the transient (Fig. 5.21, bottom), resulting in momentum forces of 43.2 kN per side. The influence of the draining process on the local heat transfer coefficients in the test module is shown in Fig. 5.22, top (corrected heat transfer coefficients recalculated from the RELAP5 heat transfer coefficients with the real heat transfer equivalent diameters, see correlations in subsection 3.2.2). Due to the very high helium velocities in the early phase of the accident the heat transfer coefficients

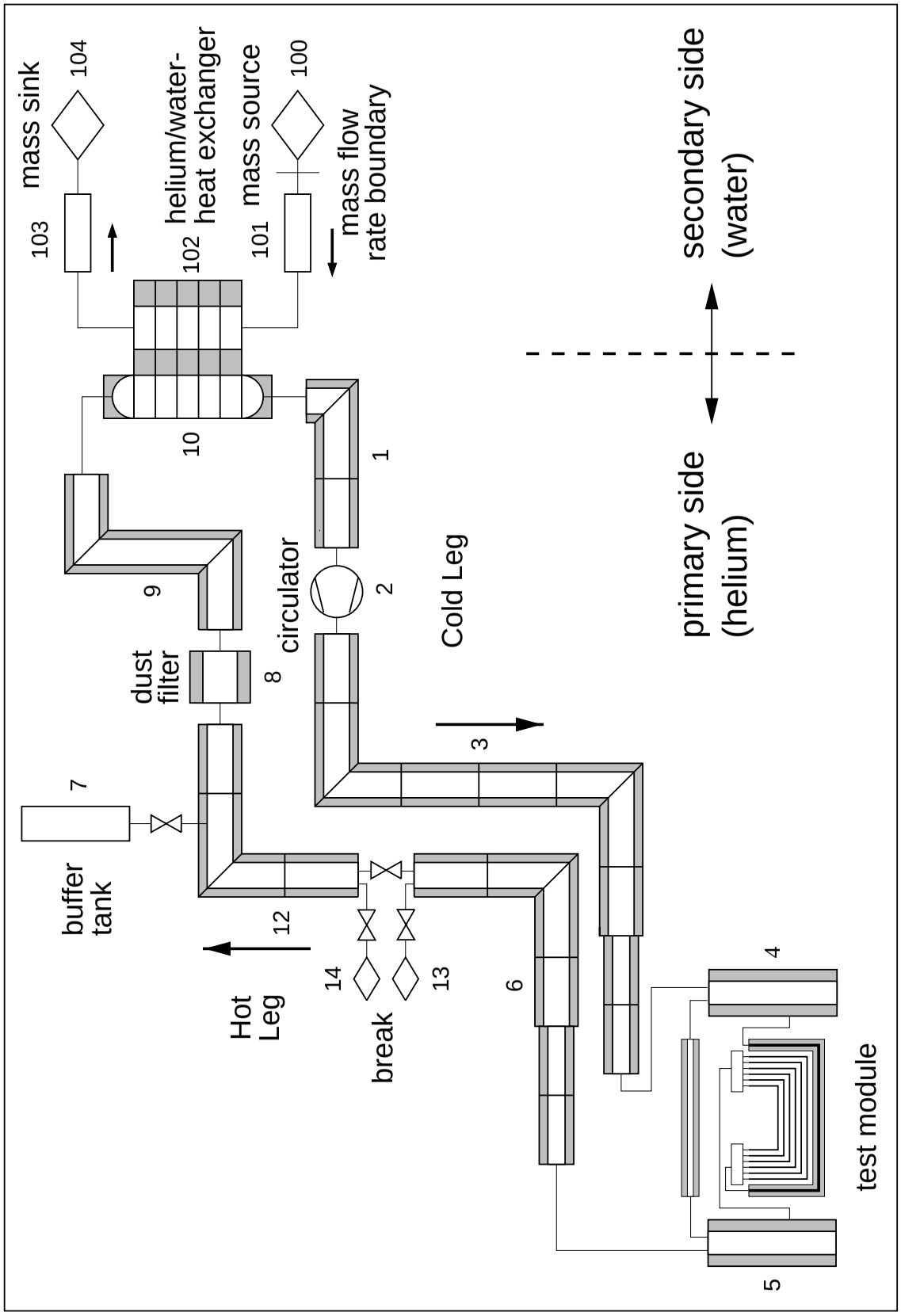

Figure 5.20: RELAP5/MOD3.1 nodalization of one cooling loop of the HCPB TBM cooling system for ex-vessel LOCA analysis.

in the FW and cooling plates cooling channels increase temporarily by factors up to three.

Histories of the helium temperatures in the TBM inlet and outlet header are plotted in Fig. 5.22, middle. Due to the expansion the helium cools down intensely. The isentropic expansion of helium at 8 MPa, 250 °C to 0.1 MPa would lead to a helium temperature of -183 °C. In the present case the cooling is mitigated by the heat transfer from the pipe walls and the cooling channel walls to the coolant. This heat transfer depends on the heat transfer coefficients, which take large values during the depressurization, as mentioned above. As a result, the helium temperature in the TBM inlet header goes down to 135 °C in the first second into the transient, rising slowly afterwards. The temperature in the outlet header is influenced by the temperature of the helium coming from the hot blanket regions and streaming to the break opening. The lowest temperature in the outlet header observed during the accident is 250 °C.

Of interest for the double-ended loss of coolant accident is the point in the circuit where the helium flow changes its direction, that is the stationary point in the loop during the depressurization. According to Fig. 5.22, bottom, which contains the histories of the helium mass flow rates at various points of the cold leg, this point turns out to be junction 4 of pipe (3), which is located at half distance between the HX and the TBM. Consequently, volume 5 of pipe (3) is the volume with the minimum helium temperature in the circuit during the accident (ϑ = -75 °C after 1.81 s, not shown).

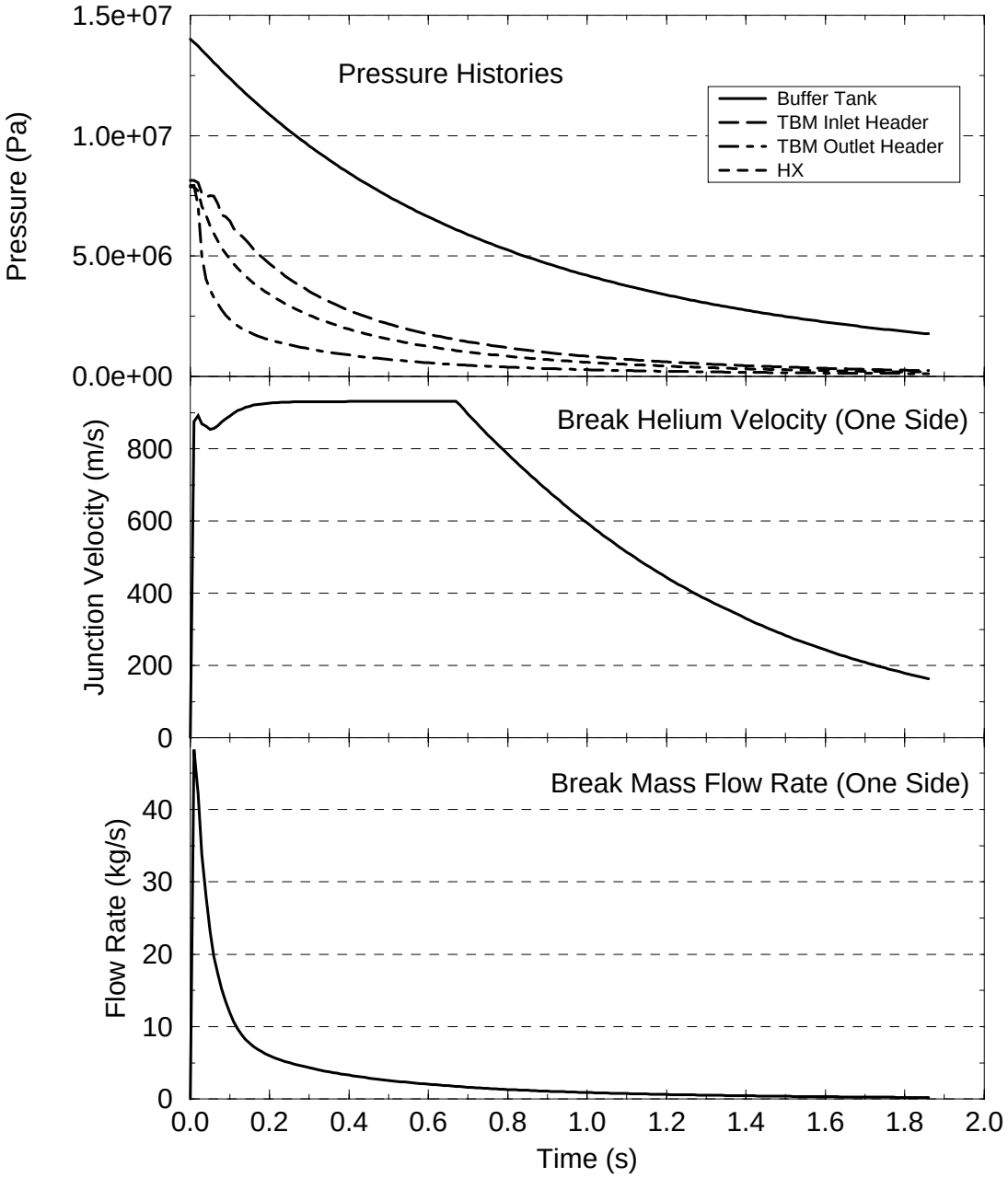

Figure 5.21: LOCA2EX: pressure histories, break helium velocity, and break mass flow rate vs. time (no plasma shutdown, no circulator trip, without HX bypass).

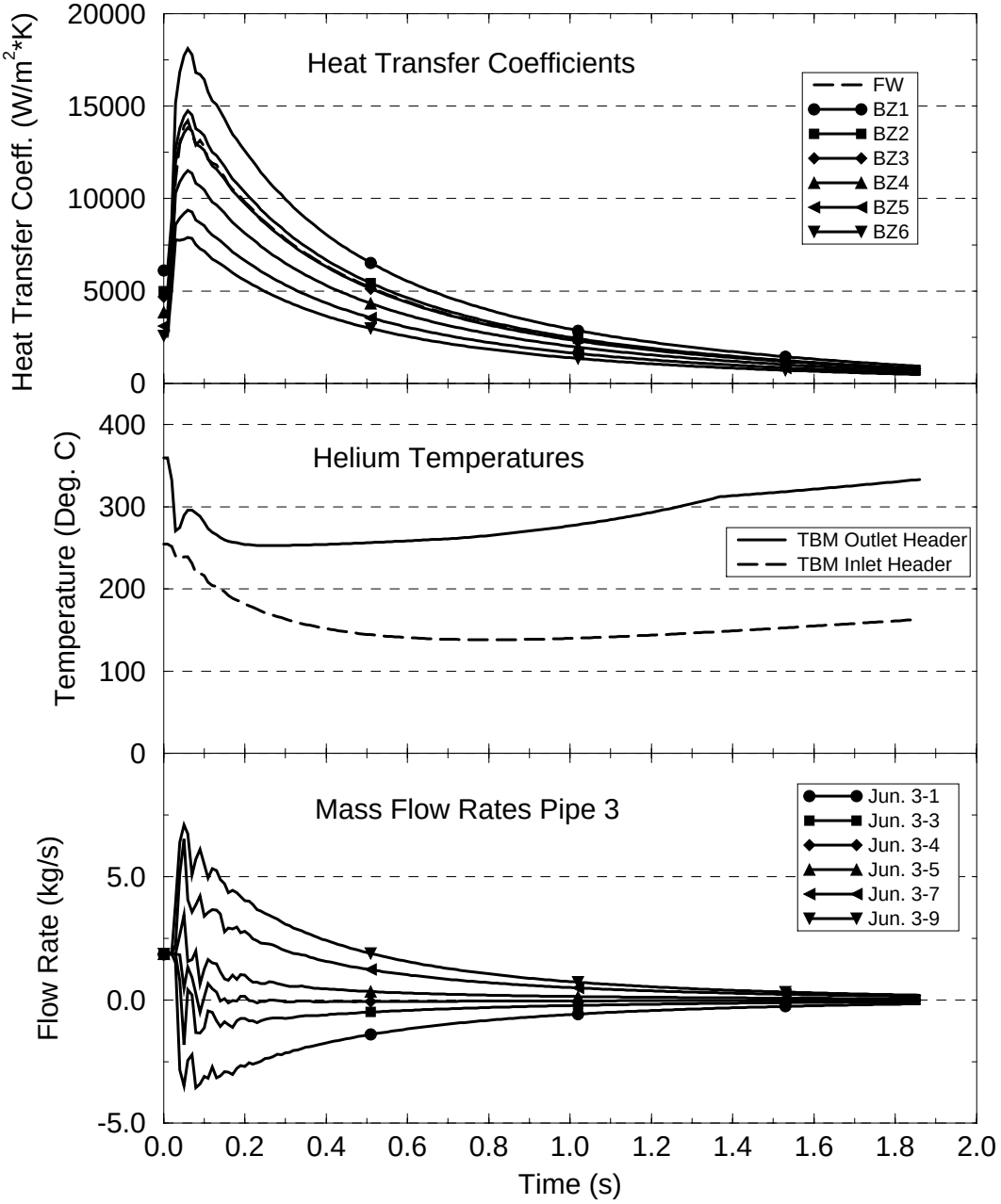

Figure 5.22: LOCA2EX: heat transfer coefficients, helium temperatures, and cold leg mass flow rates vs. time (no plasma shutdown, no circulator trip, without HX bypass).

5.2.2 In-vessel Loss of Coolant (LOCA2IN)

Accident description

The accident is characterised by a breach in the FW of the test module which extends over two adjacent FW cooling channels, thus affecting both TBM cooling loops. Spill of the helium of both cooling loops into the vacuum vessel will be the consequence. The break area per loop was assumed to equal twice the cross sectional area of one FW cooling channel:

$$A_{break,loop} = 2 \text{ x } 14 \text{ mm x } 18 \text{ mm} = 5.04 \cdot 10^{-4} \text{ m}^2.$$

The helium outflow from the TBM cooling system into the vacuum vessel is supposed to quench the plasma immediately, causing a disruption. As a more conservative scenario with respect to the temperature excursions inside the TBM a fast plasma shutdown scenario was considered which is assumed to be initiated by the control system in case the plasma should withstand the loss of coolant accident without disruption. Since no circulator trip is assumed, the heat rejection from the TBM to the secondary side will take place by forced convection at reduced helium throughput and reduced pressure.

The calculations were performed with the RELAP5 nodalization of the TBM cooling loop shown in Fig. 5.23. The break is located in volume 5 of FW pipe (20) in the toroidal center of the TBM. The vacuum vessel is modelled by single volume (50). The following parameters were used for the vacuum vessel:

Free volume:	2000 m^3
Free surface:	1500 m^2
Pressure:	1 Pa.
Surface temperature after shutdown:	150 °C.

In the RELAP5 model the surface of the vacuum vessel was simulated by a rectangular heat structure assigned to volume (50). At the right side of the heat structure a constant temperature boundary condition ($\vartheta = 150$ °C) was used. At the left side, the connecting side to volume (50), a convective boundary condition was used. The heat structure material is pure beryllium with a thickness of 10 mm, corresponding to a 10 mm beryllium layer protecting the ITER shield blanket. The break opening was modelled by a crossflow junction with a flow area of $5.04 \cdot 10^{-4}$ m^2, which connects volumes (20-5) and (50). Likewise to the LOCA2EX event, the buffer tank (7) was modelled explicitly as a single volume component.

Cases investigated

Two cases with (I) immediate plasma shutdown and (II) fast shutdown (see subsection 5.1.1) after 1 s delay were investigated. Continuous circulator operation and active temperature control system (HX bypass open) were assumed.

Results

Pressure equalization between the TBM cooling system and the vacuum vessel takes place fast within approximately 40 s. An equilibrium pressure of ≈ 20 kPa results. The situation is illustrated in Fig. 5.24, top and centre. The pressure in the vacuum vessel after depressurization of the TBM cooling loops still decreases somewhat when the initially hot helium cools down at the vessel walls to a temperature of 150 °C (Fig. 5.24, bottom).

The decrease of the flow resistance in the cooling loop is reflected by the decrease of the circulator pressure head, visualised in Fig. 5.25, centre. The resulting decrease of the total circuit mass flow rate is shown in Fig. 5.25, top. The circulator performance during

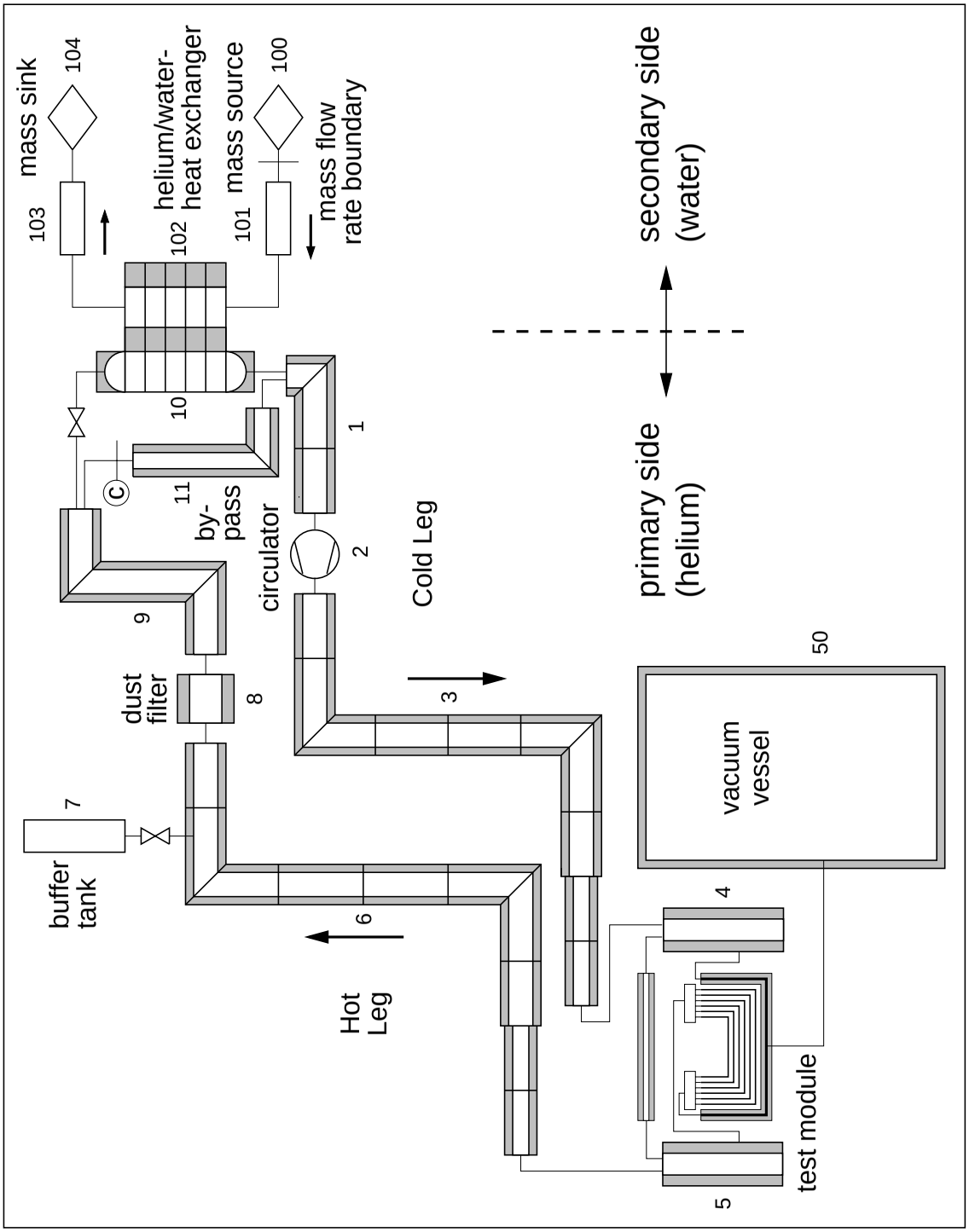

Figure 5.23: RELAP5/MOD3.1 nodalization of one cooling loop of the HCPB TBM cooling system for in-vessel LOCA analysis.

the accident is as follows: The circulator pressure head, H in unit [m], is proportional to the pressure drop divided by the helium density, $H \sim \Delta p/\rho$. Since the pressure loss in the circuit is proportional to the density, $\Delta p \sim \rho$, the circulator head H is not affected by the depressurization of the test module. Consequently, the volumetric flow rate in the circuit remains constant, since the circulator speed and the operating point do not change. Thus, the mass flow rate changes proportionally with the helium density. A mass flow rate of some grams per second after pressure equalization with the vacuum vessel ensues.

Also illustrated in Fig. 5.25, top, is the operation of the temperature control system by division of the helium flow between the HX and the HX bypass. Because of the decreased power generation in the TBM after plasma shutdown most of the helium has to be deviated across the HX bypass to keep the inlet temperature into the test module at the level of 250 °C. The success of the control action is visualised in Fig. 5.25, bottom, which shows that the helium temperature at the cold leg outlet remains in the desired range.

The temperature evolution within the first 600 s of the accident at the hottest nodes of the TBM in the more conservative case of a fast shutdown after 1 s delay is depicted in Fig. 5.26. Due to the fast decline in power generation inside the TBM no temperature overshoots occur neither in the plasma facing part of the FW nor in the pebble beds. The temperature in the part of the FW facing the breeding zone rises slowly towards a common FW temperature near 450 °C. The temperatures in the Li_4SiO_4 and beryllium pebble beds also converge towards a common temperature of $\approx$ 425 °C. No temperature excursions are expected in the further course of the accident. Consequently, the decay heat can be rejected even at a low pressure level of 20 kPa, provided the circulators remain in operation.

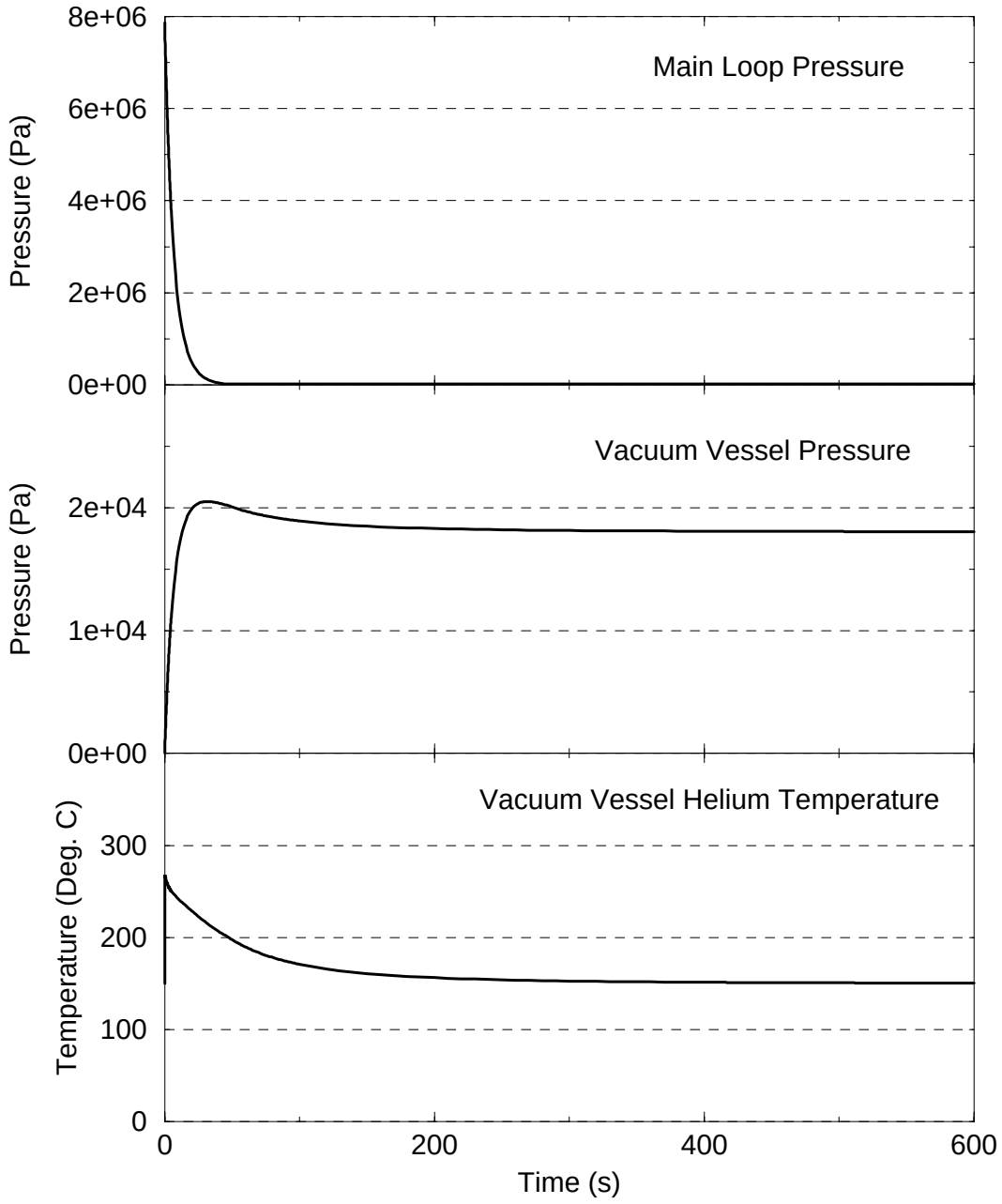

Figure 5.24: LOCA2IN case I: main loop pressure, VV pressure, and VV helium temperature vs. time (fast plasma shutdown after 1 s delay, no circulator trip, with HX bypass).

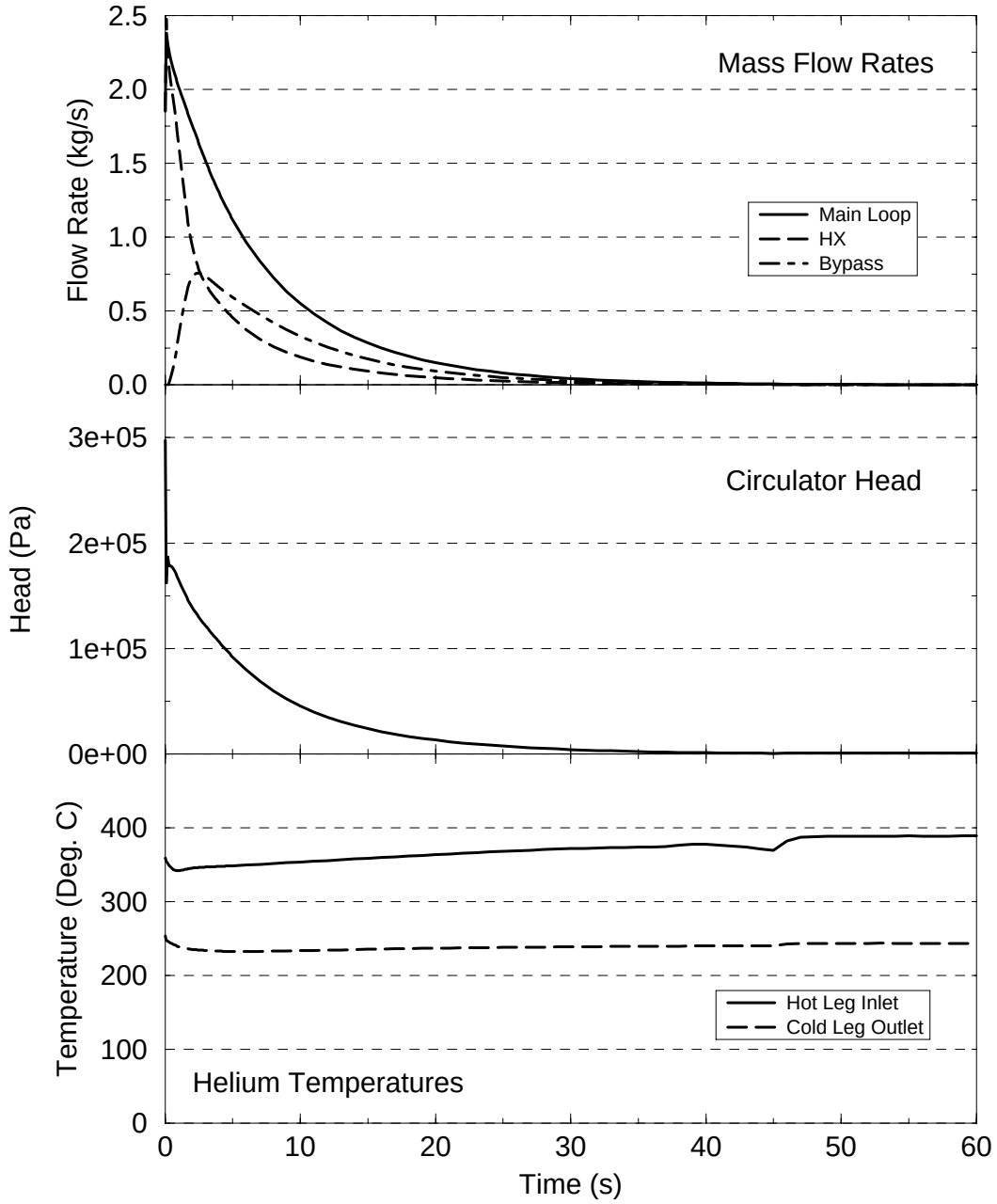

Figure 5.25: LOCA2IN case I: mass flow rates, circulator head, and helium temperatures vs. time (fast plasma shutdown after 1 s delay, no circulator trip, with HX bypass).

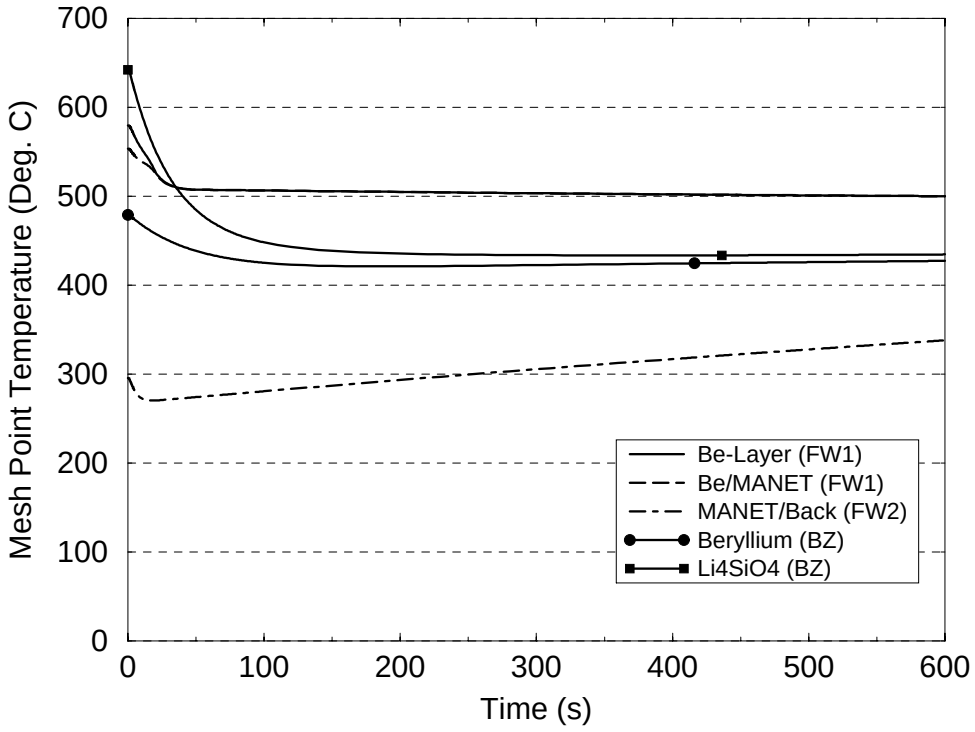

Figure 5.26: LOCA2IN case II: maximum structural temperatures vs. time (fast plasma shutdown after 1 s delay, no circulator trip, with HX bypass).

5.3 Leak Inside Test Module Accidents (LEAK2TM)

Accident description

The accident is characterised by a leak inside the test module between cooling plate channels of both TBM cooling loops and the pebble beds. Pressurization of the blanket box and the tritium extraction subsystem (TES) will be the consequence, accompanied by a fall in pressure in the primary TBM cooling loops. Continuous operation of the circulators is assumed, providing for heat rejection by forced convection from the TBM to the secondary side at reduced helium throughput and reduced pressure.

The break area per loop was assumed to be equal to the flow area of the connecting line between the TBM and the TES. According to sketches provided in [1], the inside diameter of the connecting line equals approximately 2 inch = 0.0508 m, yielding a flow area of $2.027 \cdot 10^{-3}$ m^2.

The calculations were performed with the RELAP5 nodalization of the TBM cooling loop shown in Fig. 5.27. (The Box No. 50 shown in the figure, denoted as purge gas system, represents the free volume of the TES.) The break is located in volume 3 of pipe (22), which represents the cooling plate channels in cooling zone 1 of the breeding zone in the toroidal center of the TBM (see subsection 3.2.1). The TES is modelled by a single volume (50). The following parameters were used for the TES:

Volume (for both cooling loops):	3.9 m^3 and 7.8 m^3
Pressure:	0.1 MPa
Helium temperature:	-75 °C.

The surface area and the structure of the TES were not considered in the present RELAP5 model.

The break opening was modelled by a crossflow junction with a flow area of $2.027 \cdot 10^{-3}$ m^2, which connects volumes (22-3) and (50). An equivalent pressure loss coefficient was applied to the break junction to account for the flow resistance in the connecting line which slows down the helium outflow from the cooling system into the TES. On basis of the pipe length of $L = 10$ m and a friction factor of $\lambda \approx 0.016$ a pressure loss coefficient of $\zeta = \lambda \cdot L/D = 3.15$ results ($D = 0.0508$ m).

As for the LOCA2EX and LOCA2IN events, the buffer tank (7) was modelled explicitly as a single volume component.

Cases investigated

Four cases with variation of the shutdown scenario, the circulator behaviour, and the TES volume were investigated, see Table 5.2. The TES volumes given in the table represent the fractions pertaining to one TBM cooling loop. Case III represents a bounding case that is highly unlikely. Case IV with doubled TES volume was included into the analyses to investigate the effect of a further reduced system pressure, as it is caused by the cooling of the helium on the cold surfaces of the TES after pressure equalization between the primary system and the TES.

For all transients investigated the temperature control system was assumed to be in operation (HX bypass open).

Results

Case I:

The depressurization of the TBM cooling system and the pressurization of the tritium extraction subsystem take place within 4 s. An equilibrium pressure of approximately

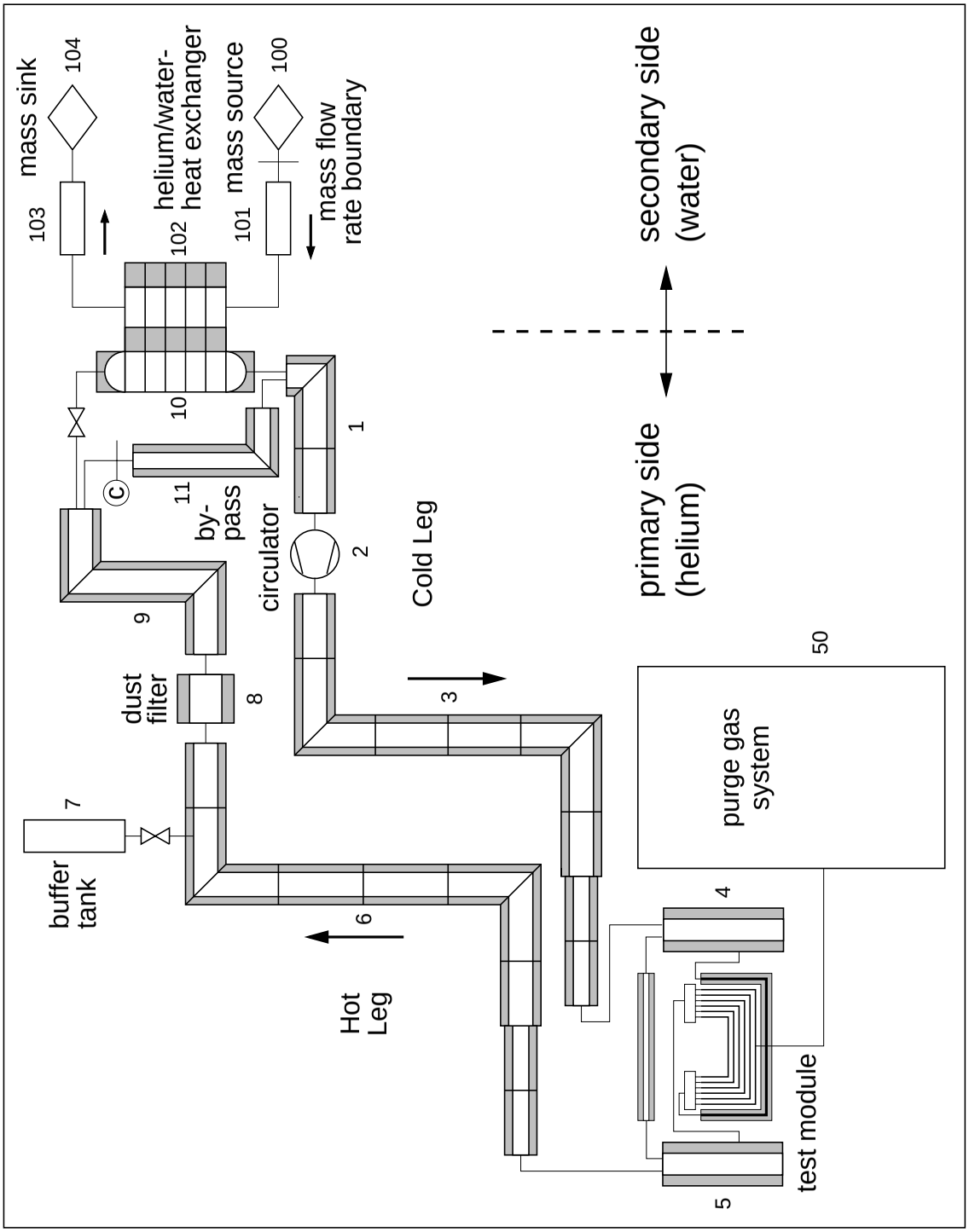

Figure 5.27: RELAP5/MOD3.1 nodalization of one cooling loop of the HCPB TBM cooling system for leak inside test module analysis.

Table 5.2:
Investigated leak inside test module accidents.

Case	Shutdown scenario	Delay time (s)	Circulator trip	Level difference TBM - HX (m)	Volume TES[1] (m^3)
I	No shutdown	inf.	no	22	1.95
II	Normal shutdown[2]	1	no	22	1.95
III	Normal shutdown[2]	1	yes	22	1.95
IV	No shutdown	inf.	no	22	3.90

[1] Fraction pertaining to one TBM cooling loop.

[2] See definition in subsection 5.1.1.

5.8 MPa results. Pressure histories for the buffer tank, the TES (purge gas system) and the primary cooling system (cold leg inlet) are depicted in Fig. 5.28, top. After pressure equalization the pressure distribution in the system is determined by the pressure head developed by the circulator. Thus, the highest system pressure prevails at the circulator discharge junction and the lowest pressure at the circulator suction junction. Since the total pressure loss in the circuit is proportional to the helium density, the pressure head developed by the circulator decreases proportional to the decrease in system pressure in the course of the accident, i.e., from the initial value of 0.3 MPa to the new steady state value of 0.22 MPa (Fig. 5.28, center).

The helium flow between the TBM cooling loop and the TES is visualised in Fig. 5.28, bottom. The flow rate achieves a maximum value of nearly 5 kg/s within a tenth of a second after initiation of the accident, declines almost linearly afterwards, and approaches zero after approximately 4 s.

The history of the total mass flow rate in the cooling loop as well as the effect of the temperature control system in the case without plasma shutdown (case I) are illustrated in Fig. 5.29. The total loop flow rate decreases proportional to the decrease in system pressure (see explanations in subsection 5.2.2), that is from 1.85 kg/s to 5.8/8 x 1.85 kg/s = 1.34 kg/s. The expansion of the helium in the cooling system leads to a decrease in temperature which causes the temperature control system to pass helium from the hot leg via the HX bypass to the cold leg to ensure the desired TBM inlet temperature of 250 °C. In the later phase of the transient, all of the helium is directed through the HX due to the elevated temperature level inside the test module.

The temperature evolution at the hottest nodes of the TBM in the case of no plasma shutdown (case I) is depicted in Fig. 5.30. The unchanged power load on the TBM in conjunction with the reduced helium throughput in the circuit causes a structural temperature rise in the TBM until a new steady state temperature profile has developed. The temperature in the Be-layer on the plasma side of the FW rises by 60 °C, the temperature in MANET at the back side of the FW at the interface to the breeding zone rises by 10 °C, and the maximum temperatures in the beryllium and Li_4SiO_4 pebble beds rise by approximately 25 °C.

Case II:

With normal shutdown after 1 s delay the temperatures develop as displayed in Fig. 5.31. Only negligible temperature overshoots appear in the FW at the beginning of the tran-

sient. In the breeding zone, the pebble beds show a decrease in temperature. Due to the forced convection flow in the circuit both the FW and the breeding zone converge fast towards the 250 °C temperature level, which is adjusted in the circuit by the temperature control system.

Case III:

The very unlikely event of the simultaneous occurrence of leaks inside the TBM and of a loss of power supply to the circulators in both loops is covered by case III. The time constant $T_{1/2}$ of the circulator, which gives the time during which the circulator slows down to half speed, was assumed to equal 6 s. The temperature excursions observed during the transient are shown in Fig. 5.32. A temperature overshoot of 180 °C occurs in FW MANET at 75 s into the accident, which is 20 °C higher than the overshoot in the corresponding LOFA2 event (case V in subsection 5.1.1) at full system pressure. The maximum transient differential temperature between front side (plasma side) and rear side (breeding zone side) of the FW is 15 °C higher than in the corresponding LOFA2 event. The pebble beds experience no temperature overshoots during the event. Both FW and breeding zone tend to equalise their temperatures and converge towards the adjusted temperature of 250 °C.

Case IV:

The depressurization of the TBM cooling system and the pressurization of the tritium extraction subsystem, in case of the TES having twice the reference volume, is shown in Fig. 5.33, top. As for case I, pressure equalization is finished within 4 s. However, the equilibrium pressure is now equal to 4.3 MPa. Accordingly, the pressure head of the circulator goes down to 0.16 MPa (Fig. 5.33, centre). The leak mass flow rate shows a similar behaviour as for case I, attaining nearly 5 kg/s immediately after occurrence of the break, and declining evenly afterwards. The main draining procedure, however, lasts about 0.5 s longer.

The temperature evolution at the hottest nodes of the TBM for case IV without plasma shutdown is given in Fig. 5.34. The evolving new steady state temperature profile is characterised by a temperature in the Be-layer on the plasma side of the FW 115 °C higher than the design steady state value. The maximum temperatures in the beryllium and Li_4SiO_4 pebble beds lie approximately 65 °C above the design steady state values.

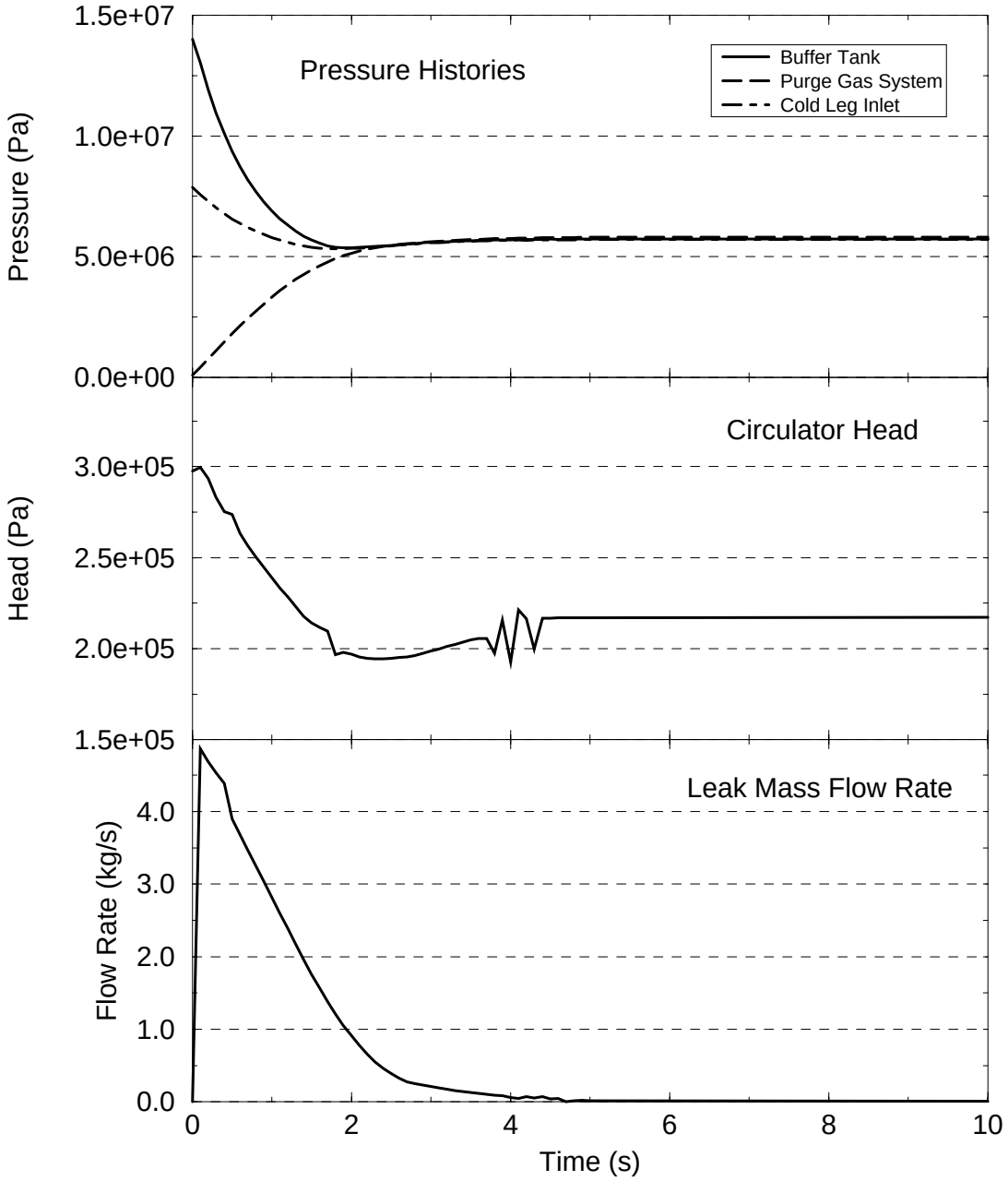

Figure 5.28: LEAK2TM case I: pressure histories, circulator head, and leak mass flow rate vs. time (no plasma shutdown, no circulator trip, with HX bypass).

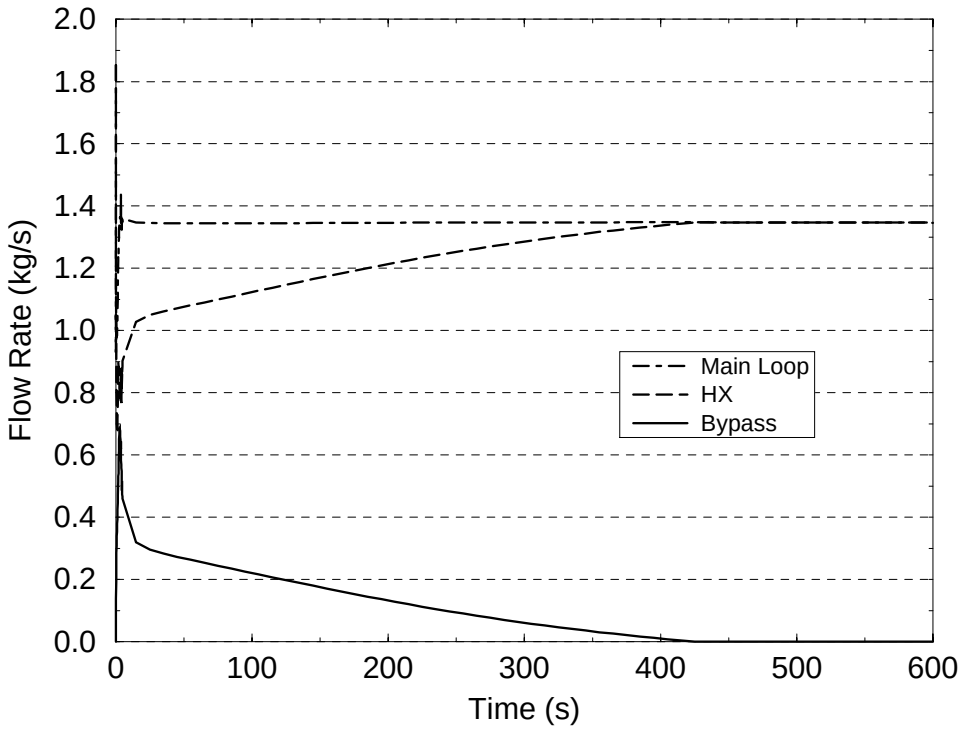

Figure 5.29: LEAK2TM case I: controlled mass flow rates vs. time (no plasma shutdown, no circulator trip, with HX bypass).

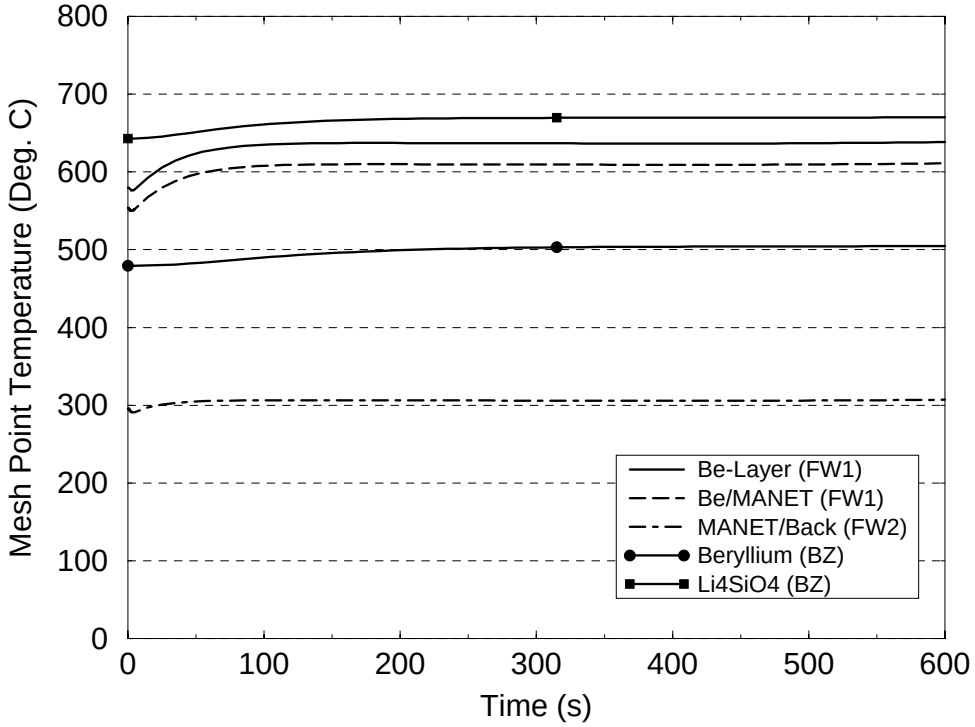

Figure 5.30: LEAK2TM case I: maximum structural temperatures vs. time (no plasma shutdown, no circulator trip, with HX bypass).

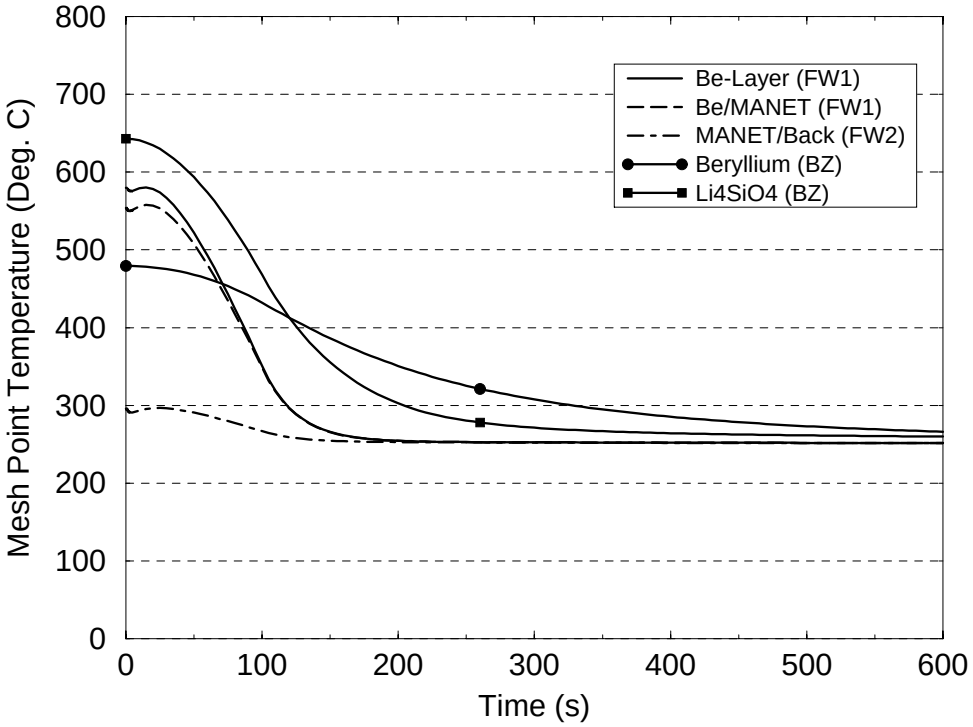

Figure 5.31: LEAK2TM case II: maximum structural temperatures vs. time (normal shutdown after 1 s delay, no circulator trip, with HX bypass).

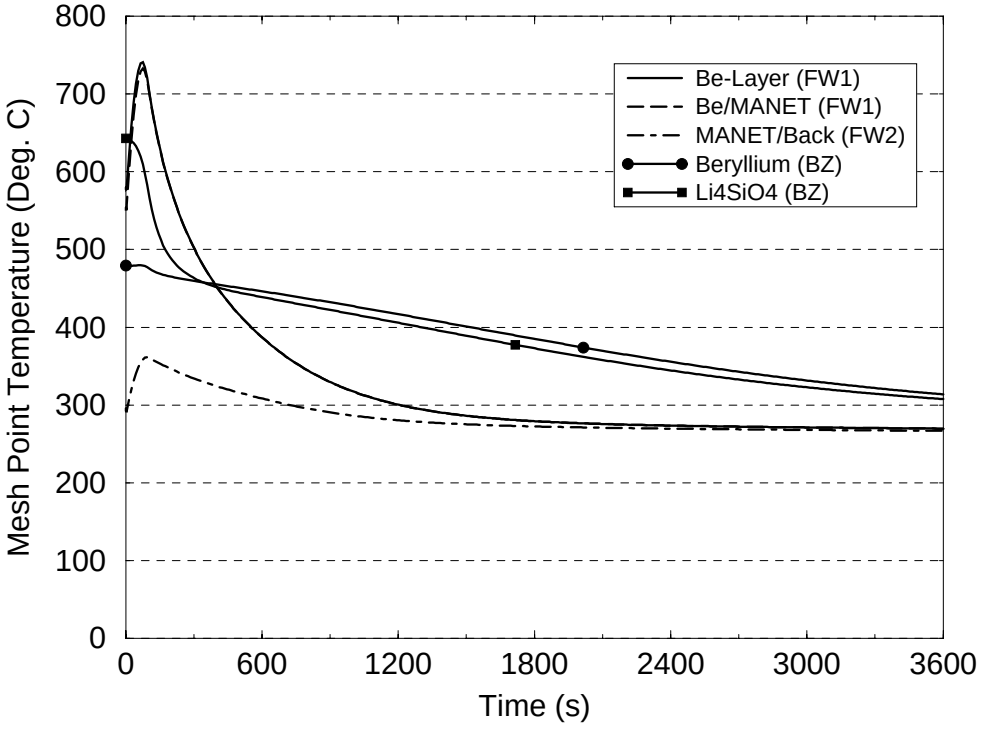

Figure 5.32: LEAK2TM case III: maximim structural temperature vs. time (normal shutdown after 1 s delay, with circulator trip, $\Delta H_{TBM/HX}$ = 22 m, T(1/2) circ. = 6 s, with HX bypass).

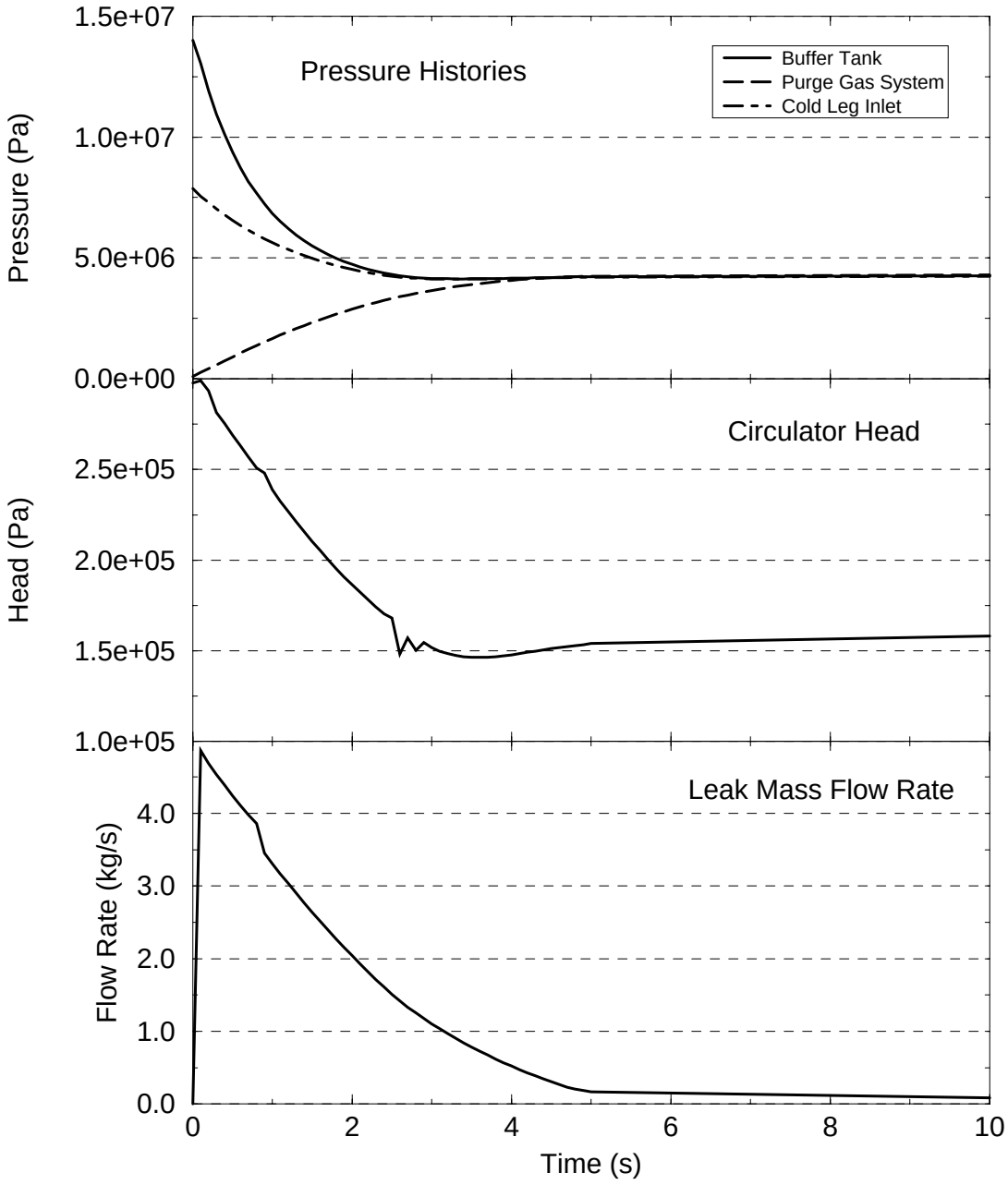

Figure 5.33: LEAK2TM case IV: pressure histories, circulator head, and leak mass flow rate vs. time (TES volume doubled, no plasma shutdown, no circulator trip, with HX bypass).

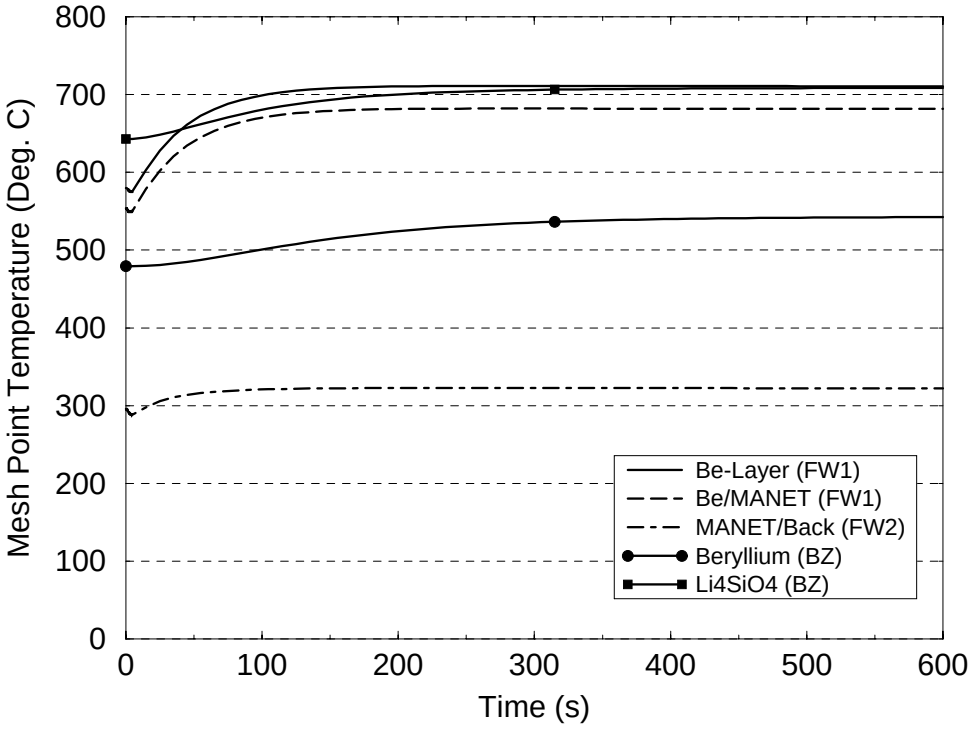

Figure 5.34: LEAK2TM case IV: maximum structural temperatures vs. time (TES volume doubled, no plasma shutdown, no circulator trip, with HX bypass).

5.4 Loss of Heat Sink Accidents

Loss of heat sink accidents following a loss of secondary coolant and, alternatively, following a total loss of flow on the secondary side were analysed. Details will be given in the following.

5.4.1 Total Loss of Heat Sink (LOHS2HX)

Accident description

The accident is characterised by a total loss of heat sink in both heat exchangers, caused by LOCAs in both secondary cooling loops. The resulting heat-up rate of the cooling system is determined by the power load on the TBM and the thermal inertia of the loop components. The analyses were conducted with the RELAP5 nodalization of the TBM cooling loop shown in Fig. 3.2 on page 18 with the secondary side piping removed. Instead of convective boundary conditions adiabatic boundary conditions were applied at the secondary sides of the heat structures pertaining to HX pipe (10) at restart of the problem from steady state.

Cases investigated

Two cases with (I) no plasma shutdown and (II) normal plasma shutdown after 10 s delay were investigated. Continuous circulator operation and active temperature control system (HX bypass open) were assumed.

Results

Case I:

The temperature evolution at the hottest nodes of the TBM in the case of no plasma shutdown within the first hour of the accident is depicted in Fig. 5.35. The whole test module experiences an unlimited steep temperature increase. The maximum temperature in FW MANET (curve Be/MANET, FW1) rises at a rate of 0.5 K/s within the first 100 s of the transient and at a rate of 0.3 K/s averaged over one hour. The temperatures in the breeder material and in the beryllium multiplier increase at mean rates of 0.2 K/s within the first 3600 s. Failure of the FW is expected to occur within the first 600 s of the accident. An in-vessel loss of coolant with succeeding quench of the plasma would be the consequence. In the hypothetical case of no FW failure, the FW MANET would reach its melting point approximately at 3000 s into the transient, whereas the breeder and multiplier would reach their melting points approximately at 2900 s and 3600 s into the transient, respectively.

Case II:

Temperature histories for the hottest nodes of the TBM in the case of normal plasma shutdown after 10 s delay are depicted in Fig. 5.36. In the early phase of the accident, the decrease in power generation leads to a decline in temperature in the whole TBM, apart from a minor temperature overshoot of some degrees centigrade in the plasma side of the FW 15 s after start of the transient. Temperature equalization in the FW, breeding zone, and between FW and breeding zone takes place. A common temperature of 350 °C is achieved 360 s after onset of the accident. The further temperature development is characterised by a common temperature rate of change of 0.04 K/s.

Note: The circulator, which has a rated power consumption of 90 kW, constitutes the main heat source in the circuit after shutdown of the plasma. Please recall that

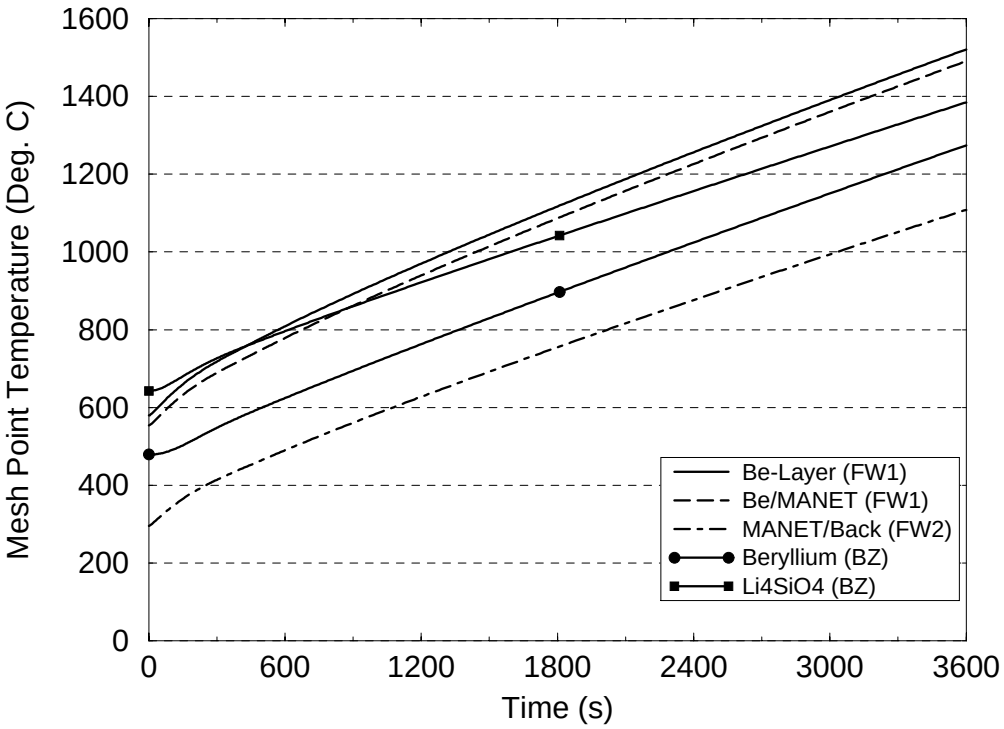

Figure 5.35: LOHS2HX case I: maximum structural temperatures vs. time (no shutdown, no circulator trip, with HX bypass).

the total decay heat in the TBM equals 38 kW immediately after shutdown and 16 kW one hour later (Table 2.6 on page 13). Since the circulator power scales with the circulator speed to the power of three, $P \sim N^3$, the power introduced into the circuit can be reduced considerably by slowing down the circulator. If this strategy should be pursued, attention has to be directed towards the evolving temperature profile inside the TBM, since the temperature equalization with the rest of the loop components slows down with decreasing throughput in the circuit, too.

5.4.2 Loss of Secondary Side Flow (LOSF2HX)

Accident description

The accident is characterised by a total loss of flow on the HX secondary sides, caused by inadvertent valve closures in both secondary cooling loops. As a result, the stagnant water in the HX on the secondary side will heat up in the course of the transient until it has reached its saturation temperature of 180 °C (constant pressure of 1 MPa supposed on secondary side). Further heat supply from the primary side will lead to evaporation of the water. The amount of heat required to evaporate all of the water contained in the HX on the secondary side ($m_{H_2O,HX} \approx 35kg$) equals approximately 70 MJ. The accident differs from the LOHS2HX accident in the way that the heat sink is not lost completely, but is still available at an elevated temperature level as long as the evaporation process is in progress.

The analyses were conducted with the RELAP5 nodalization of the TBM cooling loop shown in Fig. 3.2. The loss of flow event on the secondary side was realised by setting the

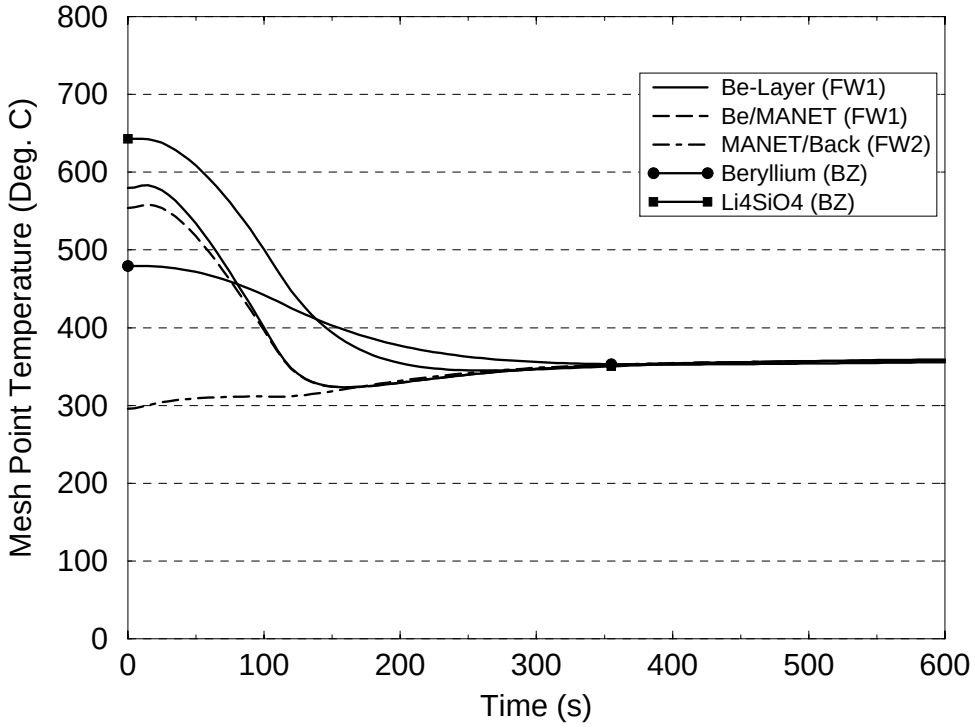

Figure 5.36: LOHS2HX case II: maximum structural temperatures vs. time (normal shutdown after 10 s delay, no circulator trip, with HX bypass).

mass flow rate in the time dependent junction located between volumes (100) and (101) to zero at restart of the problem from steady state.

Case investigated

Only one case (case I) with normal plasma shutdown after 1 s delay and simultaneous instantaneous loss of power supply to the circulators in both TBM cooling loops was investigated. The time constants $T_{1/2}$ of the circulators were assumed to equal 6 s. Further, an active temperature control system was assumed.

Results

The temperature evolution at the hottest nodes of the TBM within the first hour of the accident is depicted in Fig. 5.37. The beryllium coating of the FW and the FW MANET undergo maximum temperature overshoots of 140 °C and 160 °C within the first 100 s of the transient, respectively. In the breeder and multiplier materials no temperature excursions occur. After one hour problem time the temperatures in the FW and the breeding zone have stabilised at a temperature level between 250 °C and 300 °C.

The history of the total mass flow rate in the cooling loop as well as the function of the temperature control system are illustrated in Fig. 5.38. The total loop flow rate decreases rapidly within the first 400 s of the accident, falling from its nominal value of 1.85 kg/s to 0.05 kg/s or 2.7 % of nominal. This marks the point where the transition from forced flow to natural circulation flow takes place. After one day the natural circulation flow has decreased to 0.02 kg/s or 1.1 % of nominal.

The fraction of the helium flowing through the HX bypass varies between 25 % and 80 % around 3000 s and around 24 h problem time, respectively. The fact, that 80 % of the

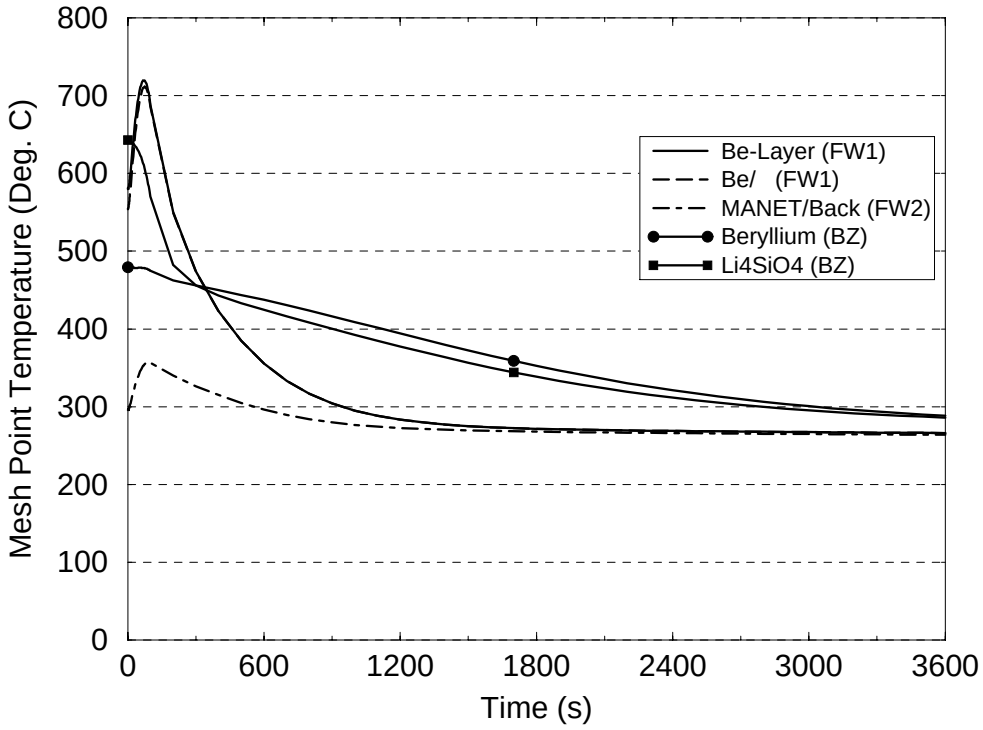

Figure 5.37: LOSF2HX: maximum structural temperature vs. time (normal shutdown after 1 s delay, with circulator trip, $\Delta H_{TBM/HX} = 22$ m, T(1/2) circ. = 6 s, with HX bypass).

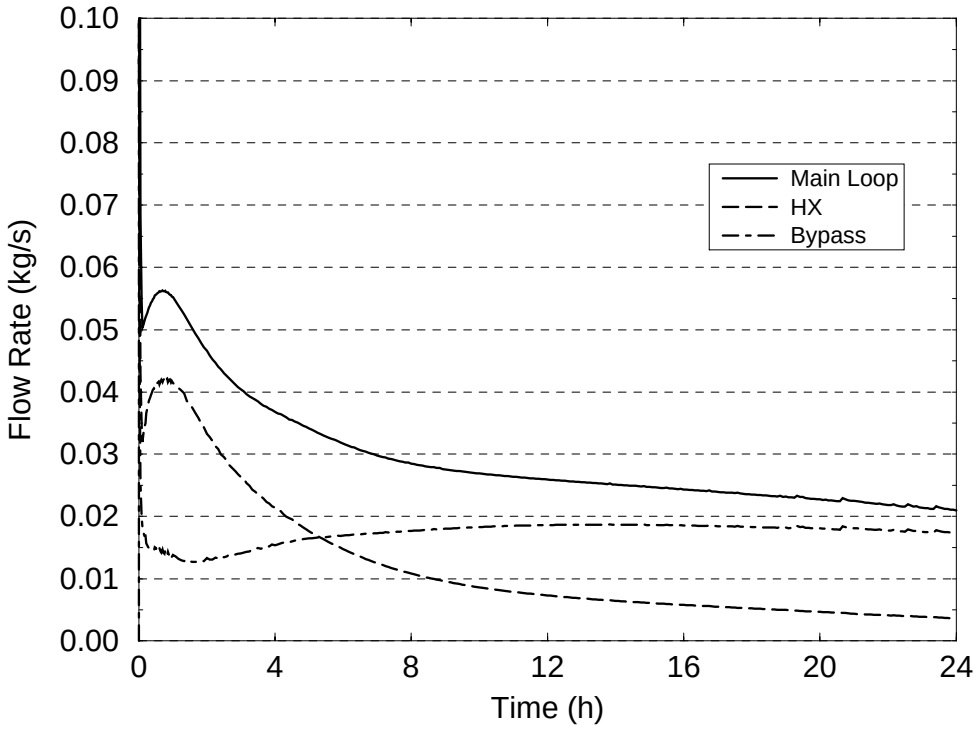

Figure 5.38: LOSF2HX: mass flow rates vs. time (normal shutdown after 1 s delay, with circulator trip, $\Delta H_{TBM/HX}$=22 m, T(1/2) circ.=6 s, with HX bypass, $\dot{m}$(0 s)=1.85 kg/s).

helium have to be directed through the HX bypass to keep up the TBM inlet temperature shows that the secondary side still constitutes an effective heat sink for the TBM even 24 h after onset of the cooling disturbance.

Histories of the water temperatures on the HX secondary side are shown in Fig. 5.39. Clearly recognisable, the water approaches its saturation temperature of 180 °C soon after start of the transient. Volume 5 of secondary HX pipe (102), located opposite the primary side helium inlet, achieves saturation first, and volume 1 of pipe (102), located at the primary side helium outlet, achieves saturation last. Temperature pulsation is observed during the course of the accident. These should be treated with caution, since the one-dimensional RELAP5 hydrodynamic model in conjunction with the specified zero flow boundary condition on the secondary side are not qualified to simulate the formation and rise of steam bubbles in a stagnant saturated fluid.

The same holds for the fraction of evaporated water (void fraction) on the secondary side of the HX shown in Fig. 5.40. Again, the curves should be treated with caution. Nevertheless, they indicate that most of the heat is transferred in the upper part of the HX (volume (102-5), Fig. 5.39). There, the highest void fractions appear during the accident. The differential temperatures between the helium and the water in the middle and in the lower part of the HX are not large enough to provide for evaporation of the water in the later phase of the transient. Generally, the decay heat generation in the test module is not intense enough to evaporate considerable quantities or even the total amount of water inside the HX.

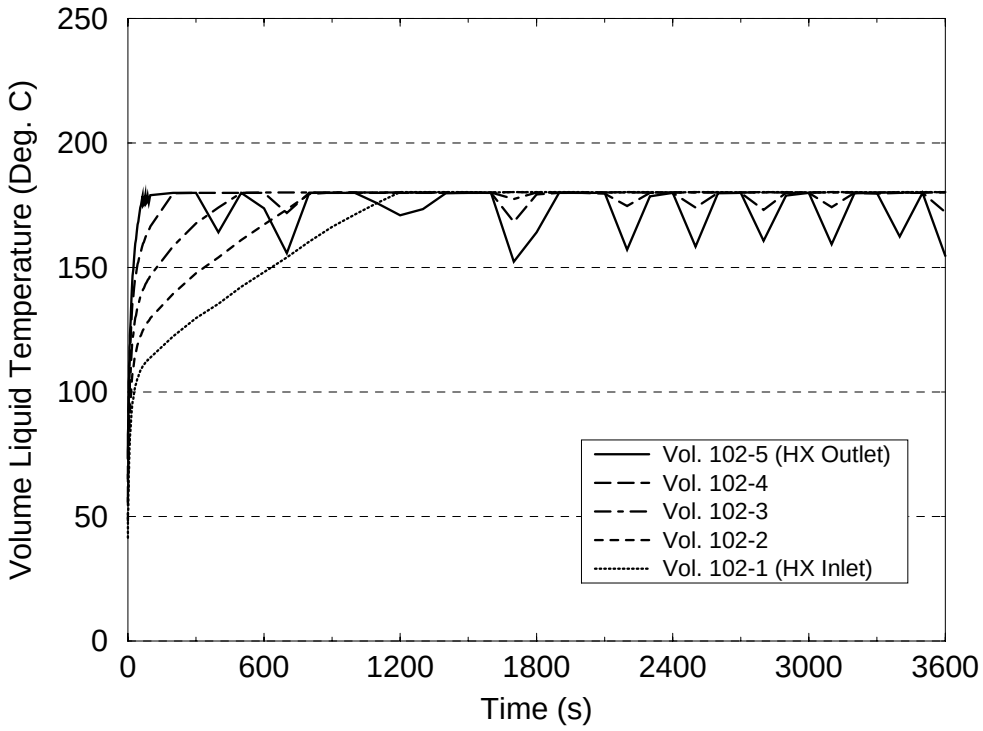

Figure 5.39: LOSF2HX: HX secondary temperature vs. time (normal shutdown after 1 s delay, with circulator trip, $\Delta H_{TBM/HX} = 22$ m, T(1/2) circ. = 6 s, with HX bypass).

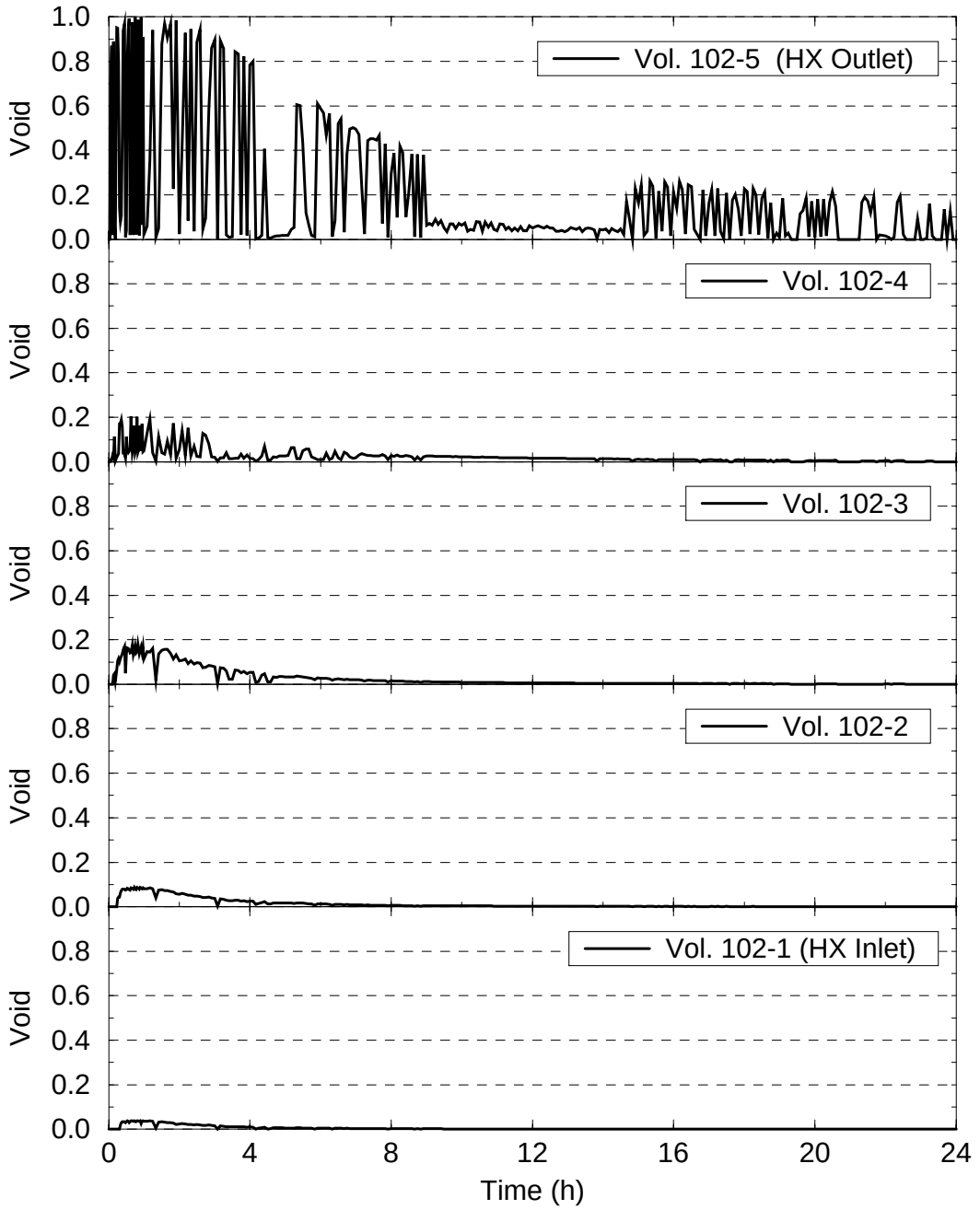

Figure 5.40: LOSF2HX: HX secondary void fractions vs. time (normal shutdown after 1 s delay, with circulator trip, $\Delta H_{TBM/HX} = 22$ m, T(1/2) circ. = 6 s, with HX bypass).

Table 5.3:
Overview of the main temperature results obtained for the cases investigated.

Accident and case	$\Delta H_{TBM/HX}$ (m)	Delay time (s)	Shutdown time (s)	$T_{1/2}$ circ. (s)	$\vartheta_{FW,max}$ (°C) MANET	$\vartheta_{BZ,max}$ (°C) Li_4SiO_4	$\vartheta_{BZ,max}$ (°C) Beryllium	$\Delta\vartheta_{FW,max}$ (°C) (FW front-rear[3])	$\Delta\vartheta_{FW,max}$ (°C) (peak-steady st.)
LOFA2-I	22	inf.	inf.	2	7 - 5 K/s	2 - 1 K/s	2 - 1 K/s	unlimited	unlimited
LOFA2-II	22	10	100	2	880	660	490	470	325
LOFA2-III	22	1	100	2	820	650	485	430	265
LOFA2-IV	22	10	100	6	770	650	470	400	215
LOFA2-V	22	1	100	6	720	<650	<480	370	165
LOFA2-VI	22	1	20	2	570	<650	<480	<285	15
LOFA2-VII	22	1	20	6	<555	<650	<480	<285	0
LOFA2-VIII	3	10	100	2	890	660	490	480	335
LOFA2-IX	0.5	10	100	2	895	660	490	485	340
LOFA2A-II[1]	22	10	100	–	1055/1275	685/815	500/815	580/0	500/720
LOFA2A-I[1]	22	1	100	–	980/1260	660/810	490/810	530/0	420/705
LOFA2A-III[1]	22	1	20	–	620/1160	<650/735	<480/735	320/0	65/605
LOCA2IN-II	22	1	20	inf.	<555	<650	<480	<285	0
LEAK2TM-I	22	inf.	inf.	inf.	610	670	505	305	60
LEAK2TM-II	22	1	100	inf.	<555	<650	<480	<285	0
LEAK2TM-III	22	1	100	6	730	<650	<480	375	180
LEAK2TM-IV[2]	22	inf.	inf.	inf.	670	710	540	380	115
LOHS2HX-I	22	inf.	inf.	inf.	0.3 K/s	0.2 K/s	0.2 K/s	unlimited	unlimited
LOHS2HX-II	22	10	100	inf.	560	<650	<480	<285	5
LOSF2HX-I	22	1	100	6	710	<650	<480	365	160

[1] Two numbers refer to short term (t < 100 s) and long term (24 hours) periods.

[2] Volume of tritium extraction subsystem doubled.

[3] The RELAP model does not account for the heat conduction in the FW ribs (see subsection 3.2.2) leading to overestimation of these values.

Chapter 6

Summary and Conclusions

This report describes the thermal-hydraulic analysis of the helium-cooled pebble bed (HCPB) test blanket module. The analysis is performed with the computer code RELAP/MOD3.1. Modeling of the complex cooling flow pattern present in the TBM, in combination with the time-dependent volumetric heat as well as surface heat flux applied to the first wall, is described in detail. The model includes also the complete cooling circuit with circulator, heat exchanger, pressure and temperature control provisions, and the coupling to the secondary cooling system.

The performance of the TBM and cooling circuit during normal operation (i.e., steady state and pulsed operation) and accidents was investigated. Four groups of accidents were analysed with a variety of input parameters: (1) loss of flow accidents, (2) loss of coolant accidents, (3) leak inside test module accidents, and (4) loss of heat sink accidents. The input parameters were essentially the following: level difference between the HX and the TBM, shutdown delay time, ramp-down time for power shutdown, circulator coast-down behaviour, and flow control in the HX bypass line.

Typical transients for pressure, temperature, velocity, and mass flow rate at various locations in the TBM and in the circuit are presented and discussed in terms of safety aspects. Peak temperatures reached during the transients and relevant differential temperatures for the cases investigated are summarised in Table 5.3 on page 100. The analyses allow to establish shutdown requirements and rules for accident management in a broad spectrum of scenarios which, in many cases, are in the hypothetical category. Generally, all accidents involving complete loss of flow require a fast shutdown within 10 to 20 s. The events with partial loss of cooling performance of the type LEAK and LOHS can cope with a normal power ramp-down time of 100 s without the threat for further damage to ITER components. Overall, no critical feasibility or safety issues are seen.

In the following paragraphs more specific results are summarised and conclusions are drawn in the order of the analyses performed.

Steady state operation

- Due to the strong decrease in heat generation in radial direction inside the test module, adjustment of the helium mass flow rates in the cooling plate channels is necessary to achieve the target function of equal helium temperatures at all cooling channel outlets. The analysis showed that the adjustment can be accomplished by introduction of orifices with varying area ratios at the inlets to the cooling channels. However, very small orifice openings at the cooling channels in the rear part of the TBM result, which are susceptible to plugging due to possibly entrained particles in the helium stream. This could lead to local overheating of the test module due to

insufficient cooling.

Pulsed ITER operation

- The analysis of the test module during pulsed ITER operation revealed that the TBM can follow the power cycles thermally, i.e. a nearly steady state condition is reached within the 1000 s full power period and the initial state condition is reached again in the dwell time between the power pulses. No heat-up of the TBM takes place with increasing numbers of cycles.

- A temperature control system is mandatory for the TBM cooling system to avoid excessive cooling of the blanket during the dwell periods and to maintain a helium inlet temperature to the TBM of 250 °C. Temperature control by division of the helium flow on the HX and on an HX bypass was found to be an effective control mechanism.

Loss of flow accidents

- A loss of power supply at the circulators with continued plasma burn will lead to failure of the FW within approximately 30 s. An in-vessel loss of coolant with succeeding quench of the plasma would be the consequence.

- The maximum temperature excursions in the TBM in cases with normal plasma shutdown, i.e. with scheduled 100 s power ramp-down, are above the acceptable margins. However, they show a strong dependence on the shutdown delay time and on the circulators' moment of inertia. Very short delay times ($t \approx 1$ s) and large circulator masses reduce the temperature overshoots. Large delay times can be compensated for by high circulators' moment of inertia. The latter could be enlarged by use of flywheels mounted on the circulator shafts.

- The situation is different if a fast plasma shutdown is executed. In this case, the temperature overshoots reduce to acceptable levels. However, this would entail the danger of a disruption.

- The long term heat removal is assured by the natural circulation which develops in the TBM cooling loops at unchanged cooling water conditions on the secondary side. Even at a geodetic level difference between the TBM and the HX of 0.5 m the natural circulation is strong enough to provide for heat removal from the TBM to the HX.

- Temperature control, e.g. by use of a HX bypass, is necessary to ensure a TBM inlet temperature of 250 °C in the long term natural circulation phase.

- A total loss of flow in both TBM cooling loops due to inadvertent valve closures leads to an unlimited temperature increase in the TBM. Fast shutdown of the plasma is mandatory to prevent failure of the FW within the first 100 s of the accident. By initiating a fast shutdown the time span for countermeasures extends to 4 – 8 h.

Loss of coolant accidents

- The simultaneous double-ended break of the hot leg pipes in both TBM cooling loops leads to rapid depressurization of the cooling circuits. The consequences are assumed to be similar to that of the total loss of flow event due to inadvertent valve

closures. Furthermore, the sudden expansion leads to intense cooling of the helium, which involves the possibility of crack formation in the structural materials due to thermal shocks.

- An in-vessel loss of coolant will lead to inherent plasma termination and pressurization of the vacuum vessel. However, the equilibrium pressure after drain of both cooling loops is two magnitudes below the design pressure of the vacuum vessel. The accident will therefore not endanger the integrity of the vacuum vessel.

- The decay heat of the TBM could be rejected by forced circulation in the cooling loops in case of in-vessel LOCAs even at the low equilibrium pressure level of 20 kPa.

Leak inside test module accidents

- A leak inside the test module between the cooling plate channels and the pebble beds leads to depressurization of the TBM cooling system and pressurization of the tritium extraction subsystem.[1] The unchanged power load on the TBM in conjunction with the resulting reduced helium throughput in the circuits causes a structural temperature rise in the TBM until a new steady state temperature profile has developed. The temperature rise in the FW will be at least 60 °C.

Loss of heat sink accidents

- A total loss of the heat sink will lead to an unlimited heat-up of the TBM and its circuit components. Without plasma shutdown, failure of the FW is expected to occur within the first 600 s of the accident. With plasma shutdown it will take several hours until the critical FW temperature is reached. This time span can be further prolonged, if the circulator, which has a rated power consumption of 90 kW, is slowed down in the course of the transient. In case this strategy should be pursued, attention has to be directed towards the evolving temperature profile inside the TBM since the temperature equalization with the rest of the loop components slows down with decreasing throughput in the circuit, too.

- A total loss of flow on the secondary side will lead to heat-up of the secondary cooling water until it has reached its saturation temperature. Further heat supply from the primary side will lead to evaporation of the water. Therefore, the heat sink is still available at an elevated temperature level as long as the evaporation process is in progress.

- Even the combination of a total loss of flow on the secondary side with a loss of power supply of the circulators on the primary side entails no severe consequences. The natural circulation flow which develops after shutdown of the plasma is strong enough to transport the decay heat from the TBM to the secondary side. Furthermore, the decay heat generation in the test module is not intense enough to evaporate considerable quantities of water inside the HX.

[1] Meanwhile the design rule that the TBM box can sustain the full system pressure, has been changed. There will be a pressure relief system which will alter the leak inside TBM accident scenario.

Bibliography

[1] M. Dalle Donne et al.: Design Description Document, European Helium Cooled Pebble Bed (HCPB) Test Blanket, FZKA 5891, April 1997.

[2] ITER Joint Central Team: ITER non-site specific safety report (NSSR-2), Volume VII, Analysis of reference events, October 1997.

[3] T. Heider et. al.: Development of fabrication techniques for the European helium cooled pebble bed breeder blanket, Proc. 19th Symposium on Fusion Technology, Lisbon, Portugal, 16-20 September 1996, (1323-1326).

[4] M. Dalle Donne et. al.: European helium cooled pebble bed (HCPB) test blanket, ITER Design Description Document, Status 15.11.1997

[5] C. M. Allison and E. C. Johnson, Eds., RELAP5/MOD3 Code Manual, Volumes I–III, NUREG/CR-5535, EGG-2596, August 1995.

[6] M. Dalle Donne et al.: European DEMO BOT Solid Breeder Blanket, KfK 5429, November 1994.

[7] U. Fischer, FZK, Private communication, August 1996.

[8] H. Tsige-Tamirat, U. Fischer FZK: Private communication 1995.

[9] P. Norajitra, FZK: Private communication, July 1994.

[10] K. Kleefeldt et al.: Safety and Environmental Impact of the BOT Helium Cooled Solid Breeder Blanket for DEMO, FZKA 5754, March 1996.

[11] Interatom: Konzeptauslegung von Kühlsystem und Spülsystem für einen NET-Testplug mit heliumgekühltem Feststoffblanket, Abschlußbericht Ident-Nr. 71.03266.4 (Nov. 1989).

[12] L. Boccaccini, FZK: Private communication, July 1996.

[13] H. Schade, E. Kunz: Strömungslehre, 2. Aufl., Walter de Gruyter, Berlin New York, 1989.

[14] J. Singh, Institute for Safety Research and Reactor Technology, Forschungszentrum Jülich: Private communication, July 1995.

[15] I. Schmuck, FZK: Private communication, 1996.

[16] P. Norajitra, FZK: Private communication, August 1996.

[17] R. Aymar, Ed.: ITER General Design Requirements Document (GDRD), S 10 GDRD 1 95-02-03 W 1.1, February 1995.